Coordination Chemistry Reviews 337 (2017) 1–33

Contents lists available at ScienceDirect

Coordination Chemistry Reviews

journal homepage: www.elsevier.com/locate/ccr

Review

SERS-based ultrasensitive sensing platform: An insight into design and practical applications

Yufeng Yuan [a,c,1], Nishtha Panwar [b,1], Stephanie Hui Kit Yap [b,1], Qiang Wu [a,c], Shuwen Zeng [b,c], Jianhua Xu [d], Swee Chuan Tjin [b], Jun Song [a,*], Junle Qu [a,*], Ken-Tye Yong [b,c,*]

[a] Key Laboratory of Optoelectronic Devices and Systems of Ministry of Education and Guangdong Province, College of Optoelectronic Engineering, Shenzhen University, Shenzhen 518060, People's Republic of China
[b] School of Electrical and Electronic Engineering, Nanyang Technological University, Singapore 639798, Singapore
[c] CINTRA CNRS/NTU/THALES, UMI 3288, Research Techno Plaza, 50 Nanyang Drive, Border X Block, Singapore 637553, Singapore
[d] State Key Laboratory of Precision Spectroscopy, East China Normal University, Shanghai 200062, People's Republic of China

ARTICLE INFO

Article history:
Received 23 December 2016
Accepted 8 February 2017
Available online 10 February 2017

Keywords:
SERS
Ultrasensitive detection
Resonance enhancement techniques
High quality plasmonic nanostructure
Highly efficient adsorption mechanism
Multifunctional integrated SERS sensing platform

ABSTRACT

Ultrasensitive detection of chemicals and biological analytes in trace or single molecular level is highly desirable in both scientific and technological fields, *e.g.*, analytical chemistry, life science, materials science, biomedical diagnostics, and forensic science, *etc*. With high sensitivity, high specificity, narrow line-widths, and multiplexed non-destructive testing capabilities, surface enhanced Raman scattering (SERS)-based sensing is the most promising approach to monitor targeted analytes in the vicinity of nanostructured surface. An insight into the recent advances of SERS-based ultrasensitive sensing platform can provide an effective reference guideline to develop an optimal detection approach for arising real-world applications. Many SERS-based review articles mainly focus on the fundamental theory of SERS, nanostructured plasmonic SERS sensors, and single molecule SERS detection. However, no comprehensive review article targeting SERS-based ultrasensitive detection strategies, their working mechanisms and illustrative practical applications has been reported yet. Hence, it is important to project the latest SERS-based ultrasensitive detection research in a review, which will present a reference guideline to develop an optimal detection approach for specific detection or monitoring of analytes in highly diluted solutions. We present a systematic classification and discussion on the recent multiple strategies to achieve ultra-high SERS detection sensitivity. We also outline a detailed analysis on the up-to-date applications *in vitro* and *in vivo*. Finally, we also discuss a new trend in SERS-based ultrasensitive sensing applications.

Contents

* Corresponding authors at: School of Electrical and Electronic Engineering, Nanyang Technological University, Singapore 639798, Singapore (K.-T. Yong).
E-mail addresses: songjun@szu.edu.cn (J. Song), jlqu@szu.edu.cn (J. Qu), ktyong@ntu.edu.sg (K.-T. Yong).
[1] These authors contributed equally to this work.

http://dx.doi.org/10.1016/j.ccr.2017.02.006
0010-8545/

1. Introduction

Ultrasensitive detection of chemicals and biological analytes is a class of important analytical science in identifying target analytes in extremely low detection levels, which provides the fingerprint signal of target analytes in a very small detection volume. In recent years ultrasensitive detection of target analytes has become critical in various scientific and technological fields ranging from analytical chemistry [1], life science [2–5], materials science [6], biomedical diagnostics [7,8] to drug discovery [9,10], food security [11,12], forensic science [13] and environment monitoring [14–16].

Detection techniques like gas chromatography (GC) [17], high performance liquid chromatography (HPLC) [18,19], capillary electrochromatography (CE) [20], gas chromatography–mass spectrometry (GC–MS) [21,22], enzyme cycling assays [23] and photoluminescence determination [24,25], *etc.*, are widely applied for ultrasensitive monitoring of chemicals and biological analytes. However, most of them are time-consuming, expensive, and require tedious sample preparation processes, which may damage intrinsic properties of analytes possessing high biological activities, especially for some DNA/RNA, enzymes, and protein molecules. Due to its highly efficient emission process, photoluminescence technique can realize single molecule detection, but the molecular structure information obtained from its broad emission band is very limited, which sometimes results in false molecular identification and recognition. Furthermore, prior to photoluminescence measurement, it is necessary to ensure the presence of chromophore in the proposed analyte system.

In recent years, SERS-based ultrasensitive sensing platform has become the most promising approach to detect targeted analytes in the vicinity of nanostructure surface because of its high sensitivity, high specificity, narrow line-widths, and non-destructive testing capabilities. Briefly, SERS events usually occur when target analytes are present near a metallic surface (Fig. 1). The SERS measurement model includes three pivotal factors for enhanced Raman signals from the adsorbed target molecules – incident light, adsorbed target molecules, and metal nanoparticles. The enhancement mechanisms explaining SERS effects are widely studied by many researchers, and documented in several excellent reviews and books [26–32]. To date, two major mechanism models, namely the long-distance electromagnetic enhancement (EM) and short-distance chemical enhancement (CE), are commonly agreed across the research community.

Plasmonics is the science to study the light-matter interactions on nano-sized metal structures. The main component of plasmonics is the metallic nanostructure, which focuses and guides light

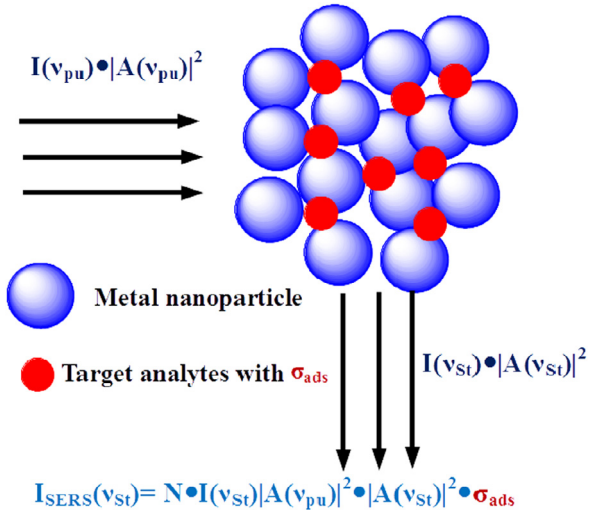

Fig. 1. Schematic of SERS detection. $I_{SERS}(\nu_{St})$ denotes the measured SERS signal intensity, $I(\nu_{pu})$ and $I(\nu_{St})$ are excitation laser intensity and Stokes scattering light intensity, respectively. $|A(\nu_{pu})|$ and $|A(\nu_{St})|$ are the enhancement factors at excitation field and Stokes scattering field, respectively. σ_{ads} describes the increased Raman cross-section of the adsorbed target analytes. N is the number of target molecules involved in SERS process.

down to nanometer distance, resulting in strong coupling between incident photons and collective oscillations of free electrons on the metal surface. Consequently, the EM mechanism stems largely from the surface plasmon resonance (SPR) process wherein the incident photons are resonant with collective oscillation frequencies of conducting electrons on the metallic surface. For target analytes, EM enhancement is non-selective and strongly dependent on distance. As the SPR enhancement effect decays exponentially as a function of distance from the nanoparticles (NPs), only the analytes approaching the metal surface obtain enormous Raman signal gain [28]. To a first approximation, SPR effects provide a maximal $|E|^4$ enhancement, where $E = E_{local}/E_{pump}$ (E_{local}: local electric field amplitude close to metal surface, E_{pump}: the original incident field amplitude) [28].

There are two basic SPR models – propagating SPR (PSPR) and non-propagating localized SPR (LSPR) [33]. PSPR can be excited on thin metal films via prism couplers or gratings, resulting in hundreds of micrometers of propagation distance. Unlike PSPR, LSPR is usually excited on the surfaces of metal NPs that are smaller than the excitation wavelength, generating resonance effects that can be tuned by the size, shape and composition [34]. SPR theory has greatly contributed to the design and development of SPR-based or SERS-based sensors through efficiently monitoring the SPR absorption band of NPs or specifically enhancing the fingerprint spectra of target analytes. Recently, our group has demonstrated a SPR-based biosensor for sensitive detection of tumor necrosis factor alpha antigen. Using a gold nanorod (GNR) as the amplification label, the detection limit is as low as femtomolar level (10^{-15} M). The huge field amplification gain is generated from plasmonic coupling between antibody functionalized gold film and antibody-conjugated GNRs [35]. More recently, our group has proposed an approach to significantly produce field enhancement through a gap between a metallic NP and a thin gain material of approximately ~100 nm. Theoretical calculation results showed that the thin gain film can provide several orders of local field enhancement, which paves a possible avenue for preparing ultrasensitive SPR-enhanced sensors [36].

Although the EM enhancement model provides major contribution to explain the SERS effects, it is insufficient to state the complete SERS phenomenon. Thus, some researchers suggested the CE mechanism model, which becomes significant on increasing the scattering cross-section of analytes adsorbed on metal surface, due to the specific interactions between adsorbates and metal, *e.g.*, electronic coupling, charge-transfer, *etc.* [37]. For identical SERS substrates, the large variation in Raman cross-sections and adsorption efficiencies of various target analytes can produce significant SERS detection sensitivity. In general, the most ideal Raman probes are heterocyclic molecules, possessing sizable Raman scattering cross-sections, larger than that of small molecules (*e.g.*, water, fatty acids, ethanol, acetone, *etc.*).

Extensive studies have been done on the optimization of SERS-active substrates, the type of adsorption mechanism, and integration of SERS spectroscopy with analytical systems (*e.g.,* microfluidic-, optofluidic-, and paper-based) to achieve ultrahigh detection sensitivity. However, there are three primary hurdles which limit the applicability of this technology into real-life. The first hindrance lies on the challenge to attain reproducible single molecule detection sensitivity in liquid medium for ultralow detection levels (*i.e.*, below femtomolar concentration) as the SERS-based detection is highly dependent on the ensemble binding of analytes in hotspot regions. Second, the fabrication of a perfect SERS substrate with highly ordered and high density hotspots is a major inhibiting factor for increasing the SERS detection sensitivity. Third, achieving quantitative analysis in highly diluted solutions remains a roadblock, due to heterogeneous liquid media, Brownian motion of analytes or nanoparticles, and laser force. In view of the present challenges, creating and developing a SERS-based sensing platform with high reproducibility, sensitivity, specificity, and efficiency would be highly preferable and valuable.

Particularly, the article is intended to present an in-depth review and discussion of SERS-based ultrasensitive sensing strategies for latest practical applications in biosensing, bioimaging, biomedical diagnostics, cancer screening/therapy, photo-thermal therapy, pollutants monitoring, drugs identification, *etc.* Using this review article as a discussion platform, we aim to promote the awareness of employing SERS for real-life detection applications, and enrich more reasonable options for fundamental research related to biosensing, bioimaging *in vitro*, and cancer therapy research *in vivo*. Our final objective is to encourage researchers to develop more novel, rapid, sensitive, reproducible, and multifunctional SERS sensing platforms for monitoring target analytes in real time.

2. Strategies for SERS-based ultrasensitive sensing

Prior to designing and constructing a SERS-based sensing platform for ultrasensitive detection, one must carefully consider and examine the following five key factors: (i) The detailed features of the proposed target analytes: are the target analytes ascribed to molecules or inorganic ions? If they belong to the molecule category, one should consider their intrinsic features, for example, molecular structure, photoluminescence, Raman scattering cross-section, electronegativity, water solubility, affinity to nanomaterial, molecular weight, *etc.* On the contrary, if the analytes are inorganic ions (*eg.*, Hg^{2+}, Cd^{2+}, Pb^{2+}, *etc.*) without Raman scattering cross-section, one should determine another suitable Raman reporter with sizeable scattering cross-section for labeling them. (ii) The selected incident wavelength for excitation of Raman scattering and SPR of nanoparticles (*e.g.,* ultraviolet, visible and near infrared (NIR) excitation window), which depends on the absorption band of target molecules or nanoparticles. (iii) Once the incident light is selected, the enhancement features of SERS substrates play an important role in amplifying Raman signals and further developing detection sensitivity. The plasmonic nanostructure in a metal containing nanostructure system is a prerequisite in producing SERS event. The coordination of metal ions/nanoparticles in creating plasmonic nanostructures plays an important role in generating huge surface plasmon resonance effects [38]. Metallic substrates employed for SERS usually focus on single composition-based coinage nanomaterials (*e.g.*, gold, silver, aluminum and copper) and composite-metal nanomaterials (*e.g.*, alloy, metal-organic frameworks, and magnetic nanostructures). Additionally, metal-free substrates refer to non-metal nanostructures such as semiconductor silicon, carbon-based materials and paper-based SERS substrates. Metal-free materials have further expanded the options of SERS substrates for practical applications [39]. However, it must be highlighted that noble metal containing systems are also widely involved in the design of novel carbon-based hybrid nanomaterials and silicon-based hybrid nanomaterials, mainly because of the SPR effects of the metal ions/nanoparticles coordination in plasmonic hybrid nanostructures. (iv) The adsorption mechanism between target analytes and SERS substrates is also important, because it is highly related to the adsorption efficiency, which indirectly influences the SERS intensity. Besides the surface modification of plasmonic nanostructures by using coordination molecules, the coordination mechanism between targeted molecule and plasmonic nanostructures also enables to further improve SERS effects [38]. (v) The place that SERS sensing experiments will be performed: are they performed *in vivo* or *in vitro*? Given identical analytes, the sensing strategy

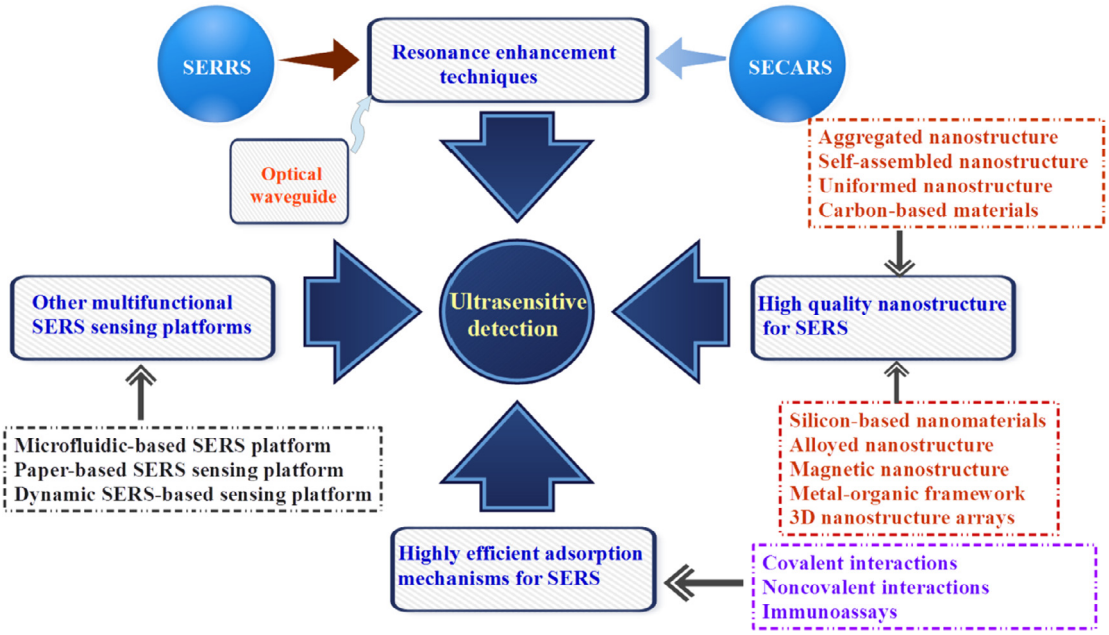

Fig. 2. Efficient strategies for SERS-based ultrasensitive detection.

will not be identical for *in vivo* and *in vitro* locations. Once these five factors have been carefully considered, one can proceed to design and prepare the construction of SERS sensing.

In principle, the signal intensity is highly dependent on the excitation wavelength, SPR features of nanomaterials, increased Raman scattering cross-sections of adsorbed target analytes, and the adsorption interaction mechanism between target analytes and nanomaterials. Thus, multiple efficient strategies are proposed to achieve ultrasensitive detection sensitivity, as shown in Fig. 2 and described below.(i) *Resonance enhancement techniques*: Besides SPR enhancement produced by the interactions between nanomaterials and incident photons, both molecular electronic transition resonant excitation [40,41] and molecular coherence [42] can produce additional enhancement effects, which significantly contribute to the SERS detection sensitivity. For example, surface enhanced Raman resonance scattering (SERRS) and surface enhanced coherent anti-Stokes Raman scattering (SECARS) spectroscopy mainly originates from resonant excitation of molecular electronic transition, and optical coherence techniques, respectively. Many recent findings demonstrate the ability of SERRS [43,44] and SECARS [45,46] to achieve the SERS signals with single molecule sensitivity. In addition, optical waveguide integrated optics and devices are an ideal option to achieve high electric field gains, due to their high light harvesting effect. In the later part of this review, we will present and discuss their latest practical applications in SERS sensing.(ii) *High quality nanostructure for SERS:* It is widely agreed that the EM enhancement mechanism, which stems largely from SPR, mainly contributes to the total SERS enhancement. At fixed excitation wavelength, the enhancement performance of SPR is highly related with the nanomaterials used, which are essential for achieving ultrasensitive detection sensitivity. The material properties of nanostructure, *e.g.*, morphology, size, composition, preparation, and stability, *etc.*, play a key role in producing SPR electromagnetic enhancements. The excellent SERS enhancement features of different nanostructures will be discussed in the review article.(iii) *Highly efficient adsorption mechanism for SERS:* For target analytes, CM enhancement mechanism is highly related with the increased Raman scattering cross-section of analytes adsorbed on the nanomaterials. Therefore, the adsorption mechanism between adsorbed analytes and nanomaterials is an important factor which affects enhancement of SERS detection sensitivity. High adsorption efficiency does not only increase CM enhancement gain, but also improves immobilization efficiency as well as capturing target analytes in the hotspots zone, resulting in a highly reproducible SERS signal. To date, several adsorption interaction mechanisms such as covalent bond adsorption, non-covalent adsorption, and immunoassays are reported and proposed. Analytes with active heteroatoms such as sulfur and nitrogen, can efficiently bind to the metal surface via covalent bonding [47]. Particularly, the non-covalent interaction mechanism is interesting because it can bind analytes onto the surface with minimal distortion of the analytes and metal substrate. Some widely reported non-covalent adsorption methods are charge-selective mechanism, hydrophobic interactions, and π-π stacking interactions, *etc.* In addition, owing to its strong and specific recognition reaction between antibody and antigen, immunoassays combined with SERS [48] are also be employed to improve SERS detection sensitivity, which will be reviewed in the corresponding section.(iv) *Multifunctional SERS sensing platform:* This platform allows one to incorporate SERS spectroscopy with some analytical platforms (*e.g.*, microfluidics, optofluidics, and capillary electrochromatography, *etc.*) to address SERS signals fluctuations or blinking in highly diluted solutions and is emerging as a powerful quantitative analysis tool for various biological applications. In addition, paper-based SERS sensing platform and dynamic SERS detection method from wet state to dry state of plasmonic nanoparticles are also introduced into the review article because of their ultrahigh detection sensitivity. In the following part, multifunctional SERS-based sensing platforms will be comprehensively reviewed and discussed.

3. Resonance enhancement techniques

3.1. SERRS spectroscopy

The SERRS phenomenon arises when the excitation laser is resonant with the electronic transition of analytes. Here, the Raman

cross-section of target analytes can be significantly enhanced by several orders of magnitude, due to molecular resonant excitation. In many papers, SERS and SERRS are not distinguished, but they do have different properties. Compared to SERS, there is a huge additional enhancement observed in SERRS mechanism. Moreover, the SERRS intensity is wavelength-dependent. To date, SERRS spectroscopy has advanced to the individual resonant molecule detection sensitivity, because both molecular resonant effect and SPR enhancement contribute to produce extremely strong Raman scattering signals. The luminescent dyes or fluorescent protein molecules (*e.g.*, Rhodamine 6G (R6G), crystal violet, and malachite green, proteins, and antibodies *etc.*) are good candidates for SERRS study, due to their sizable Raman scattering cross-sections and strong optical absorption in the visible window.

The early seminal observations in the visible window clearly showed chances for single molecule detection limit using SERRS spectroscopy is potentially viable. In early studies, aggregated silver colloid was the most common substrate as its broad SPR absorption range could efficiently match with resonance excitation of Raman scattering. Nie and Emory [49] demonstrated the intrinsic SERS enhancement factors on the order of 10^{14}–10^{15} because of excitation laser line (514.5 nm) and electronic absorption of R6G molecule Soon after, Xu et al. [50] successfully detected the molecule vibrations of single hemoglobin protein molecules using induced hot silver nanoparticles. Recently, Zhou et al. [51] demonstrated a novel double-stranded DNA detection approach through SERRS. In the study, there is no SERRS signal of fluorescent dye SYBR Green I in the absence of double-stranded DNA. However, when SYBR Green I is specifically bound to a double-stranded DNA, a DNA–dye complex can be formed with green light emission. Under the illumination of 532 nm laser, the SERRS phenomenon was achieved with a linear range of 0.13–13 ng μL^{-1} and a detection limit of 6.6×10^{-12} g μL^{-1}.

In the ultraviolet (UV) window, aluminum (Al) nanomaterials have more effective plasmonic response than gold and silver, because Al nanomaterials can produce strong plasmonic resonance in the UV light region.[52–54] Notably, some important target analytes such as DNA/RNA bases, biological coenzyme couple NAD^+/NADH, $NADP^+$/NADPH, and explosives TNT *etc.*, prefer to absorb light in the UV region. Thus, Al nanomaterials are ideal substrates for achieving ultrasensitive UV SERS detection. For example, Shankar et al. [55] reported a deep UV SERRS-based ultrasensitive detection method for adenine molecules using high ordered Al NP arrays. Under the excitation of laser (257 nm) that well matched with Al NP arrays, a zeptomole (10^{-21} M) detection sensitivity was achieved. Later, they also demonstrated an ultrasensitive detection approach for explosives TNT. The Al NP arrays can provide a real-time detection level of TNT down to 10^{-18} g in quantity [56].

It has been confirmed that the analytes with large Raman scattering cross-section can be detected by SERRS in extremely low concentration. However, achieving the sensitive detection of analytes with extremely small Raman scattering cross-sections is an issue that remains to be addressed. To date, a reasonable strategy used is by means of indirect measurement. For instance, Qu et al. [57] demonstrated a silver NP probe (SPRA band, 420 nm) for ultrasensitive and indirect detection of formaldehyde using 3,5-diacetyl-1,4-dihydrolutidine (DDL, absorption band, 415 nm) on Ag surface. The chosen 457 nm incident light satisfies the conditions of SERRS effects, affording a low detection sensitivity of 10^{-11} M.

Near infrared (NIR) light (~700–900 nm) can penetrate much more deeply through living cells or biological tissues, up to several centimeters in optimal cases [58]. Therefore, most biomedical applications are achieved in the NIR window, where the biological tissue absorption coefficients are over two orders of magnitude lower than in blue and ultra-violet light. In the NIR windows, gold nanomaterials are the most often employed plasmonic resonance materials for bioimaging and photo-thermal imaging *in vivo*. The commonly used Raman molecules for SERRS detection in NIR window are cyanine derivatives [59–61].

In recent years, noninvasive photo-thermal imaging has drawn a great deal of attention because of large absorption cross-section of nanomaterials within the NIR region. Despite of low penetration energy loss, NIR light is highly desirable for specific cell treating using heat generating nanomaterials since it possess no damage to adjacent normal tissue. For example, a novel SERS-encoded gold nanorods (SPR band, 790 nm) were designed, although not perfectly matched with NIR excitation source 785 nm, but provide strong optical absorption at 810 nm for photo-thermal heating [61]. Due to resonance excitation enhancement, SERS signal of IR-792 molecules is most intense in contrast with other SERS active molecules, *e.g.*, DTTC-765, DTDC-655, Nile Blue, malachite green, *etc.* Moreover, IR-792 molecules could be detected in attomolar concentrations *in vitro*. After injecting IR792-coded gold nanorods into mice right flank tumor, the Raman spectra of tumors showed IR-792 NRs signatures have little background signal from PEG-NRs alone or from saline. More importantly, under the irradiation based on 810 nm diode laser, saline injected mice did not reach temperatures above 40 °C, while IR792-coded NRs-injected tumors rapidly heated to ablative temperatures above 75 °C, highlighting a potential avenue for integrated bioimaging and photo-thermal therapy *in vivo*.

Later, novel thiophene-substituted chalcogenopyrylium (CP) dyes were designed as SERRS nanoprobes for biomedical imaging *in vivo* [62]. The novel nanoprobes are well matched with NIR laser resource 785 nm, and contain three important components: a gold core in the inner layer, the CP dye adsorbed on gold core, and an encapsulating silica outer layer. Interestingly, the Cp-dye 3-based nanoprobes have a detection limit of 100 aM compared to *IR792*-based SERRS nanoprobes with 1 fM. The ability of Cp-dye 3-based nanoprobes to characterize tumor tissue *in vivo* was performed by using an epidermal growth factor receptor (EGFR)-targeting antibody. The bioimaging results showed that the SERRS signal intensity enhanced by Cp-dye 3-based SERRS nanoprobes was approximately 3-fold stronger than IR792-based SERRS nanoprobes. In addition, Harmsen et al. [63] prepared SERRS gold nanostars (75 nm), which featured a star-shaped gold core with NIR absorption band, a Raman reporter (IR-780) resonant in the NIR window, and a silica-based encapsulation shell. Under 785 nm diode laser irradiation, the gold nanostars can perform precise, visual biomedical imaging *in vivo* for tumor premalignant lesions of pancreatic and prostatic neoplasias with a detection limit of 1.5 fM.

More recently, they also demonstrated high precision biomedical imaging *in vivo* based on real-life mouse brain tumors using integrin-targeted SERRS NPs with a detection sensitivity of femtomolar level [64]. In the study, the SERRS NPs were prepared as reported in [62,63]. Then, the integrin-targeted SERRS NPs were synthesized by a heterobifunctional linker, poly(ethylene glycol) (*N*-hydroxy-succinimide 5-pentanoate) ether *N′*-(3-maleimidopropionyl) aminoethane (NHSPEG4k-Mal), which can bridge cyclic RGDyK peptides and SERRS NPs. After the injection (26 fM/g) into a grade IV astrocytoma (GBM)-bearing mouse, the integrin-targeted SERRS NPs can monitor tumor cell migration through the brain, as shown in Fig. 3. Compared to normal brain tissue, strong SERRS signals with a good profile were observed in bulk tumor (Fig. 3a). Moreover, the RGD-SERRS signal can also be

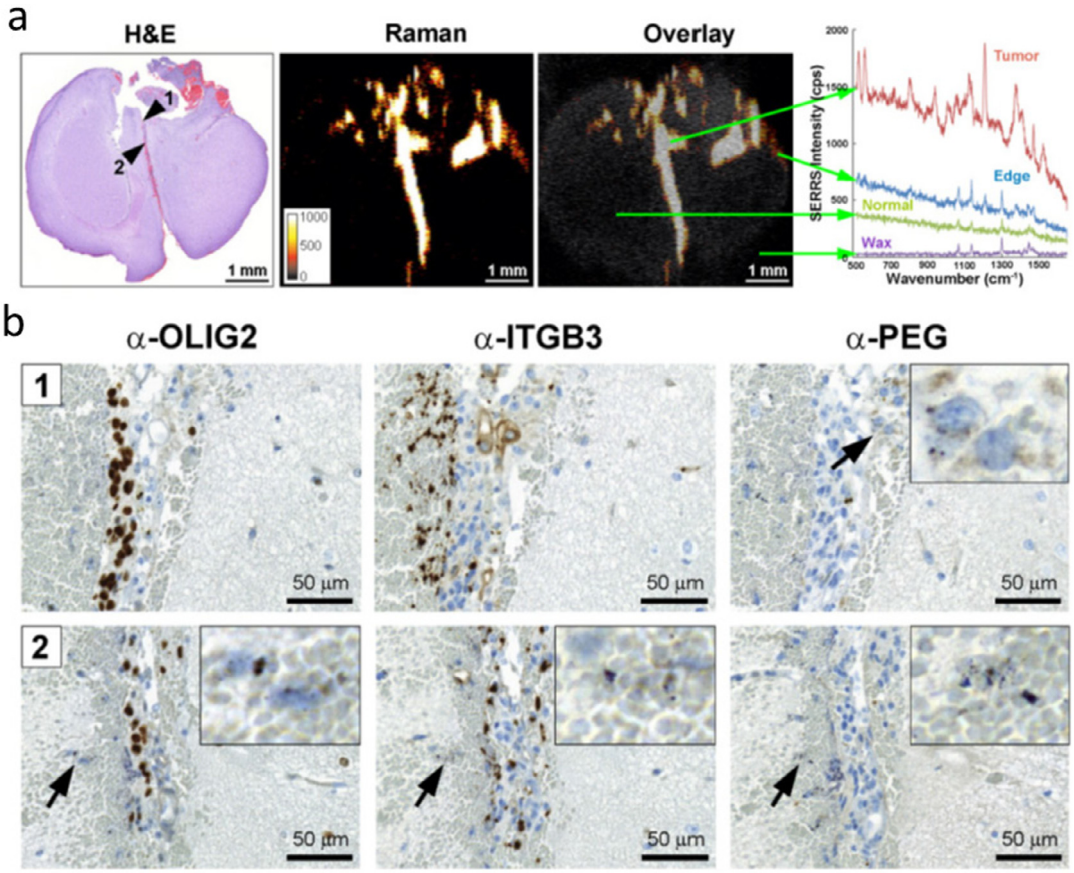

Fig. 3. The detection of microscopic tracts of tumor cell migration through the brain by integrin-targeted SERRS nanoparticles. (a) SERRS signal in a paraffin-embedded coronal brain section (1-mm thickness) after i.v. injection of RGD-SERRS nanoparticles in a GBM-bearing mouse. The pronounced 1200 cm^{-1} peak of the RGD-SERRS-NP is only present in the tumor bulk and tumor edge and not in the normal brain tissue. (b) Immunohistochemistry analysis of two regions along the midline. Upper panels (region indicated by arrowhead 1 in A): OLIG2 staining confirmed tumor cell invasion along the midline. Lower panels (region indicated by arrowhead 2 in a): The RGD-SERRS nanoparticles accurately outlined the linear microscopic (2–3 cells in diameter) tumor infiltration, extending from the superiorly located bulk tumor all the way into the inferior areas of the brain. Insets show magnified regions. (Reproduced from Ref. [64] with permission of ivyspring International Publisher.)

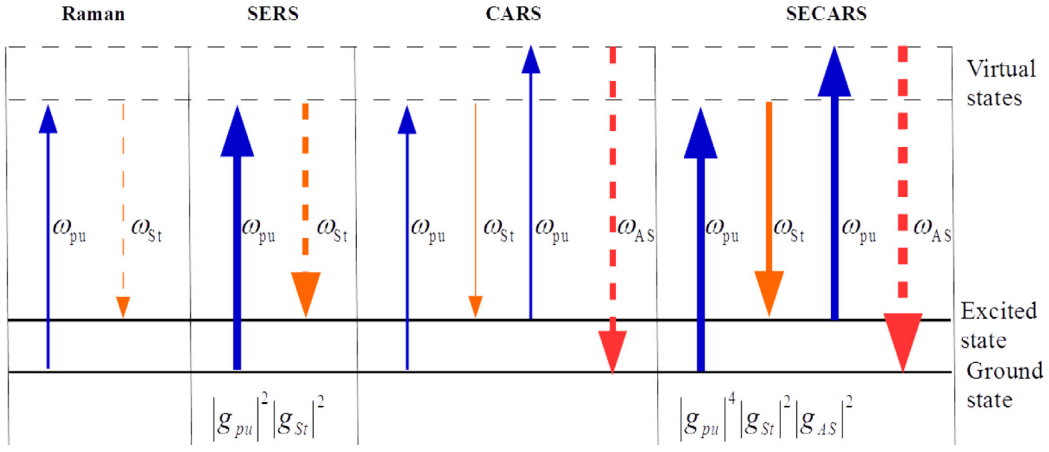

Fig. 4. Energy level diagram depicting the four types of Raman processes.

detected near the medial septum, which was penetrated by GBM cells. The proposal of cell migration was confirmed by immunohistochemistry analysis of two regions (arrowhead 1 and arrowhead 2 in Fig. 3a). Overall, the approach using integrin-targeted SERRS NPs shows a great potential in the biomedical field.

3.2. SECARS spectroscopy

Besides resonant absorption enhancement technique, nonlinear optical coherent technique, which has higher enhancement factors than linear spectroscopy, can also be employed for ultrasensitive

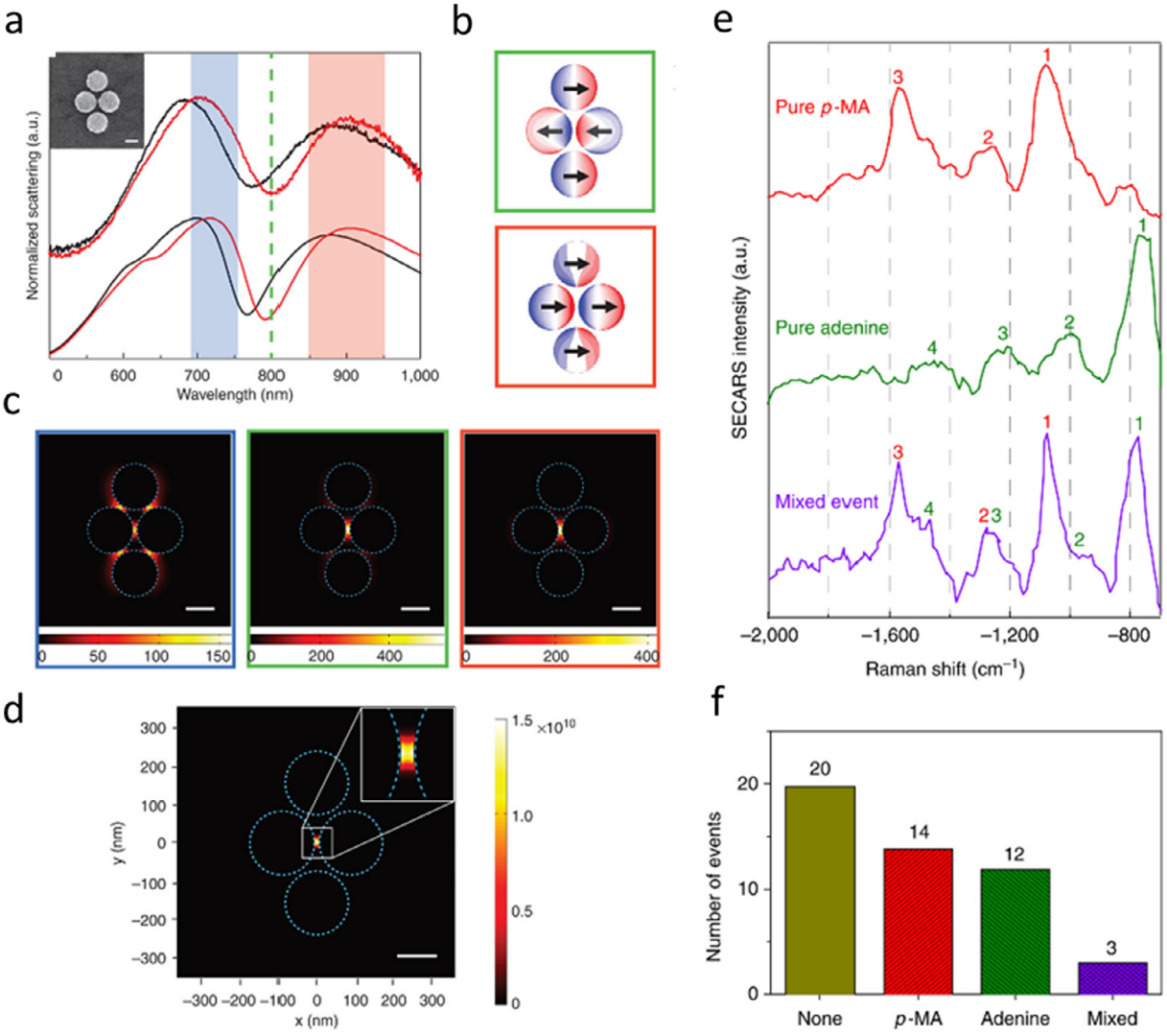

Fig. 5. Properties of the monolayer p-MA molecule coated quadrumer. (a) Experimental and simulated scattering spectra of a single quadrumer before (black) and after (red) the p-MA absorption. (b) Charge densities of the quadrumer pumped at 800 nm (green) and 900 nm Stokes (red), with respect to the subradiant and superradiant modes. (c) Field enhancement intensity (g^2) distribution at the anti-Stokes (left), pump (middle) and Stokes (right) frequencies for the p-MA 1070 cm^{-1} mode evaluated at mid-height of the quadrumer. (d) SECARS enhancement ($G_{SECARS} = G_{pg}^4 g_{St}^2 g_{AS}^2$) map for the mode in c. The maximum enhancement factor is $\sim 1.5 \times 10^{10}$ in the central gap, and significantly lower ($\sim 2.5 \times 10^6$) in the four peripheral gaps. Scale bar, 100 nm. (e) Single-molecule SECARS detection of bianalytes. (a) Three representative SECARS spectra showing a pure p-MA event (top), a pure adenine event (middle) and a mixed event (bottom). (f) Histogram of occurrences of none, pure p-MA, pure adenine and mixed molecules from one sampled array of 49 quadrumers. (Reproduced from Ref. [72]with permission of Nature Publishing Group.)

detection [65]. The best example for SECARS spectroscopy is coherent anti-Stokes Raman scattering (CARS), a nonlinear optical four-wave mixing process that employs molecular coherence [66,67].

In CARS, the pump (ω_{pu}) and Stokes (ω_{St}) fields interact coherently through the third-order susceptibility of the material, generating an anti-Stokes signal $\omega_{AS} = 2\omega_{pu}$-$\omega_{St}$. Albeit CARS has much higher sensitivity than spontaneous Raman scattering, it is not however high enough for monitoring or detecting analytes in extremely low concentrations. One strategy to achieve higher sensitivities is to employ SPR technique based on nanostructures to enhance the CARS signals. If the input (ω_{pu}, ω_{St}) or output (ω_{AS}) frequencies are in resonance with the collective excitation of SPR in the nanostructure, the surface enhanced CARS (SECARS) signal from molecules adsorbed onto the nanostructure is significantly enhanced. SECARS can attain greater signal enhancement than that of SERS or CARS alone, because electromagnetic enhancement factor (G) in SECARS is given by the equation $G \sim |g_{pu}|^2 |g_{St}|^2 |g_{AS}|^2$ (Fig. 4). However, the obtained enhancement (G) in SECARS is quite small and much smaller than that in SERS, because the SERS phenomenon is a two-photon process, while the SECARS is a third-order nonlinear process. In principle, the CARS signal is enhanced if any of the light pump, Stokes, or anti-Stokes light is in resonance with the SPR from metallic nanoparticles. The most ideal plasmonic SECARS configuration is when the frequency of pump photon, Stokes photon, and anti-Stokes photon are simultaneously resonant with the frequency of nanostructure in the same spatial sites.

The theoretical prediction of SECARS effects from target analytes on silver NP surface was proposed by Chew et al. [68]. In 1994, Liang et al. showed that not only the CARS signal is significantly enhanced, but also the signal-to-noise ratio is significantly increased because of the addition of silver nanoparticles [69]. Earlier reports discussed the feasibility of combining SPR and CARS for higher detection sensitivity. However, the SECARS background signal, originating from metal and water, limited the detection sensitivity of molecules. Koo et al. [70] demonstrated an ultrasensitive SECARS detection of deoxyguanosine monophosphate (dGMP) and angiotensin at single molecule level with the help of aggre-

gated silver nanoparticles, picosecond laser excitation in a collinear geometry, and polarization control for background suppression. It is important to note that, the pump, Stokes and anti-Stokes photons cannot be simultaneously enhanced by colloidal NPs because the narrow surface plasmon absorption (SPA) of their one and only band. Thus, it is necessary to design plasmonic SECARS substrates with more versatile features than the conventionally used SERS substrates.

Recently, novel plasmonic Fano resonance substrates, *i.e.*, four coupled nanodisks, were proposed and designed [71]. Typically, the Fano resonance substrates have one dip and two shoulders, arising from the interference between bright and dark plasmon modes, which can match the pump, Stokes and anti-Stokes photons in the SECARS process. Thus, the single molecule SECARS spectra of biological molecules p-MA and adenine are successfully achieved and verified through a statistically rigorous bi-analyte method (Fig. 5) [72].

In order to achieve the strongest enhancement effect by SECARS, novel plasmonic surface enhancement nanovoids were designed by Steuwe and coworkers [73]. In the study, there is a strong additional enhancement of $\sim 10^5$ over CARS, and SECARS is at least 10^3 times sensitive than SERS. The presence of nanovoid surfaces generates a broad plasmonic absorption region such that the pump, Stokes, and anti-Stokes light can simultaneously resonate with nanovoids. In addition, the high performance SECARS imaging of benzenethiol monolayer paves the way for ultrasensitive monitoring of adsorbed molecules on plasmonic nanostructure surface by using SECARS. Very recently, He et al. [46] have explored a strategy to regulate hotspots in the same spatial position in SECARS process by optimizing three asymmetric Fano resonance gold disks, producing an enhancement factor of $\sim 3.8 \times 10^{12}$, approaching single molecule detection sensitivity.

Unlike SERS employing continuous incident light, the main light source for SECARS are time-resolved lasers with high intensity and repetition frequency. Amazingly, a wave packet vibration of a single molecule can be captured and recorded in real time by time-resolved SECARS (tr-SECARS), equipped with individual dipolar nano-antenna (a gold dumbbell, *trans*-1,2-*bis*-(4-pyridyl) ethylene (BPE) molecule linked with two gold nanospheres), similar to a plasmonic dimer, which is a perfect hotspot for single molecule sensitivity [74]. The SECARS imaging of gold dumbbell distribution was performed by a femto-second laser scanning CARS microscope system, showing that the wave packet vibration of single BPE molecule based on gold dumbbell can be readily seen through the SECARS response. In addition, the idea in which the signal originating from single molecule level was confirmed by tracking the probability distribution function statistic of the noise, which can uniquely distinguish between one, two and many molecule responses. Therefore, with the assistance of SPR nanostructure, tr-SECARS has great potential for individual molecule or atom imaging.

3.3. Optical waveguide-based SERS spectroscopy

Optical waveguides, which integrate optics and devices on the microscale, are also explored for high electric field gains, due to their significant light harvesting effect. In an optical waveguide layer, a concentrated laser beam is reflected into a thin film with a certain angle using a semicylindrical prism. When the thickness of thin film is well matched with the high refractive index ($\boldsymbol{n}$), *i.e.*, $\boldsymbol{n}$ (prism) > $\boldsymbol{n}$ (film) > $\boldsymbol{n}$ (substrate), the incident light gets concentrated and thus the optical field is significantly enhanced. Moreover, it is very easy to obtain low cost waveguide materials, including semiconducting materials (*e.g.*, SiO_2, Ta_2O_5, ZnO, and MoO_3) [75–78] and polymeric materials (polyimide and poly (diallyldimethylammonium chloride (PDDA)) [79,80], which can strengthen the charge-transfer between target analytes and waveguide layer. Thus, the introduction of optical waveguide into SERS can further develop the SERS detection capability compared to isolated SERS detection. Interestingly, the optical waveguide plays multiple roles in improving incident light coupling, guiding and collection of the Raman scattered-light.

There are various types of waveguide structures used for SERS detection, *e.g.*, semicylindrical prism, planar, and tapered waveguides, *etc.* [76,79,81]. A SERS-active sensing layer comprising of metal NPs or film is fixed on the SERS substrate. Recently, optical waveguide-based SERS detection has demonstrated promising potential for various applications [82–84]. Gu et al. designed an ultrasensitive SERS substrate based on optical waveguide-enhanced SPR model. A Kretschmann-type prism coupled the incident light into the SiO_2 waveguide forming a concentrated EM field. Several resonance modes, such as TE0, TE1, and TE2 modes are formed in this waveguide. At the SPR resonance condition, the Ag nanoparticles (size ranging from 40 to 70 nm) assembled on the waveguide surface further enhance the EM field. The configuration can achieve stronger EM enhancement factor than single silver NP, yielding a 1000 times enhancement in the SERS signal for realizing ultrasensitive SERS detection of 4-MBA [80]. Fu et al. [82] demonstrated a novel immunoassay measurement of human IgG by using dielectric and porous anodic alumina (PAA) waveguide-based SERS spectroscopy. In the study, the SERS signals were amplified by the enhanced electric field SERS due to waveguide resonance. In addition, self-assembled silver NPs on the surface of PAA waveguide provide a more intensive electromagnetic field due to the plasmonic coupling between Ag NPs and waveguide modes. The detection limit of human IgG down to 0.1 ng mL^{-1} was obtained. Quite recently, a tapered waveguide composed of ultra-sharp ZnO nanocones@Ag film@Au NP has been demonstrated with single molecule SERS detection capabilities of benzenethiol (10^{-19} M), R6G (10^{-17} M), and adenine (10^{-17} M), due to its excellent light trapping and waveguide effects [81].

In addition to the plasmonic waveguide configuration decorated with metal NPs or films as above mentioned, microstructured optical fibers have been considered as a promising waveguide device for designing next generation multifunctional SERS sensing platform, which can efficiently incorporate SERS spectroscopy and plasmonic devices [85]. Wang et al. demonstrated a highly sensitive, porous SERS-active optrode, where Ag NPs were *in situ* deposited on an optical fiber end through laser-induced polymerization method [86]. The porous structure can load several Ag NPs, which provide strong electromagnetic enhancement for SERS. When the as-prepared optical fiber sensor is combined with a microfluidic chip, the SERS quantification of organic pollutants and pesticides can be achieved with a detection limit 1.0×10^{-8} M. More recently, our group developed a solid core-photonic crystal fiber (SC-PCF) SERS sensing platform, which is capable of quantifying the sialic acid level on a single cell with a 2 fM sensitivity [87]. The SC-PCF-based waveguide can be employed to acquire ultrasensitive SERS signals, due to its high detection volume, low signal loss, low external interference and long-distance monitoring. The Raman tag, 4-dihydroxyborophenyl acetylene (DBA) selectively binds with sialic acid on the cell membrane using phenyl-boronic moiety, as shown in Fig. 6a–c. Thus, the sialic acid SERS detection can be realized by exploiting the Raman peak located at 2000 cm^{-1}, which belongs to the alkyne functional group. Interestingly, our SC-PCF-based SERS platform (Fig. 6e) is designed to allow DBA-tagged HeLa cell mixed with Au NP solution to be pumped through a side channel. The propagated laser light in the central solid core can interact with DBA-tagged HeLa cell along the entire length of the fiber, and thus three dimensional SERS signals of

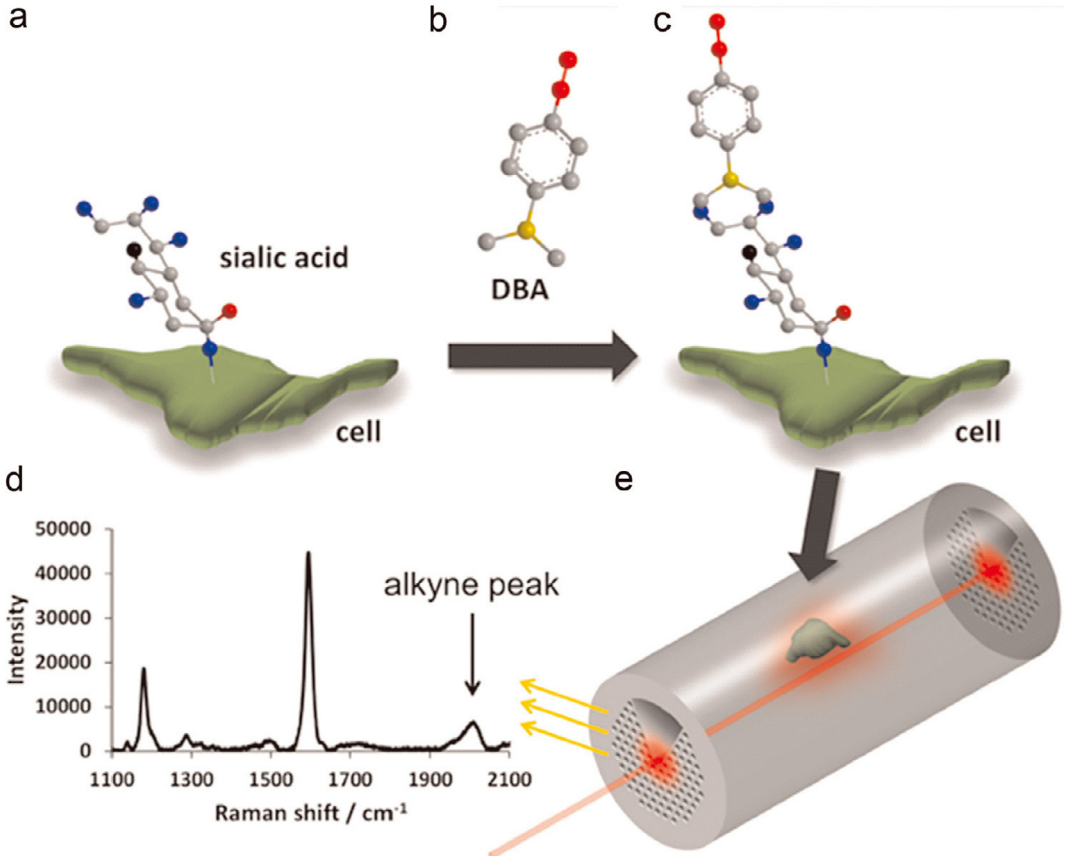

Fig. 6. Sialic acid SERS detection mechanism (a) Molecular structure of sialic acid. (b) Molecular structure of DBA. (c) DBA-bonded sialic acid on the membrane of a cell at the C-8,9 diol of sialic acid. (d) Output Raman spectrum with a peak at 2000 cm^{-1} showing the presence of alkyne group from DBA. (e) SC-PCF for detection of sialic acid on a single cell using SERS method. (Reproduced from Ref. [87] with permission of Elsevier B. V.)

samples with extremely low concentrations can be obtained, indicating that our designed SERS sensing platform is a potential diagnostic tool to evaluate sialic acid-related diseases in real-time.

4. High quality nanostructure for SERS-based detection

The enhancement feature of SPR is highly dependent on the types of nanomaterials used for testing, which is essential for achieving ultrasensitive detection. Variations of nanostructures properties such as morphology, size, composition, surface modification, dielectric parameter and stability, *etc.*, play an important role in producing SPR-driven EM enhancements. During the past decades, many types of excellent nanostructures, *e.g.,* aggregated nanostructure, self-assembled nanostructure, uniformed plasmonic nanostructure, alloyed nanostructure, carbon-based material, silicon-based nanomaterials, magnetic nanostructure, metal-organic frameworks, and three-dimensional nanostructure arrays, *etc.*, have been designed and developed for SERS-based ultrasensitive detection study. To clearly understand their enhancement features, the SERS enhancement features of these nanostructures are discussed in the following sections.

4.1. Aggregated nanostructure

Aggregated nanostructures are the earliest sensing platforms for SERS-based ultrasensitive detection. The most frequently used types of substrates are simple silver aggregates, which are commonly prepared by the reduction of silver nitrate with sodium citrate acid at the boiling condition (Lee–Meisel method) [88]. Under laser irradiation, the broad absorption ranges of nano-aggregates in the size range of 10–150 nm are well suited to support and generate metallic SPR enhancement, which is sufficient for single molecule detection. To efficiently excite metallic SPR, the SPR absorption band of Ag NPs make a significant impact in producing SERS effects. When the target analytes contain active atoms, such as sulfur or nitrogen, the activation of silver colloids is usually done via the analytes themselves, by controlling various colloidal aggregation states. However, when the target molecules cannot induce colloidal aggregation, salt-induced (potassium chloride or sodium chloride) aggregation can solve the problem, due to the variation of surface charge. Early studies [26,49,50,89,90] in SERS-based single molecule detection showed that the detection sensitivity largely depended on the random absorption sites (hotspots) of nano-aggregates by addition of activator solutions. Recently, an ultrasensitive detection approach for ozone has been reported by using aggregated Au NPs as SERS substrate. Based on ozone oxidization and RhS–I_3 particle formations, the Rhodamine S (RhS) acts as the Raman reporter to monitor ozone level, achieving a detection limit of 9.0×10^{-10} M [91]. One main advantage of aggregates is that the randomly encountered hotspots have unusually high enhancement efficiencies. However, the so-called hotspots hold a meagre proportion (<1%) of the total surface area for adsorption [92,93], which results in an extremely poor statistics of ultrasensitive detection events. In addition, another significant drawback of aggregated substrates is that the hotspots of aggregates are extremely difficult to repeat or predict. Thus, the morphology and size of the aggregated NPs need to be precisely controlled for producing reproducible SERS signals.

In order to overcome these limitations, electron beam lithography (EBL) techniques are widely employed to design and fabricate high quality nanostructures [94]. Unlike the nano-aggregates induced by target analytes and activator agents, the morphology of nanoparticles in EBL can be uniquely constructed, controlled and tuned using computer-aided design software. With the help of EBL, it is feasible to create random, reproducible nano-aggregates for SERS detection. Many random aggregated cells with different morphologies are prepared by EBL. By spectral mapping, the SERS activity of the combinatorial cell arrays create uniform 5×10^8 enhancement factors, which are well suited to SERS-based sensitive detection [95]. More recently, aggregated Ag NPs-based SERS were introduced into an ELISA signal generation system for ultrasensitive detection of prostate specific antigen (PSA) [96]. The sensing platform employed multiple signal amplification to obtain higher Raman signal, including the additional SERS enhancement of aggregated Ag NPs and the high enzymatic activity of catalase. Using this technique, PSA can be detected at ultralow concentration, in the order of 10^{-9} ng mL^{-1}, which is very useful for cancer recurrence prognosis for patients. Yang et al. [97] reported a highly sensitive SERS approach for selective detection of arsenic ions by using cationic polymer (PDDA) and 4-mercaptopyridine (4-MPY)-modified Au@Ag nanoparticles (Au@AgNPs). In the study, arsenic ions can specifically interact with the Ars-3 aptamer, and form an As(III)–aptamer complex, resulting in aggregated 4-MPY-modified Au@AgNPs complexes. Using 4-MPY molecule as Raman reporter, the arsenic ions levels can be determined with an extremely low detection limit of 0.059 ppb.

4.2. Self-assembled nanostructure

Owing to their uniform size, shape, strong inter-particle plasmonic coupling, and reproducible enhancement hotspots, self-assembled plasmonic nanostructures with well-ordered assemblies for SERS sensing, have received wide attention compared with irregular nanoaggregates discussed in the previous section. The lack of sufficient hotspots limits the SERS enhancement capability of individual nanoparticle, therefore, precisely controlling them into larger size assemblies is an attractive approach to create huge plasmonic enhancement effects. To date, several strategies have been devised to achieve nanostructured assemblies by electrostatic interactions [98,99], hydrophobic interactions [100,101], covalent bonding [102,103], and specific bio-recognition interactions [104,105], *etc.*

The charged nanostructures can bind oppositely charged polymeric films to form self-assembled monolayers via electrostatic interactions. For example, an assembly of gold nanorods-embedded Raman reporter (4-ATP) on silica particles was shown as excellent SERS substrates, affording a detection limit of 0.01 ng mL^{-1} for human immunoglobulin G (h-IgG) in immunoassays [106]. In addition, Li et al. [107] synthesized plasmonic assemblies of truncated octahedral (TOH) Au NPs by using poly (diallyldimethylammonium chloride) via electrostatic interactions. Interestingly, using human immunoglobulin (h-IgG) as targeted analytes, a detection limit of 36.56 fg mL^{-1} can be obtained.

Hydrophobic interactions are based on the aggregated tendency of nonpolar molecules in water solution. To date, numerous practical applications have shown that hydrophobic interaction mechanism is an efficient approach to prepare self-assembly of plasmonic nanoparticles with various morphologies and sizes. Zhong et al. [108] reported a simple approach for preparing a self-assembly of gold nanoparticles onto a poly (methyl methacrylate) (PMMA) template by using hydrophobic interactions. The as-prepared SERS substrates can reproducibly detect malachite green (MG) isothiocyanate with a concentration as low as 0.1 nM. More importantly, the SERS-active sensor can perform *in situ* detection of MG residual on real-life fish, with a lowest *in situ* detection limit of down to 0.1 μM.

Thiols-type molecules are widely used as linkers for creating hotspots, because they can strongly bind to the metal surface and form self-assembled monolayers via covalent bonding. Generally, the asymmetric thiol linker sometimes spontaneously produces non-uniform coalescences with poor enhancement capability [109], while the symmetric linker molecules usually generates ordered dimeric assemblies containing a number of hotspots [110]. This happens due to strong plasmonic coupling as result of the linker-enhanced local electromagnetic field in the junctions between two NPs. Recently, Fabris et al. [111] presented a novel Raman tags for cancer cell imaging based on dimeric assemblies of spherical Au NPs. Several hot spots were obtained by plasmonic coupling of inter-nanoparticles, which were linked by a small and rigid dithiolated molecule. After incubation with human glioblastoma cells for a short time, the Raman tags can provide faster, highly sensitive SERS mapping for cancer detection.

In terms of specific bio-recognition interactions, the most commonly used plasmonic sensor is the DNA-based nanostructure assembly. DNA is an ideal candidate for assembly due to its good availability and excellent bio-compatibility. Nowadays, DNA-based nanostructure assemblies are a class of perfect plasmonic SERS substrates for ultrasensitive detection, due to their high sensitivity and specificity. Wu et al. [112] demonstrated a SERS biosensor called the assembly of Ag-trimers, for ultrasensitive detection of cancer biomarker, alpha fetoprotein (AFP). The assembly of Ag-trimers sensor was prepared via the AFP aptamer. The detection limit of AFP in human serum can approach to sub-attomolar level, about 0.097 aM. Heavy metal ions – Hg^{2+} and Ag^{+} can specifically interact with DNA bases thymine (T) and cytosine (C), respectively, forming strong and stable T–Hg^{2+}-T and C–Ag^{+}-C complexes. Thus, DNA-based plasmonic sensors are perfect probes for monitoring Hg^{2+} and Ag^{+} in real time. Xu et al. [113] developed an assembled Au NP chain sensor for ultrasensitive assay of mercuric ions (Hg^{2+}). The mercuric ions can regulate the transformation of single-stranded DNA to form double helical DNA using thymine–Hg^{2+}–thymine (T–Hg^{2+}–T) interaction. With the aid of DNA modified-Au NP chain, a detection limit of mercuric ions in drinking water as low as 0.45 pg mL^{-1} is possible. Moreover, Li et al. [114] developed an approach for simultaneous detection of Hg^{2+} and Ag^{+} by using the assembly of triple Raman reporter-encoded gold nanoparticle trimers. In the study, three identical Au NPs were modified by three different DNA molecules (DNA1, DNA2, and DNA3), respectively. A Y-shaped DNA framework was constructed by introduction of DNA4 and DNA5 molecules, which were partially complementary with DNA3. Next, three different Raman reporters, aminothiophenol (ATP), nitrothiophenol (NTP), and 4-methoxy-α-toluenethiol (MATT), were employed to further modify the entire surface of Au NP-DNA1, Au NP-DNA2, and Au NP-DNA3, respectively (Fig. 7). When Hg^{2+} or Ag^{+} appeared individually, the Au NP dimers were assembled by forming T-Hg^{2+}-T or C-Ag^{+}-C complexes, producing enhanced Raman signals of MATT or ATP. However, when Hg^{2+} and Ag^{+} coexisted, Au NP trimers were obtained, and the SERS signals of all the three Raman reporters were considerably enhanced than that of dimmers. With the help of Au NP trimers, the simultaneous detection limit of Hg^{2+} and Ag^{+} was 1.69 pg mL^{-1} and 1.71 pg mL^{-1}, respectively.

More recently, Xu et al. [115] designed a DNA-driven plasmonic assembly named self-assembling nanopyramid, labeled with a Raman reporter (Cyanine 5), for monitoring telomerase in living K562 cells. In the study, the as-prepared plasmonic probes were Au nanopyramids composed of four gold nanoparticles embedded with single-stranded DNA sequences, which could be comple-

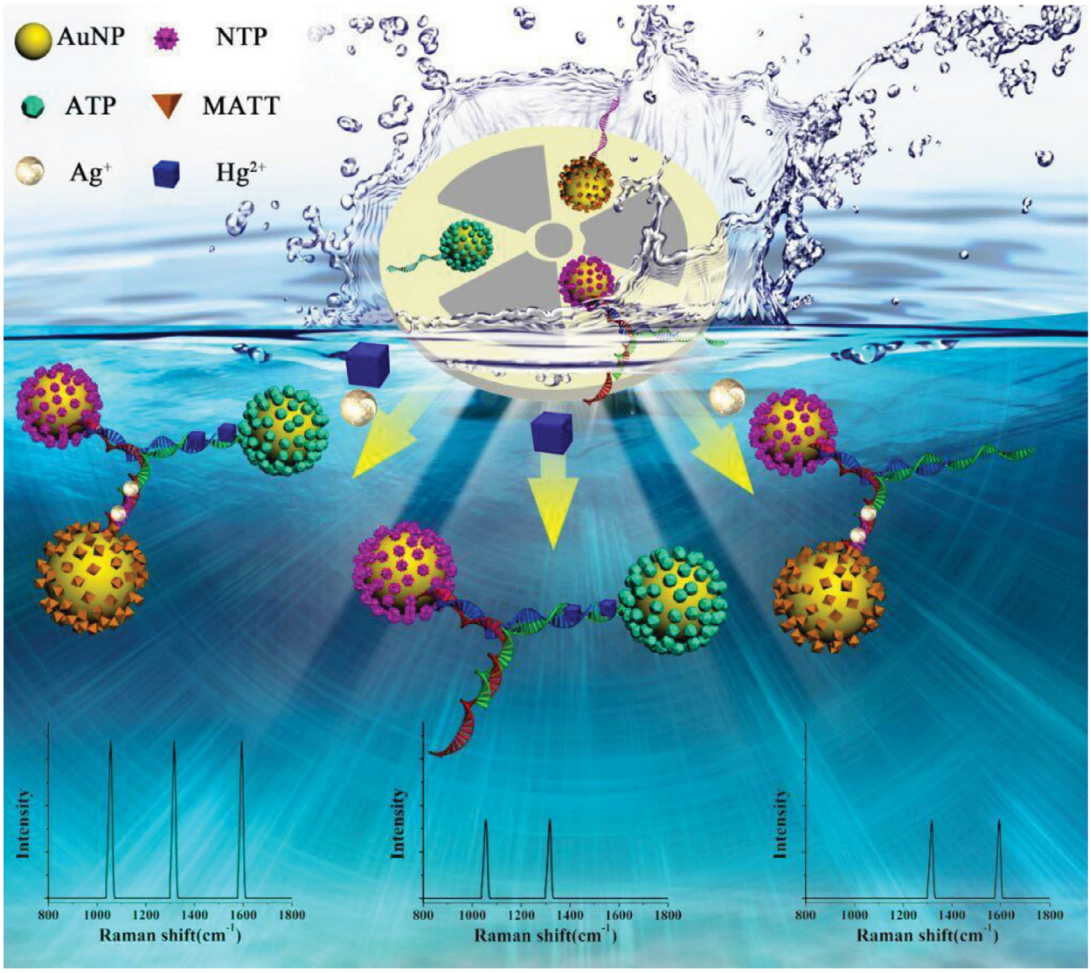

Fig. 7. Detection of mercury and silver ions based on the Au NP assemblies. (Reproduced from Ref. [114] with permission of Wiley-VCH Verlag GmbH & Co. KGaA, Weinheim.)

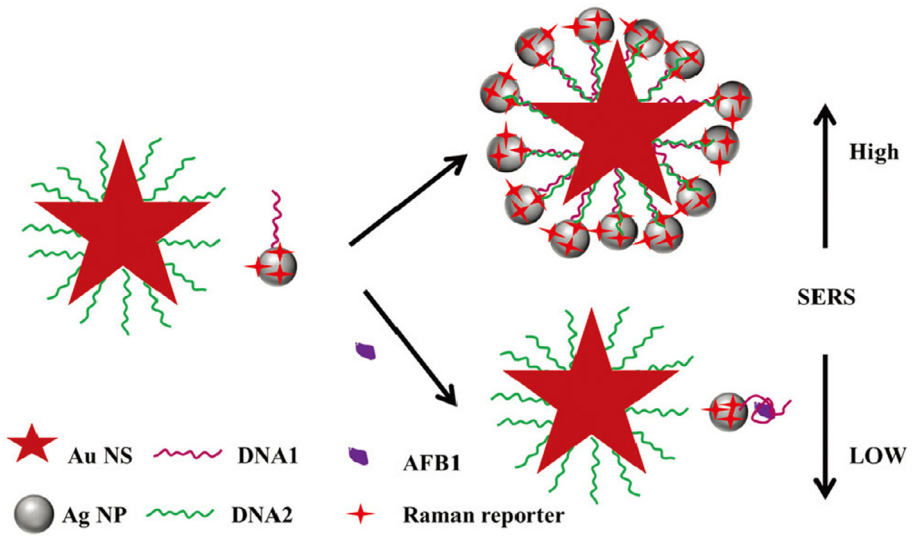

Fig. 8. Scheme of AFB1 detection based on the SERS method using Au NS core–Ag NP satellite assemblies. (Reproduced from Ref. [119] with permission of The Royal Society of Chemistry.)

mented by the Raman reporter sequence (RS) and telomerase primer (TP). In the presence of the telomerase and deoxynucleotides, the TP was extended, and meanwhile the inner DNA chain was immediately replaced, resulting in a reduced trend for SERS signal intensity. The SERS signals exhibited a linear range from 1×10^{-14} to 5×10^{-11} IU, with a detection limit of 6.2×10^{-15} IU. Similarly, Shi et al. [116] also developed a strategy for ultrasensitive SERS detection of telomerase activity. The quadratic SERS signal ampli-

fication was achieved by telomerase-triggered Ag NPs assembly incorporating with silver ions-mediated cascade amplification. With the help of the interesting quadratic amplification, the detection limit was down to a single HeLa cell.

4.3. Uniformed plasmonic nanostructure

Unlike nanoscaled aggregates, uniformed plasmonic nanostructures have almost uniform shape, regular size, and dielectric constant, indicating their reproducible plasmonic enhancement capability. One of the most important properties is that, the morphology of nanostructure can define and manipulate its SPR features. The ability to control nanostructures with uniform morphologies makes it possible to acquire SPR enhancement. Particularly, single gold or silver nanosphere cannot meet the demand of ultrasensitive detection, due to lack of efficient enhancement hotspots. Thanks to the development of nanofabrication technology, plasmonic nanostructures can be tailored with desired shapes. Various alternative uniform plasmonic nanostructures (*e.g.,* nanostars, nanoflowers, nanopyramids, and nanosatellites, *etc.*) with perfect and reproducible SERS hotspots have been successfully synthesized, and their ultrasensitive SERS detection capabilities have been tested.

4.3.1. Plasmonic nanostars

Compared to spherical or smoother plasmonic NPs, the NPs with sharp tips demonstrate much higher sensitivity for external environment changes and larger local field enhancement gain because of their lightning rod effects. Increasing spiked or sharp features on plasmonic nanostructure is a useful strategy to generate higher EM effects [117]. Thus, spiky-type plasmonic NPs are ideal SERS substrates for sensing. Herein, gold nanostars are a class of novel spiky plasmonic NPs with a spherical core and many outward branching sharp tips. Both the branch angle and the radius of the sharp tips are the two important factors in influencing the SERS enhancement efficiency. In addition, the anisotropic shape of gold nanostars can generate huge plasmonic coupling between the core and the tips, thereby enhancing the EM field close to the particle. Moreover, the gold nanostars also show a tunable optical property from the visible to NIR window, offering the option to yield ultrahigh enhancement factors. Lee et al. [118] fabricated an ultrasensitive SERS substrate composed of high density gold nanostars assembled on silver films. Using gold nanoparticles as seeds, gold nanostars were synthesized using a seed-mediated method. Then the gold nanostars were assembled on silver films. In the plasmonic platform, multiple plasmonic couplings such as nanostar–silver film, nanostar-nanostar, and core-sharp tips, can contribute to huge EM field gains, resulting in an aM (10^{-18}) level of detection capability for explosive 2,4-dinitrotoluene.

In addition, the gold nanostars can also be employed in food safety. For instance, a SERS-active sensing platform composed of aflatoxinB1 aptamer (DNA1) modified silver nanoparticles and complementary sequence (DNA2) modified gold nanostars were constructed for tracing AFB1 [119]. First, both DNA1-modified Ag NPs and DNA2-modified Au nanostars formed a super architecture named gold nanostar core-silver NP satellites, as shown in Fig. 8. In the absence of AFB1, the Raman reporter ATP on Ag satellites showed quite intense SERS signals, due to the huge plasmonic coupling in the sensing platform. However, in the presence of targeted molecules AFB1, the AFB1 aptamer (DNA1) preferred to bind with the AFB1 molecules so that the gold nanostar core-silver NP satellites architecture decomposed into dispersed nanoparticles with decreased SERS signals. For AFB1, the SERS sensing platform has yielded a linear detection range from 1 to 1000 pg mL^{-1} and a detection limit of 0.48 pg mL^{-1}.

4.3.2. Plasmonic nanoflowers

The large surface area and abundant hotspots for SERS in the Ag or Au-based flowerlike nanostructures render them useful for practical applications such as biosensing [120,121] and bio-imaging [122–124]. Dandapat et al. [125] developed a strategy to engineer novel Ag hierarchical building blocks for monitoring methylene blue. In the study, the plasmonic Ag nanostructures were fabricated by consecutively injecting 4-mercaptobenzoic acid, trisodium citrate, and ascorbic acid into silver nitrate solutions as reducing agents. Interestingly, the Ag nanostructures possess numerous Ag petals, and nanosized gaps of Ag petals are filled with small Ag NPs, indicating that there are lots of hotspots in the novel Ag hierarchical building blocks. Owing to the highly enhanced electric field gain, the SERS signals of methylene blue can be obtained when the detection concentration is as low as 100 aM.

Similarly, an approach to synthesize green, eco-friendly, and ultrasensitive SERS sensor based on rose petals was reported by Chou et al. [126]. In the study, a high density Ag NP array on rose petals can be fabricated by the addition of Ag NPs suspension because of hydrophobic interaction. The nanosized gaps of Ag NP arrays can significantly amplify the electric field intensity. Once consecutive target analytes (R6G) solution was placed onto the Ag NP arrays, the R6G molecules get concentrated and are captured by the high-density NP arrays during the evaporation process. Thus, the SERS signals of R6G molecules increase dramatically. With the help of novel petal-based substrate, a measurable and reproducible SERS detection limit for R6G is as low as femtomolar level (10^{-15} M).

4.3.3. Plasmonic nanopyramids

Plasmonic nanopyramids support both localized and propagating SPR, and have demonstrated excellent SERS detection capability. For example, ordered, inverted Au nanopyramids were employed to detect nitro-based explosives, providing reproducible detection limits of tens of pg (10^{-12} g) [127]. In addition, Wang et al. [128] demonstrated the single molecule detection strategy for dopamine and serotonin using a graphene deposited Au nanopyramid platform. The Au nanopyramids decorated with single graphene layer possess high density hotspots, resulting in ultrahigh SERS enhancement factors. In a short time of 1 s, dopamine and serotonin is detected and distinguished at the single molecule level.

Notably, pyramid-type nanocomposites can also be employed for SERS detection in practical applications. For instance, Zhao et al. [129] designed an ultrasensitive SERS sensor named silver decorated-gold pyramids, to monitor vascular endothelial growth factor (VEGF). The sensing platform composed of gold nanopyramids and a specific Raman reporter 4-NTP modified-Ag NPs. In the absence of VEGF, the 4-NTP modified-Ag NPs are well integrated with gold nanopyramids, resulting in quite intense SERS signals of 4-NTP. However, in the presence of VEGF, the 4-NTP prefer to bind VEGF so that Ag NPs get released from the adsorption sites of Au nanopyramids, leading to reduced SERS signals of 4-NTP. Thus, the detection concentration of VEGF can be quantified by measuring the SERS intensity of 4-NTP, achieving a detection limit as low as 22.6 aM.

In addition, a novel SERS sensor encoding silver pyramids for ultrasensitive, simultaneous, and multiplexed detection for disease biomarkers such as PSA thrombin, and mucin-1 was designed by Xu et al. [130]. In the study, the SERS sensor was a silver pyramid composed of four Ag NPs, which was modified by identical Raman reporter 4-ATP. Owing to strong plasmonic coupling between four Ag NPs, the silver pyramid can be used to monitor single biomarker PSA (Fig. 9a). However, when the other three Ag NPs were modified by Raman reporter molecules 4-ATP, NTP, and MATT, respectively, the DNA frame encoded specific disease biomarker aptamers was

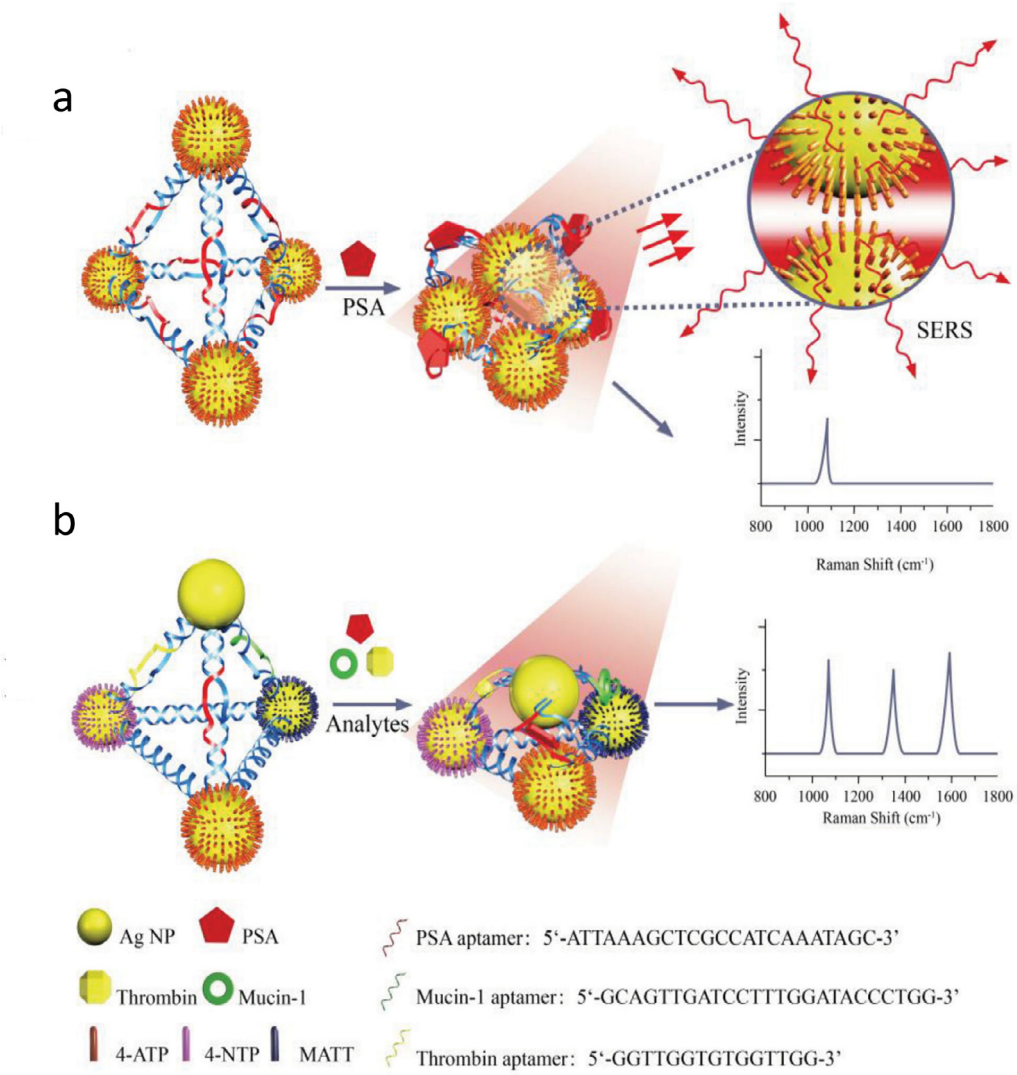

Fig. 9. Scheme of Ag pyramids self-assembled by DNA frame for SERS analysis of biomarkers. (a) Ag-pyramid-mediated singlet SERS assay for PSA, Ag NPs were modified with 4-ATP, PSA aptamers were inserted in each side of DNA frame. (b) SERS encoded multiple Ag-pyramidal detection of biomarkers (PSA, thrombin, and mucin-1), three Ag NPs in each pyramid were modified with 4-ATP, NTP, and MATT, respectively, and three aptamers were inserted in three sides of the DNA frame, respectively. (Reproduced from Ref. [130] with permission of WILEY-VCH Verlag GmbH & Co. KGaA, Weinheim.)

employed to form Ag pyramids. Due to the specific bio-recognition interaction, the presence of designated disease biomarkers could alter the geometries of Ag pyramids by shortening the gap length, resulting in large SERS enhancement (Fig. 9b). More importantly, the Ag pyramids sensing platform can reach a detection limit of at least aM level, paving a way for performing early disease diagnosis and biomarker screening assays in clinical science.

4.3.4. Plasmonic nanosatellites

Plasmonic nanosatellites-type structures composed of a metallic core and multiple satellite NPs around the core, demonstrate intense plasmonic coupling between high density satellite NPs. The strong plasmonic coupling remarkably increases the EM field intensity between the core and satellite NPs, resulting in enormous enhancement in hotspots. Consequently, the design of nanosatellites-type structures offers a new path to construct high quality SERS sensing platform.

Recently, Feng et al. [131] demonstrated a novel plasmonic nanostructure platform including gold nanorods (Au NRs) as core and multiple Ag NPs as satellites for biomarker Mucin-1 sensing. In the study, the Raman reporter 4-ATP modified-Ag NPs and Au NRs were functionalized by the aptamer for Mucin-1 and its partial complementary sequences, respectively. In the absence of Mucin-1, the Au NRs core-Ag NPs satellite nanostructures were well constructed through DNA hybridization. Many SERS hotspots were produced by plasmonic coupling between Au NRs and Ag NPs, generating intensive SERS signals of 4-ATP in the absence of Mucin-1. However, in the presence of Mucin-1, the specific bio-recognition interaction between aptamer and Mucin-1 allowed satellite-Ag NPs release from gold nanorods. Thus, the SERS intensity of 4-ATP notably decreases with increased detection concentration of Mucin-1, providing a detectable limit of 4.3 aM. Similarly, Ma et al. [132] developed an ultrasensitive SERS sensor for PSAs by using aptamer directed core-satellite nanostructures, affording for a detectable limit for PSAs down to 4.8 aM.

4.4. Carbon-based materials

It is undoubtedly that carbon-based materials which possesses large surface area with high capacity of adsorption sites such as graphene, graphene oxide, carbon nanotubes, are a class of emerging platforms for gathering target molecules. Graphene is an excel-

lent, uniform, two-dimensional material with single carbon atom layer packed into a honey-comb plane structure. Graphene oxide (GO), a good alternative for graphene, can be treated and functionalized by various chemical approaches. Graphene and GO nanomaterials attract considerable attention in SERS-based sensing applications due to their excellent CE effects arising from charge-transfer between graphene/GO and target analytes. The rich aromatic rings (π electron systems) in graphene/GO structure are good adsorption sites, which can efficiently capture aromatic target analytes through interesting π–π stacking interaction mechanism, showing that GO is a preferred option for aromatic molecule detection. Also, the negatively charged oxygen-based functional groups in GO structure can capture positively charged target analytes via electrostatic interaction mechanism. Moreover, since the surface plasmon frequency of graphene/GO lies in the mid-infrared or terahertz region, isolated graphene and GO are not believed to produce EM enhancement effects in visible and NIR window. It is impossible for single graphene or GO nanomaterials to achieve high SERS detection sensitivity using only CE effects. Fortunately, the drawback can be addressed by attaching noble metal NPs (*e.g.*, Ag and Au).

4.4.1. Graphene/GO-based hybrid nanostructure

Various graphene/GO-based hybrid nanostructures such as Ag NPs@GO, Au NPs@GO, Ag NPs@graphene nanosheets, Ag nanoshells@GO, Au/Ag NPs@GO@Au/Ag NPs sandwich, and Au NPs@GO@Ag NPs sandwich, *etc.*,[133–137] are reported for ultrasensitive SERS detection. Fan et al. [138] reported an ultrasensitive SERS substrate for HIV DNA detection. The SERS platform was synthesized with GO attached onto popcorn-shaped gold nanoparticles, which yielded high CE gain as well as supported huge EM gain due to the gold nanopopcorn tip with concentrated EM field. With the assistance of the GO-based hybrid nanomaterials, a detectable limit of fM (10^{-15} M) is achieved, opening a new avenue for sensitive HIV DNA detection in the biomedical field. In addition, Liu et al. [137] designed a novel hybrid material sensor for ultrasensitive detection of TNT using SERS. The SERS substrates were constructed by p-aminothiophenol (PATP) functionalized Ag NPs attached to graphene nanosheets. Interestingly, the Raman reporter PATP can be paired together to form azo compounds model. The target molecule TNT and hybrid sensor can serve as π-acceptor and π-donor, respectively. The π–π stacking interaction between them can effectively induce many hotspots, which can guarantee a detectable SERS signal of TNT as low as 10^{-11} M.

Under NIR light irradiation, GO incorporated with Au nanostructures are also ideal candidates for drug delivery and photothermal therapy (PTT) due to their high drug-loading capacity, excellent therapeutic effect and high photothermal conversion efficiency. Recently, a novel multifunctional sensing platform based on GO and Au NP core polyaniline shell (GO-Au@PANI) nanocomposites was designed for SERS imaging and PTT cancer ablation *in vivo* [139]. In the study, PANI showed good NIR absorption with excellent stability and low cytotoxicity, which highlighted its potential to be used as a photothermal absorber decorated Au NPs surface. With the help of π-π stacking and electrostatic interaction mechanism, the as-prepared GO-Au@PANI nanohybirds was prepared by Au@PANI core-shell composites attached to GO nanosheets. When a small amount of GO-Au@PANI entered the cancer cells, intensive SERS signal from PANI was generated. Through measuring the signal intensity of PANI, the GO-Au@PANI nanocomposites can work as a NIR SERS probes to perform *in vivo* bio-imaging in 4T1 cancer cells. Moreover, high performance photothermal ablation for cancer cells was also demonstrated *in vitro* and *in vivo*. Thus, the multifunctional theranostic and sensing platforms for integrated real-time SERS imaging and photothermal therapy can be an excellent option for cancer therapy.

4.4.2. Graphene quantum dots-based hybrid nanostructure

Graphene quantum dots (GQDs) are a new type of zero-dimensional graphene nanosheet, which are derived from 2-dimensional graphene sheets. GQDs have attracted extensive attention in optoelectronic devices, bio-imaging, and photochemical catalysis because of its excellent photoluminescence and electronic properties. Besides their potential applications, GQDs-based hybrid materials can also be employed to perform SERS sensing study, which has been paid little attention by scientists. For example, sensitive detection of hydrogen peroxide (H_2O_2) and glucose was realized by using DNA-mediated silver NP and GQDs hybrid compound (DNA-mediated Ag NP@GQDs) as a sensing platform [140]. More recently, Ge et al. [141] designed and synthesized a highly sensitive SERS substrate named silica (SiO_2) supported Ag NPs and GQDs compounds for R6G detection. Under UV light irradiation, the GQDs solutions were used to reduce Ag^+ and synthesize Ag-GQDs nanocompounds. With the help of electrophoresis deposition technique, the nanocompounds were captured by a SiO_2 supported Si substrate. Due to π–π stacking interaction, the SERS signals of Rhodamine 6G (R6G) molecules on Ag-GQDs compounds were considerably enhanced. More importantly, the spatial gaps between Ag NPs and GQDs are the hotspots sites for enhancing the Raman scattering signals of R6G, providing a detection limit of 8×10^{-14} M.

Besides its excellent photoluminescence feature, GQDs also possess strong simultaneous Raman scattering background, making it possible to perform dual-mode detection based on its fluorescence and Raman scattering. Recently, a novel dual-mode sandwich-typed immunoassay platform was designed to monitor tuberculosis CFP-10 antigen [142]. In the study, the newly designed magnetic Fe_3O_4–Au–GQDs nanocomplex can simultaneously work as a SERS sensor and fluorescence imaging platform. The magnetic plasmonic nanomaterials (Fe_3O_4-Au NPs) act as SERS substrate, while GQDs are the reporter of fluorescence and Raman signals. Both high quality SERS mapping and fluorescence imaging were successfully obtained with a highly sensitive detection limit of 0.0511 pg mL^{-1}.

4.4.3. Carbon nanotubes-based nanostructure

In carbon-based material family, carbon nanotubes (CNTs) are one typical member with cylindrical nanostructure containing highly ordered carbon atoms covalently linked in a hexagonal geometry. To date, the single-walled nanotubes (SWNTs) and multi-walled nanotubes (MWNTs) are the main substrates for science research. SWNTs are a single layer of graphene cylinders, while MWNTs have multiple layers. The tube diameters of CNTs can be tailored to as small as 1 nm while the lengths can reach up to several centimeters. Owing to its extraordinary optical and electronic properties such as large surface area, highly hollow, light mass density, and unique charge-transfer capacity, *etc.*, CNTs have been exploited in designing desirable optical platforms for chemicals and biological molecules sensing and imaging *in vitro* and *in vivo* [143,144].

SWNTs possess huge Raman scattering cross-section and well-known, intensive, sensitive and tunable Raman bands (G^+, G^-), making them ideal Raman labels for biosensing. SWNTs-based Raman label for protein detection in ultralow concentrations was introduced in [145]. In the study, protein human serum albumin (HSA) was immobilized on gold-coated glass slides by self-assembled cysteamine monolayer covalently linked with a six arms, branched poly(ethylene glycol)-carboxylated terminated PEG. Then, PEGylated phospholipids functionalized SWNTs were performed to incubate with antibody named goat anti-mouse

immunoglobulin G (GaM-IgG), which are employed to capture analyte (antibody HSA). As a result of strong plasmonic coupling in sandwich model, the Raman bands of SWNTs attributed to breathing vibration mode (below 500 cm^{-1}), longitudinal G^+ and transverse G^- mode (1590 cm^{-1}) were significantly enhanced. Because its high signal-to-noise ratio and narrow peak width, the G-mode signal intensity can be employed to achieve quantitative detection of antibody HSA, affording a detection limit down to 1 fM.

In addition, CNTs decorated with metal NPs provide higher SERS detection sensitivity than isolated CNTs, because both EM and CE enhancement effects contribute to the SERS signals. A sensitive sensor composed of single wall CNTs and deposited gold nanoparticles, was reported for monitoring Hg vapor concentration [146]. Due to strong plasmonic coupling between the Au NPs and CNTs, an extremely low detection limit down to 2 ppb was achieved. Recently, Zhang et al. [147] demonstrated a highly efficient SERS sensor prepared via decoration of walled carbon nanotube/gold nanoparticle (CNT/AuNP) hybrid nanocomposites onto a filter membrane. The coupling between high density gold nanoparticles, inter-carbon nanotubes can produce numerous hot spots, guaranteeing their strong SERS enhancement capability. When the detection concentration of MG was reduced to 1 pM, the characteristic band at 1615 cm^{-1} corresponding to MG could still be measured. More recently, a novel SERS sensor for monitoring heavy metal ions such as (Pb^{2+}, Hg^{2+}, and Cd^{2+}) was reported [148]. In the study, the substrate, namely $CoFe_2O_4$ NPs functionalized-porous anodic alumina (PAA) membrane, was used to grow long helical-structured carbon nanotubes (CNTs) with a diameter of less than 20 nm. The SERS sensor CNTs/PAA exhibited a high sensitivity of up to 1 ppb for heavy metal ions. Compared to their corresponding bare solutions, the normalized sensor response values are about 22, 16, and 10 for Pb^{2+}, Hg^{2+}, and Cd^{2+}, respectively.

4.5. Silicon-based nanomaterials

With ultrahigh surface-to-volume ratio, excellent biocompatibility, convenient surface modification, and sensitive response, silicon (Si) nanomaterial is one of the most important semiconductor materials, which have shown great potential for practical applications, such as optoelectronic devices, catalytic analysis, bioimaging, biosensing, cancer diagnosis and therapy, *etc*. [149,150]. Silicon materials incorporated with noble metal nanoparticles (Ag or Au) can further develop the SERS effects because of strong charge transfer between semiconductor Si and metal surface. Thus, Si-based hybrid nanomaterials are superior to isolate Au NPs or Ag NPs sensors, due to their higher enhancement capability and better reproducibility. In the past decades, various Si-based hybrid nanomaterials such as Ag/Au NPs-decorated silicon nanowires [151,152], Ag/Au NPs-decorated silicon nanocones [153], Ag NPs-decorated silicon nanospikes [154], Au/Ag NPs-decorated silicon wafers [155] *etc*., have been prepared for SERS sensing.

Ag/Au-decorated Si nanowires are the most widely used substrates for SERS sensing. Galopin et al. [156] synthesized Ag nanoparticles decorated Si nanowires by (Ag NPs) using *in situ* deposition technique. The as-prepared Si-based hybrid composites could reach a detection limit of 10^{-14} M for R6G. He et al. [157] developed an ultrasensitive DNA sensor by *in situ* fabrication of Ag NPs on Si nanowire, providing a lowest detection of 1 fM. Zhang et al. [158] deposited Ag NPs coated with silica layers onto highly ordered silicon nanowire array (SiNWA) by using chemical *etch*ing and metal reduction approaches, and used as SERS substrates, with a detection limit for R6G as low as 10^{-16} M. In addition, Peng et al. [159] demonstrated an ultrasensitive SERS sensor for R6G, fabricated by depositing Au NPs on etched Si nanowires, observing a detection limit of 10^{-11} M. Recently, a sensitive SERS sensor for tracing Hg^{2+} was presented, fabricated using Au NPs decorated-Si nanowire array. In the presence of Hg^{2+}, intensive SERS signals could be detected by forming thymine-Hg^{2+}-thymine base complex, resulting in a lowest detection concentration of 1 pM (0.2 ppt) for Hg^{2+} [160].

Furthermore, highly ordered Si nanocone arrays decorated with Au/Ag NPs have also shown their excellent SERS enhancement capability. The ultrasensitive SERS signals of R6G were achieved at concentrations as low as 10^{-15} M [153]. Also, reusable Si nanospikes decorated with Ag nanoparticles were fabricated by femtosecond laser pulses writing and *in situ* grown methods. They yielded a detection limit of 1 pM for R6G when used as SERS-active substrates [154].

4.6. Alloyed nanostructure

Among all the noble metals, Ag is the best plasmonic enhancement material but it gets oxidized easily in air. However, gold possesses the best biocompatibility, which can be employed to hinder the oxidation of Ag while improving its stability. When pure Ag nanostructures cannot exhibit satisfactory optical properties, alloying is an efficient strategy to tailor the plasmonic property of Ag-based nanostructures. To date, several types of Ag-based alloy nanostructures are prepared and reported [161,162].

One popular substrate used for SERS is the Ag-Au alloyed nanostructure, which can be prepared by the reduction of $HAuCl_4$ and $AgNO_3$ at different molar ratios. Recently, Zhao et al. [163] showed a double detection approach for ochratoxin A (OTA) and aflatoxin B1 (AFB1) using Ag@Au core-shell nanoparticles. In the study (see Fig. 10), two SERS tags were prepared by embedding 4-NTP and 4-ATP at the junction between Ag core and Au shell, respectively. Then the metal surface of Ag@4-ATP@Au NPs and Ag@4-NTP@Au NPs were modified by the aptamer-O and aptamer-A, respectively. Probe-O/Probe-A functionalized magnetic nanoparticles (MNPs) were employed to capture SERS tags via hybridization interactions, leading to formation of MNPs@Ag@4-ATP/4-NTP@Au NPs core-satellite complexes. The MNPs@Ag@4-ATP/4-NTP@Au NPs composites showed strong SERS enhancement effects, due to the strong plasmonic coupling between the approaching satellite Ag@Au NPs as well as plasmonic coupling between the Ag core and Au shell. In the presence of OTA and AFB1, both of two target molecules compete with probes on MNPs for combining with the aptamers, resulting in the release of Ag@Au NPs and further reduction in the SERS signal of Raman tags. The obtained detection limits of OTA and AFB1 are 0.006 ng mL^{-1} and 0.03 ng mL^{-1}, respectively.

Meanwhile, an ultrasensitive approach for monitoring bisphenol A (BPA) in water was performed by using DNA-embedded Au/Ag alloyed NPs [164]. Thiolated probe DNA was embedded on the surface of Au NPs (40 nm) prepared by citrate-reduction procedure. Next, DNA-embedded Au NPs were encapsulated with a silver shell to enhance the Raman signals. Finally, Cy3-labeled aptamer was combined with DNA-embedded Au/Ag NPs via DNA hybridization. In the presence of BPA, aptamer DNA molecules are released from surface of NPs, forming a stable aptamer–BPA composite. Herein, the SERS signals of aptamer DNA molecules gradually decrease with increasing BPA concentration. The ultrasensitive quantification of BPA can be achieved by monitoring the SERS signal reduction. There is an ultrasensitive detection limit of 10 fM for BPA, which is expected to have potential applications in sensing hazardous materials.

4.7. Magnetic nanostructure

Magnetic nanostructures including nanoparticles and nanocomposites exhibit novel physical and chemical features compared to single component nanomaterials. The presence of magnetic field in the magnetic nanostructures can efficiently induce

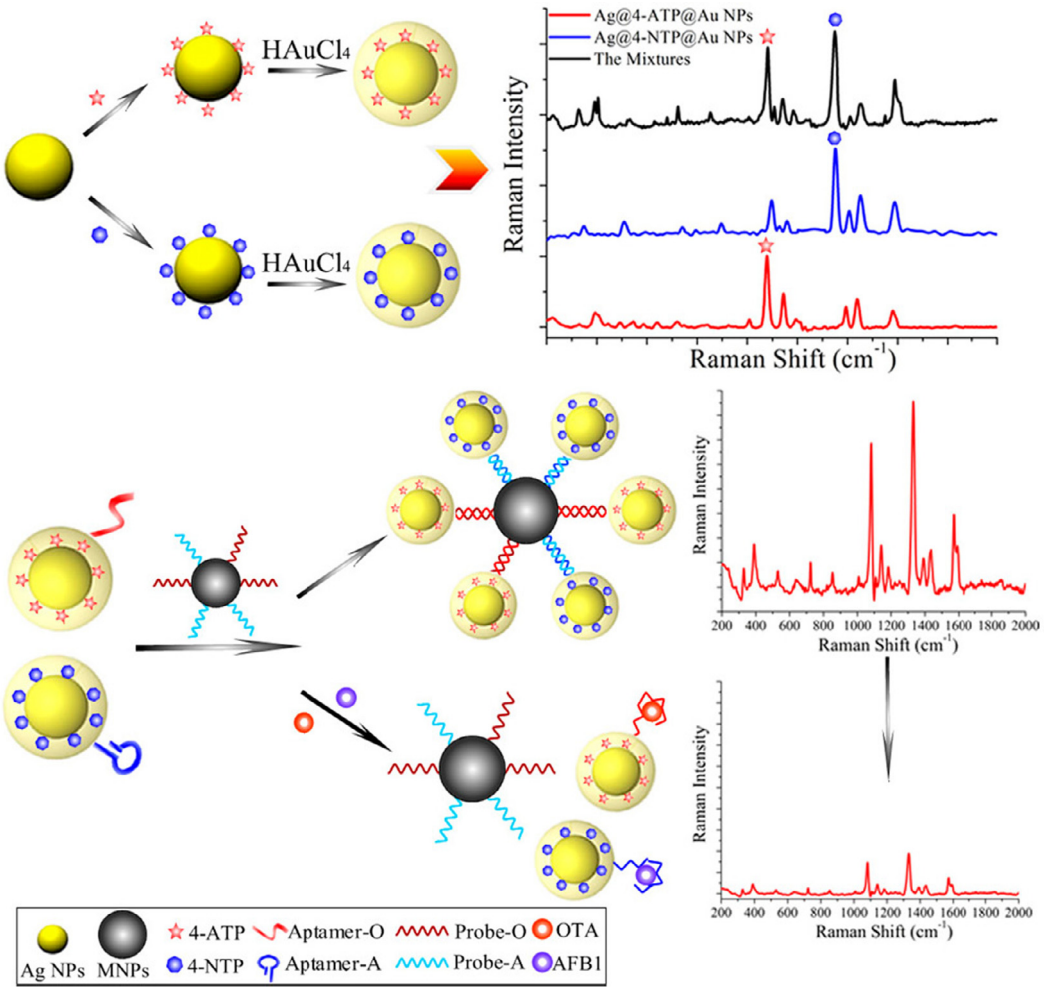

Fig. 10. Schematic of simultaneous detection of OTA and AFB1 using SERS labels embedded Ag@Au CS NPs. (Reproduced from ref [163] with permission of American Chemical Society.)

electromagnetic enhancement hotspots, making them ideal candidates for SERS-based sensing. With their unique magnetic responsiveness, magnetic nanostructures have developed as a powerful analytical tool for bioimaging [165], biosensing and fast separation of target analytes (*eg.*, chemicals, biomolecules, bacteria, and living cells) [166–168].

Among numerous magnetic nanostructures, the core-shell structured nanocomposites are well known magnetic hybrid systems used for SERS sensitive detection. For example, Hu et al. [169] fabricated silver-coated Fe_3O_4@SiO_2 composite microspheres with excellent ferromagnetic and SERS properties. Using R6G molecule as target analytes, the SERS signals can be measured in concentrations as low as 1 fM (10^{-15} M). Recently, Song et al. [170] have demonstrated novel silver-deposited silica-coated Fe_3O_4 magnetic particle (Fe_3O_4@SiO_2@Au) for ultrasensitive detection of MG. The as-prepared Fe_3O_4 particles were coated with silicon shell, resulting in formation of Fe_3O_4@SiO_2 magnetic particles. Next, the surface amination of Fe_3O_4@SiO_2 particles was performed by poly (allylamine hydrochloride) (PAH). Through electrostatic interaction mechanism, the product Fe_3O_4@SiO_2@Au particles were yielded by mixing Fe_3O_4@SiO_2 magnetic particles and Au NPs solutions. The resulting Fe_3O_4@SiO_2@Au magnetic particles show a good magnetic separation activity toward MG molecules. Moreover, there is a sensitive SERS response in the range from 10 fM to 100 μM, generating an ultralow detection limit of 2 fM.

In terms of biosensing, magnetic nanostructures have presented great potential capability. For instance, Zengin et al. [171] described a simple and highly sensitive sandwich assay for monitoring tau protein by using anti-tau protein functionalized hybrid magnetic (Fe_2O_3) nanoparticles incorporated with anti-tau immobilized Au NPs, providing a detection limit less than 25 fM. Pang et al. [172] designed a novel, superparamagnetic and ultrasensitive platform named multifunctional Fe_3O_4@Ag magnetic NPs, which can be used for microRNA determination and duplex-specific nuclease signal amplification. With the aid of DNA/RNA hybridization, the microRNA molecules can be captured and immobilized on the surface of Fe_3O_4@Ag NPs. In the presence of endonuclease duplex specific nuclease (DSN), one target microRNA molecule can rehybrid a number of DNA probes to open signal-amplifying recycling. Moreover, the superparamagnetism of Fe_3O_4@Ag NPs allow a direct quantitative analysis of microRNA concentration. The obtained detection limit of microRNA was as low as 0.3 fM, triggering a novel approach for microRNA detection in point-of-care clinical diagnostics.

In addition, Zhang et al. [167] demonstrated a multifunctional magnetic Fe_3O_4–Au core–shell NP platform for simultaneous detection of bacterial cells by using SERS. Because of the strong magnetic property of the Fe_3O_4 core, the Fe_3O_4–Au core–shell NPs can be concentrated into a small dot under an external magnetic field. Interestingly, the small dot shows relatively strong plas-

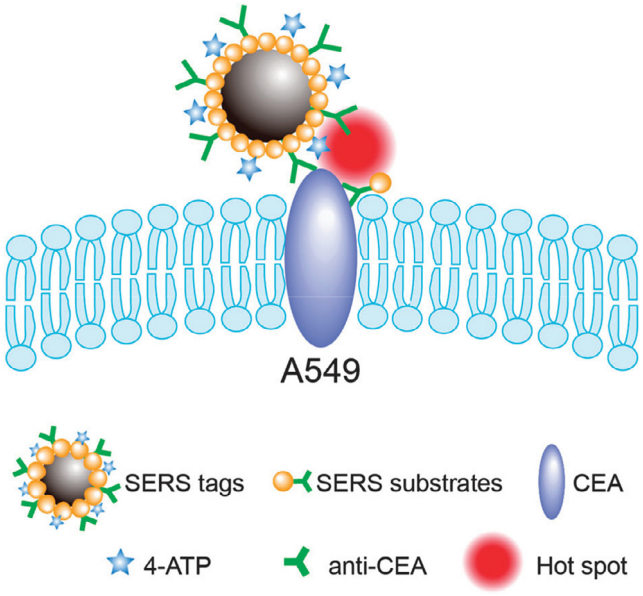

Fig. 11. Schematic illustration of the formation of sandwich structures and SERS hot spots when both SERS tags (anti-CEA/4-ATP/Fe3O4–Au NPs) and SERS-active substrates (anti-CEA/Au NPs) were bound to the CEA, which was expressed on the A549 cell surface, based on the specific antigen-antibody interactions. The formation of the SERS hot spots at the junction of SERS tags and SERS-active substrates results in an enhanced SERS signal of the Raman reporter, which could be used to detect cancer-related membrane proteins on cancer cell surfaces. (Reproduced from ref [173] with permission of The Royal Society of Chemistry.)

monic enhancement property because of the nanostar-shaped gold shell and high density of hotspots induced by magnetic stacking. Taking advantage of both magnetic and SERS features, the novel platform can provide a detection limit of bacteria better than 0.1 ppb. More recently, Qiu et al. [173] demonstrated an ultrasensitive SERS approach for detecting living cancer cells by Fe_3O_4-Au hybrid NPs substrates, which are labeled with a Raman reporter molecule 4-aminothiophenol (4-ATP) and an antibody of carcinoembryonic antigen (CEA). The SERS tags and anti-CEA-labeled Au NPs serve as SERS substrates to improve SERS detection sensitivity. In the presence of CEA positive-expressed lung cancer cells A549, a sandwich configuration (Fig. 11) between SERS tags and SERS substrates was formed at the surface of living cancer cells, due to specific antigen-antibody recognition mechanism. The sandwich model can provide excellent SERS hotspots in the gap of SERS tags and SERS substrates. Thus, the SERS signals of Raman reporter 4-ATP can be successfully measured on cell surfaces. This approach shows ultrahigh detection sensitivity, where CEA is measurable at ultralow A549 cells concentrations of 10 cells mL^{-1}.

4.8. Metal–organic frameworks

Metal–organic frameworks (MOFs) are a class of important porous crystalline materials that combine metal ions or metal ions clusters with rigid organic ligands via a coordination interaction [174,175]. In addition, MOFs possess many advantages such as large surface area, good stability, high porosity, tailorable chemistry, ordered and tunable nanostructure cavities [176], making them promising candidates for SERS substrates (*eg.*, Ag or Au

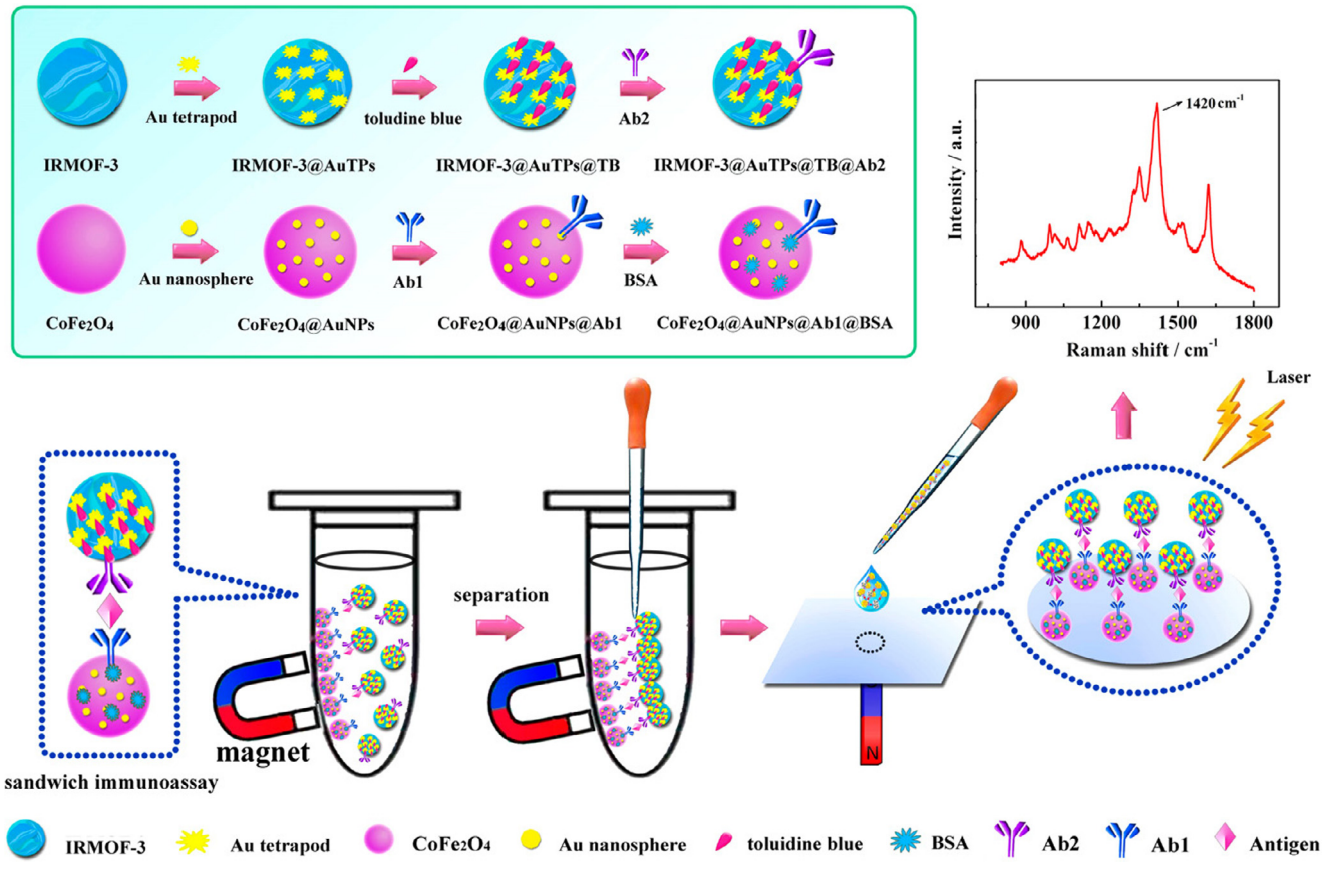

Fig. 12. Schematic diagram of the SERS-based immunosensor for the detection of NT-proBNP. (Reproduced from Ref. [183] with permission of American chemical society.)

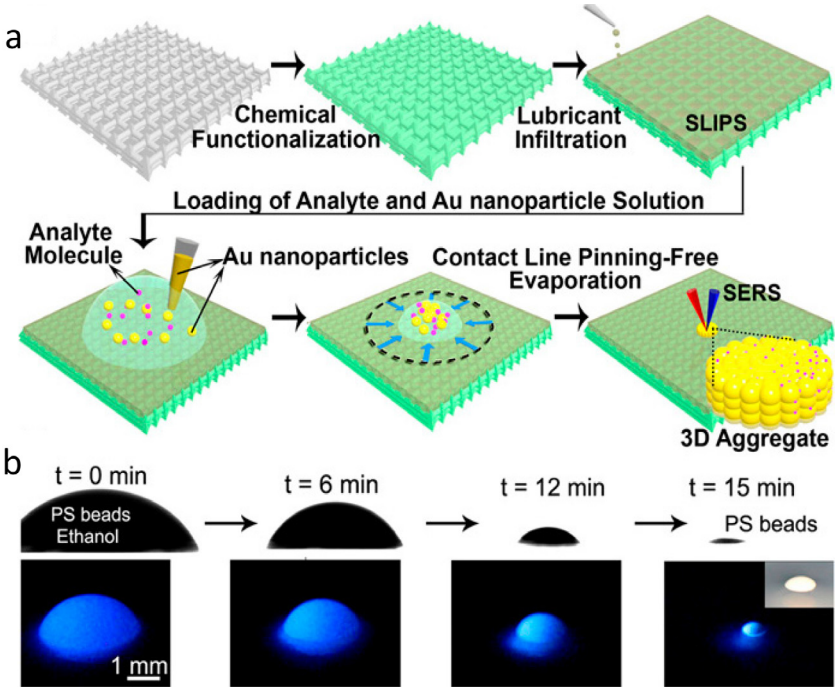

Fig. 13. (a) Schematic illustration explaining the concept of SLIPSERS. Upon analyte loading on SLIPS substrate, 3D aggregated are formed, that facilitate SERS detections. (b) Pictorial view of the SLIPSERS effect using luminescent PS spheres dispersed in ethanol. (Inset) Optical image of the enriched PS sphere aggregate. (Reproduced from Ref. [190] with permission of Clearance Center, Inc.)

embedded frameworks) [177–180] for monitoring targeted analytes.

Through a solution impregnation approach, ultrasensitive SERS substrates were *in situ* fabricated by embedding gold nanoparticles (Au NPs) into a solid matrix MIL-101 that can efficiently load Au NPs and prevent them from migration [181]. The as-prepared Au NPs/MIL-101 composites not only incorporate localized surface plasmon resonance enhancement property of Au NPs, but also possess high adsorption capability of MOF for target molecules, resulting in concentrated molecules in the vicinity of hotspots. Using the Au NPs/MIL-101 composites as SERS substrates, the detection limits of R6G and benzadine is down to 41.75 fM, 0.54 fM, respectively. Likewise, another ultrasensitive SERS substrate for monitoring dopamine was prepared by *in situ* synthesis of Ag NPs on the surface of a solid matrix MIL-101(Fe) [182]. The as-synthesized SERS substrate exhibit high adsorption performance and thus can capture and concentrate analytes in the vicinity of the enhancement hotspots generated by high density Ag NPs. Using dopamine as targeted analytes, there is a good linear detection range from 1.054 pM to 210.8 nM, and a detectable limit approximately 0.32 pM can be obtained.

Lately, an ultrasensitive SERS-based immunosensor for monitoring biomarker N-terminal pro-brain natriuretic peptide (NT-proBNP) was designed by synthesizing MOFs combining magnetic NPs (Fig. 12) [183]. In this study, the three-dimensional framework MOF-3 (IRMOF-3) with amination moieties was employed to synthesize IRMOF-3@Au tetrapods (Au TPs)@toluidine blue (TB), which act as excellent SERS substrates for biomarker monitoring due to their large surface area of IRMOF-3 and abundant hotspots generated by Au TPs. Then the second anti-NT-proBNP (Ab2) was further immobilized on the surface of IRMOF-3@Au TPs@TB, resulting in a formation of immunosensor IRMOF-3@AuTPs@TB@Ab2. To develop the detection sensitivity of the immunosensor, magnetic nanocomposites ($CoFe_2O_4$@Au NPs) were used to immobilize primary antibodies (Ab1) and BSA to form CoFe2O4@AuNPs@Ab1@BSA. With the help of sandwich immunoassay protocol, magnetic separation, and magnetic enrichment approaches, the enhanced Raman band at 1420 cm^{-1} ascribed to Raman reporter TB was used to label the concentrations of biomarker NT-proBNP. Finally, the multifunctional SERS platform could provide a detection limit of NT-proBNP as low as 0.75 fg mL^{-1}.

4.9. Three-dimensional nanostructure arrays

It is well-known that hotspots are essential for ultrahigh SERS gain because of their excellent EM magnitude, desirable for ultrasensitive sensing. In the past decades, most reported hotspots for SERS have been found in zero-dimensional tip-like, one-dimensional rod-like, two-dimensional planar nanostructures [184–187]. Nevertheless, the ordered SERS substrates from zero to two-dimension space have quite limited hotspots compared to three dimensional nanostructures. Therefore, it is highly desirable to fabricate plasmonic nanostructures with uniform and high density hotspots for practical applications. The three-dimensional (3D) nanostructure has shown great promises for SERS-based sensing applications due to extraordinary intense plasmonic coupling. A 3D SERS substrate is much superior to a 2D substrate, as it offers larger surface area for capturing more analytes, highly ordered metal NPs distribution, high density hotspots for giant enhancement in 3D space, and excellent repeatability.

A simple and novel 3D hotspots matrix that can maintain hotspots in 3D space between every two neighboring Ag NPs, was created by evaporating a droplet of trisodium-citrate reduced Ag NPs colloids on a hydrophobic silicon wafer (contact angle $\sim 107°$) that treated with fluorosilane [188]. During the evaporation process, the inter-particle gaps become smaller so that the Ag NPs are orderly deposited on the silicon wafer surface. Unlike dry state SERS substrate, the 3D geometry show excellent particle dispersity, and uniformed inter-particle distance, both of which can produce a large number of hotspots and huge Raman enhancement. The hotspots can serve as trapping wells to gather more molecules. Interestingly, even a single molecule of R6G (0.5 aM) located in the 3D

hotspot matrix can generate a significant SERS signal with good repeatability. Wang et al. [189] demonstrated a novel, sensitive and simple SERS platform with 3D hotspots. The SERS platform was a single droplet of concentrated Ag NPs with analytes deposited on a highly hydrophobic cover glass. Due to liquid adhesive force, solvent evaporation, and hydrophobic interaction existing in the platform, the hotspots were generated into a 3D space. The resulted 3D hotspots demonstrated an ultrasensitive detection for R6G molecules with a lowest detection limit of 10 aM.

Another ultrasensitive SERS sensing platform named slippery liquid-infused porous SERS (SLIPSERS) for enriching and delivering analytes into a specific SERS detection area in both aqueous and non-aqueous liquids was reported (Fig. 13) [190]. In the study, the slippery substrate was prepared by infiltrating Teflon membranes (pore size, 200 nm) with a perfluorinated liquid (DuPont Krytox GPL 100). The preparation process guaranteed that the substrate surface is immiscible to both the aqueous and non-aqueous phases. When one droplet of analytes and Au NPs or Ag NPs mixture solutions was deposited on SLIPSERS, the mixture droplet evaporated at a constant contact angle without obvious pinning at the contact line, until the Au NPs aggregated together to form a three-dimensional nanoaggregate, which is a high-quality hotspot for SERS detection. Moreover, the sensing platform can perform ultrasensitive detection in most commonly used aqueous and non-aqueous solvents (*eg.*, ethanol, acetone, toluene, and dichloromethane, *etc.*) when the concentrations of targeted analytes are in the order of attomolar level. With the help of the SLIPSERS platform, the quantified detection levels of R6G molecules range from 750 fM to 75 aM.

Furthermore, various 3D nanostructured composites such as branched nano-trees [191], nano-butterfly wing [192], branched nanodendrites [193], nanoporous cylinder arrays [194], nanoring cavity arrays [195], colloidosomes [196], laser writing of 3D blocks [197], Au@Ag nanorod arrays [198], *etc.*, have been synthesized for SERS detection, greatly enriching 3D SERS substrate family members and providing more options for pursuing ultrasensitive SERS detection sensitivity. Li et al. [199] designed an ultrasensitive three-dimensional plasmonic architecture named gold triangle nanoarrays for protein biomarker human immunoglobulin G detection. In the presence of protein biomarker, the antibody molecules immobilized on gold triangle nanoarrays because of immunoassays recognition interaction, and were then linked with the gold nanostar@Raman reporter@silica, forming a 3D sandwich nanocomposites and high density hotspots in 3D space. With the aid of SERS immunosensor, a low detectable limit of human immunoglobulin G protein was 7 fg mL^{-1}. Recently, Li et al. [200] reported a novel SERS substrate named Ag NPs decorated PAN-nanohump arrays with large-scale 3D hotspots. The SERS substrate was prepared by printing polyacrylonitrile (PAN) films with uniform nanohump arrays and Ag NPs depositing approaches. Interestingly, high density 3D hotspots could be obtained by tuning the curvature of flexible PAN film during Ag-depositing process. The synthesized Ag-NPs@PAN-nanohump array films exhibited excellent SERS performance in the detection of explosives TNT, with low detection limit of 10^{-12} M.

Notably, the semiconductor material (*eg.*, Silicon [201], ZnO [202], and TiO_2 [203,204]) functionalized-3D plasmonic arrays also shown outstanding performance in ultrasensitive detection via SERS. For example, Huang et al. [201] developed a 3D SERS substrate with cactus-like nanostructure for monitoring MG. In the study, the plasmonic substrate was synthesized by growing many silicon nanoneedle scaffolds on Ag dendrites and decorating with Ag NPs, respectively. The hierarchical scaffolds possess a number of high-density hotspots, resulting in huge amplification of SERS signals. Using MG as targeted analyte, a low detectable limit with good reproducibility is down to 10^{-13} M. A novel and efficient SERS 3D substrate named Gold@silver/silicon pyramid (Au@Ag/3D-Si) was designed to probe R6G [205]. The SERS substrate was composed of silicon pyramid arrays, 30 nm Ag film deposited on silicon pyramid, 10 nm Au film outside Ag film. The stable SERS response of Ag film, chemical stability of Au film and the large field enhancement capacity of 3D-Si pyramids, contributed to superior detection sensitivity. Using R6G as probe molecule, the performance of Au@Ag/3D-Si substrate is far better than 3D-Si, Ag/3D-Si and Au/3D-Si substrate, indicating that it is possible to create more opportunities for label-free SERS detections in the future. In addition, Tan et al. [203] designed a large-scale 3D nanostructure by decorating silver NPs on TiO_2 nanorods scaffold. The as-prepared 3D nanostructure demonstrated excellent SERS enhancement capability due to presence of high density hotspots in Ag NPs. Taking the advantage of 3D nanostructure, a detection limit of MG was as low as 1 pM. Later, Dai et al. [204] developed an ultrasensitive 3D SERS substrate based on TiO_2 nanowire arrays to target R6G, and the achievable detection limit was 10^{-15} M.

5. Highly efficient adsorption mechanism for SERS

In general, intensive SERS signals are generated when the target analytes have high affinity to SERS substrate. Highly efficient adsorption mechanism is quite helpful to develop the SERS detection sensitivity for the target analytes located in the vicinity of nanostructure surface. Such target molecules containing active moieties such as thiol group (–SH), and cyanide (–CN), can be adsorbed via covalent bonding. In addition, the heterocyclic molecules such as pyridine, bipyridine, adenine, *etc.*, prefer to interact with metal surface via their active atoms. The charged analytes can also be captured by oppositely charged SERS substrate. However, not all the target analytes in nature exhibit strong affinity to nanoscaled surface, such as single cyclic aromatic molecules (*eg.*, benzene, toluene, nitrobenzene, phenol, *etc.*) and polycyclic aromatic hydrocarbons (PAHs, *eg.*, biphenyl, naphthalene, fluorene, anthracene, pyrene, *etc.*). Thus, it is still a challenge for detecting the target molecules with poor affinity to metallic surfaces. Therefore, it is necessary to choose a reasonable adsorption mechanism towards nanomaterial substrates for different kinds of target analytes. To date, several well-known adsorption mechanisms used for SERS detection have been proposed, such as covalent bonding, hydrophobic interaction, charge-selective mechanism, π-π stacking interaction, and immunoassays, *etc.* These as-proposed mechanisms will be outlined and discussed along with their practical applications in the following sections.

5.1. Covalent bonding

For target analytes with thiol group, the formation of covalent bonds (Ag–S and Au–S) is usually employed to immobilize target analytes on noble metal surface [206,207]. The target analytes containing diazonium moiety prefer to react with other aromatic diazonium groups via forming a diazo bond [208]. Acting as important Raman reporters for monitoring the biological molecule DNA, fluorescent dyes are also used to attach with DNA by covalent bonding [209,210]. In addition, due to specific covalent binding for hydroxyl, the boronic acid moiety is used to perform sensitive SERS detection of dietary source glucose and fructose [211,212]. Recently, a sensitive detection strategy for monitoring heavy metal ions (Hg^{2+}) was designed by using strong covalent bonding mechanism [213]. In the study, the 2-mercaptoethanesulfonate functionalized silver NPs exhibited intensive SERS signals due to the formation of Ag-S bonding. However, as the binding capacity between mercury and sulfur is stronger than that of between silver and sulfur, the presence of Hg^{2+} prevents the adsorption of 2-

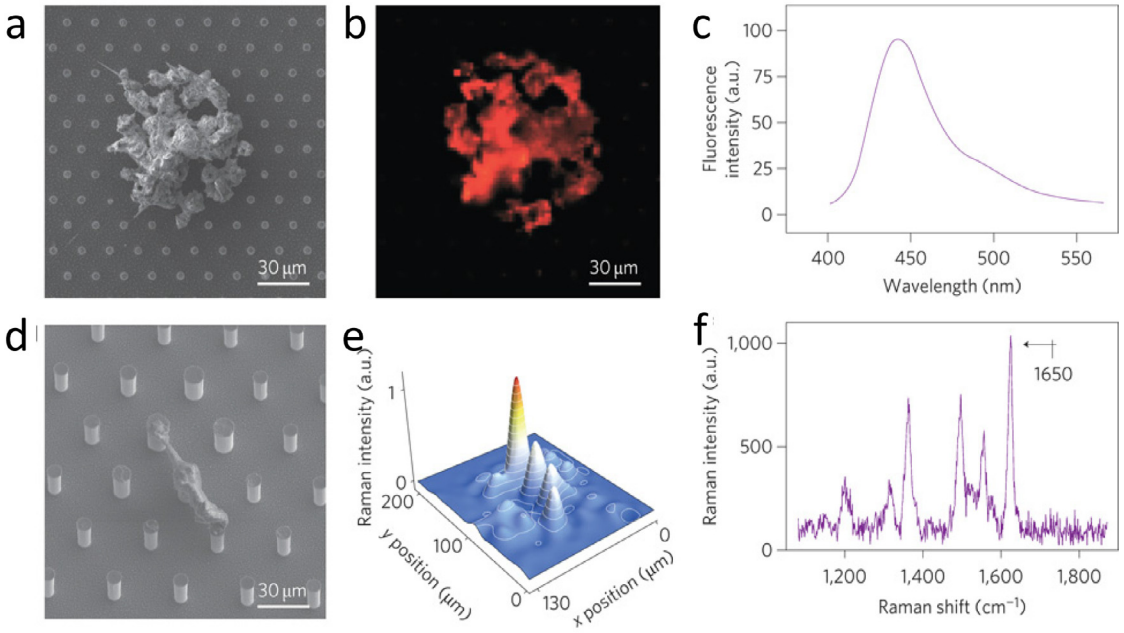

Fig. 14. SERS mapping process with plasmonic nanostructure arrays on super-hydrophobic surfaces. (a) SEM image of solute precipitation from a 1 fM solution of rhodamine. (b, c) Fluorescence optical image and spectrum rhodamine. (d) SEM image of solute precipitation from a 10 aM solution of rhodamine. (e, f) Raman intensity map of Rhodamine and its spectrum. (Reproduced from Ref. [221] with permission of Nature Publishing Group.)

mercaptoethanesulfonate on Ag NPs surface. The as-obtained SERS intensities of 2-mercaptoethanesulfonate decrease with the increasing concentrations of Hg^{2+}. Using the Raman band at 795 cm^{-1} for quantitative analysis, a reliable detection limit of Hg^{2+} is as low as 2.4 nM L^{-1}. Moreover, an interesting SERS-based sensor for monitoring thrombin in low concentrations was reported [214]. The Au NPs were first functionalized with a Raman reporter 4-ATP. Typically, the 4-ATP possesses two moieties, one of which is the thiol group (-SH) used to bind Au NP via covalent bonding, while the other is a diazonium moiety, capable of reacting with aromatic residues of thrombin protein by forming a diazo bond. Finally, the covalent linked thrombin was introduced into a substrate coated with silane and glutaraldehyde, resulting in the formation of a sandwich model 4-ATP@thrombin@antithrombin@heparin. The detection limit of thrombin with the sandwich model is recorded at 10^{-13} M.

5.2. Hydrophobic interactions

Wettability is an important property for plasmonic nanostructures because it defines the capability of maintaining contact with a liquid. As is well known, hydrophilic surfaces should have affinity to the target molecules with good solubility in water, resulting in shrinking of the target molecule droplet and rapid evaporation due to large surface contact. However, hydrophobic surfaces too allow a deposited liquid droplet to evaporate and maintain its quasi-spherical shape during the volume reduction process. Briefly, super-hydrophobicity can be classified when a quasi-spherical water droplet on metal surface possesses a contact angle greater than 150° and a planar angle less than 10° [215,216]. For SERS detection, hydrophobic surface enables to control and concentrate water-insoluble target molecules on plasmonic enhancement hotspots area. Essentially, both hydrophobicity and hydrophilicity can act as a working mechanism employed in SERS-based practical applications. Particularly, if a substrate surface possesses both highly hydrophobic and hydrophilic moieties, it can act as a multifunctional organic solvent–water separation platform system for detection of environment pollutants such as polycyclic aromatic hydrocarbons (PAHs) and pesticides. In general, there are two steps to prepare hydrophobic metal surface, the first is construction of nanometer or micrometer scaled structure, second is modification of the surface by using low surface energy molecules [217,218]. Thus, hydrophobic interaction mechanism has become an efficient approach for SERS-driven detection [189,219,220].

For example, novel plasmonic nanostructure arrays with super-hydrophobic surface are prepared by multiple micro-nano fabrication processes [221]. In the study, clean Si wafer is coated with a positive resist layer through optical lithography technique. Then, a Ag layer is grown on the treated-Si wafer based on the reduction of metal Ag^{+} using electroless deposition method. The hydrophobic surface is achieved by coating a thin film of polymer Teflon onto the cylindrical pillar structure arrays prepared by reactive ion etching process. When a droplet of R6G water solution (a diameter, 2 mm; initial concentration 1 fM) is deposited on the superhydrophobic device, the precipitation solute of R6G gets concentrated and precipitated onto a small area nearby the silver nanostructures due to high hydrophobic interaction, as confirmed by SEM and fluorescence imaging (Fig. 14a-b). Using the extremely small concentration of R6G (10 aM), the resulting SERS mapping analysis (1650 cm^{-1}) demonstrates that the hotspots induced by hydrophobic interaction mechanism can provide ultrasensitive detection capacity (Fig. 14d–f).

In addition, a super hydrophobic plasmonic substrate named Ag decorated polystyrene (PS) nanotubes was prepared by melting PS onto an anodized alumina (AAO) template and subsequent silver evaporation. The super hydrophobic SERS substrate is capable of achieving a ultralow detection limit of 400 ppt level for organic pollutant crystal violet [222]. Recently, Jayram et al. [223] synthesized super hydrophobic silver decorated zinc oxide (ZnO) nanostructure thin films by using thermal evaporation method. Prior to Ag deposition process, the treated ZnO nanowires thin films show super hydrophobic property possessing a contact angle of 163°. Taking the advantage of super-hydrophobicity, the as-prepared SERS substrate can provide a reproducible detection limit of R6G

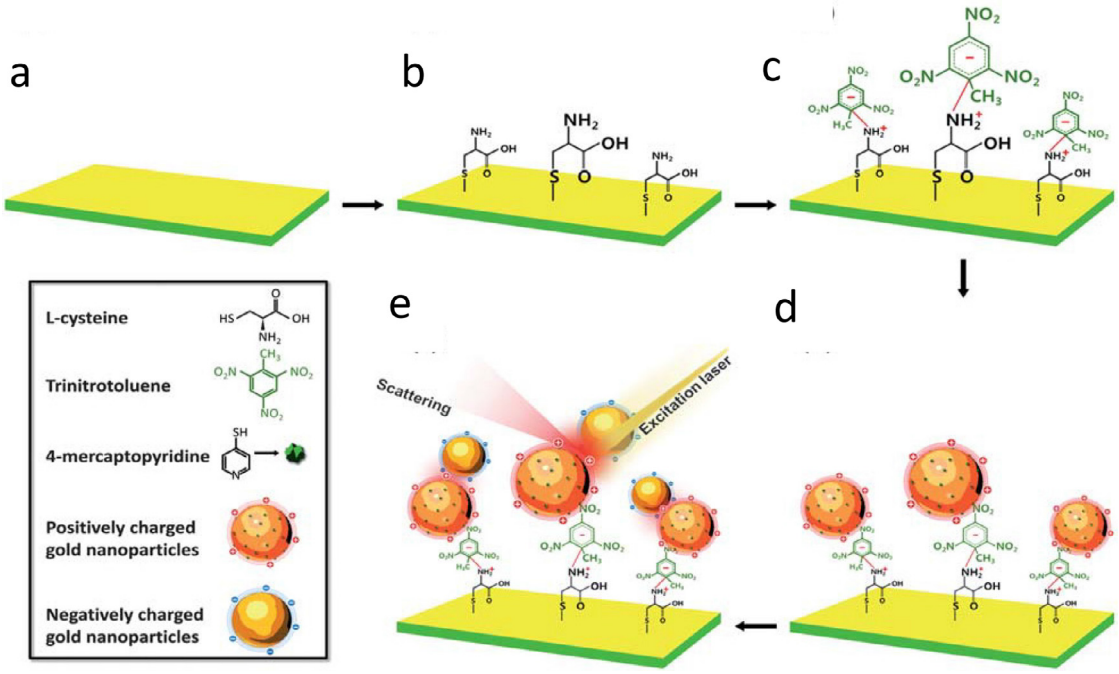

Fig. 15. SERS-based TNT detection using electrically charged nano-dumbbells: (a–f) Functionalization steps to produce nano-dumbell structures on gold substrate. (Reproduced from Ref. [232] with permission of The Royal Society of Chemistry.)

as low as 10^{-10} mol L^{-1}. Thereafter, they designed another type of SERS substrate named silver coated copper oxide (Ag@CuO) nanoflowers thin film, which can efficiently incorporate superhydrophobic property with high enhancement ability of Ag@CuO nanoflowers. Using R6G as target molecules, the SERS substrate can provide a detection limit of 10^{-10} mol L^{-1} [224].

5.3. Charge-selective mechanism

Similar with wettability, electronegativity determined by Zeta potential, is another important property of nanomaterials. With the help of charge-selective mechanism, the charged SERS substrates prefer to capture oppositely charged target analytes. For example, Ag NPs deposited on negative- and positive-type Si wafers have demonstrated enhanced SERS signals for positively charged molecule acridine orange and negatively charged dye molecules fluorescein, respectively [225]. In addition, for positively charged dye R6G, Ag NP on negative-type porous Si nanostructures are obviously superior to the corresponding positive-type Si nanostructures [226]. Moreover, Baik et al. proposed that the Ag NPs deposited on p- and n-type Si nanowires exhibit higher charge selectivity than the Au NPs [227]. Thus, charge-selective adsorption mechanism can be considered as an efficient way to capture charged molecules using n-type and p-type substrates.

In many SERS-based charge selective detection studies, trinitrotoluene (TNT) is one of the commonly used target analytes via charge-selective adsorption mechanism [228–232]. Recently, an ultrasensitive SERS-based detection system for 2,4,6-trinitrotoluene (TNT) by the electrostatic interaction mechanism between positively and negatively charged gold nanoparticles was proposed [232]. The TNT molecule can induce L-cysteine modified gold substrates to form a Meisenheimer complex with a negatively charged aromatic ring which is employed to immobilize the 4-mercaptopyridine (4-MPY) modified-Au NPs (positively charged) through electrostatic interactions (Fig. 15a–c). More importantly, with the help of another type of negatively charged Au NPs because of electrostatic interaction, the generated nano-dumbbells structure can provide many enhancement hotspots for SERS (Fig. 15d-e). Thus, the SERS signals of TNT are greatly enhanced. The measurement results show that the nano-dumbbells structure can provide an ultra-sensitive detection limit of 1 pM and a linear response ranging from 9 to 180 nM, proving its strong potential in detecting various explosive materials.

Moreover, charge-selective-based SERS platform can also be used to detect mercury ions [233], food dyes [234,235], biological proteins and enzymes [236,237]. Recently, Chen et al. developed a simple and sensitive sensing strategy for recognition and detection of trypsin based on the electrostatic adsorption interaction. The polycationic protamine not only served as a substrate for enzyme hydrolysis but also acted as a medium for SERS enhancement, which could bind negatively charged 4-MPY-functionalized AgNPs and induce their aggregation. A detection level down to 0.1 ng mL^{-1} for trypsin was obtained [238].

5.4. π-π stacking interaction

In natural substances, especially in various biological and non-biological systems, π-π stacking effect is a well-known non-covalent interaction mechanism, occurring in aromatic rings containing π electrons. Indeed, π-π stacking interaction plays a pivotal role in DNA/RNA bases stacking [239,240], protein folding [241,242], supramolecular architecture design [243], material science [244], chemicals and biological analytes recognition [245]. In SERS study, π–π stacking interaction is particularly interesting because it can efficiently bind aromatic target analytes on metal surface without destroying the morphology of nanoparticles and distortion of the target analytes. Thus, for the aromatic analytes that do not interact with metal surface, π-π stacking interaction is the most promising approach to improve the adsorption efficiency between aromatic analytes and SERS substrate, and further achieve ultra-high SERS detection sensitivity.

Polycyclic aromatic hydrocarbons (PAHs) are a class of organic materials, which contain two or more than two aromatic moieties. Although they have sizable Raman scattering cross-sections, they

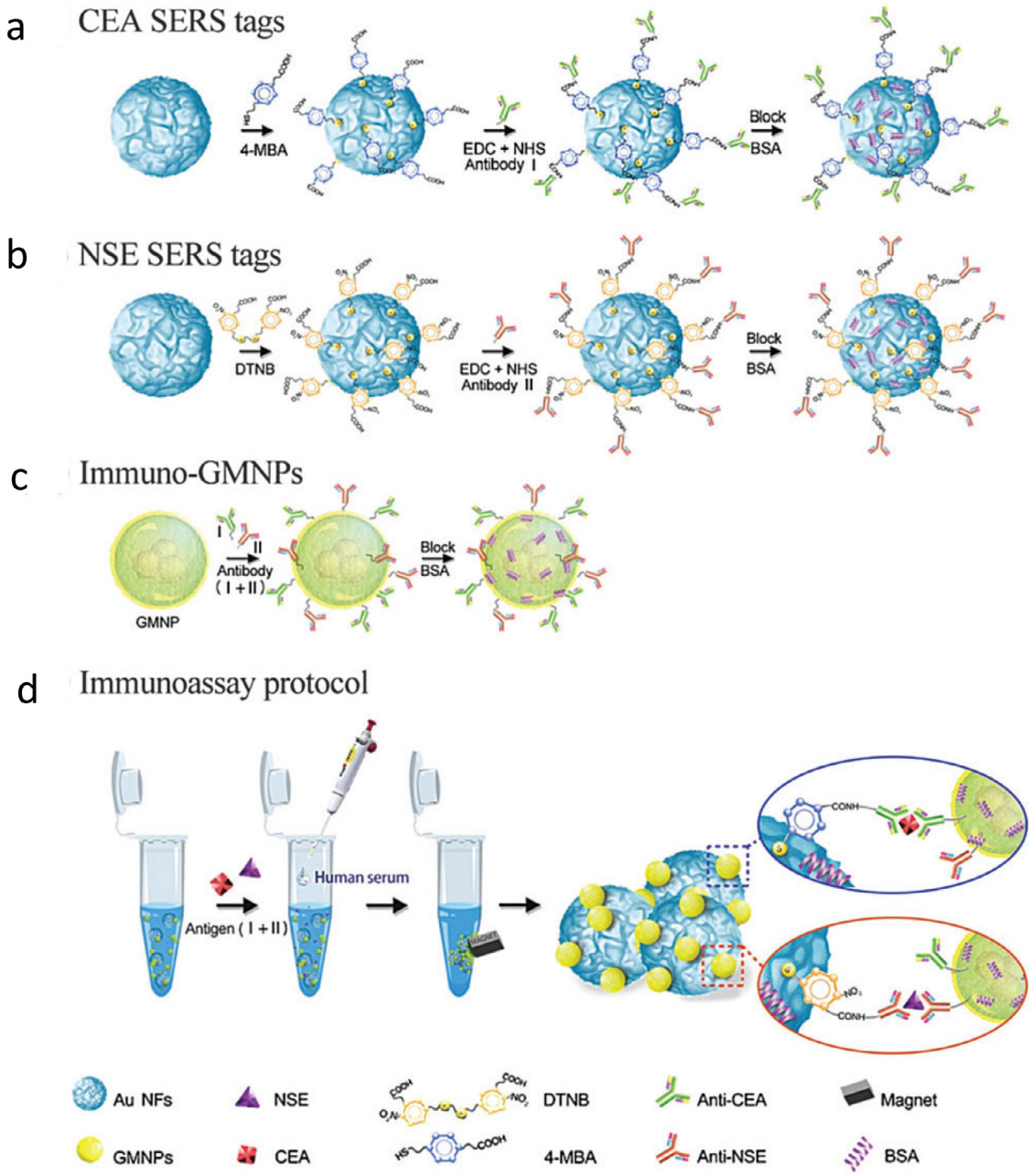

Fig. 16. Illustrative schematic of the design of SERS tags and immune-GMNPs, and the sandwich immunoassay for combination assay of CEA and NSE. (Reproduced from Ref. [252] with permission of The Royal Society of Chemistry.)

exhibit feeble SERS spectra when they are directly deposited on bare metal surfaces because of their poor affinity to metals. Fortunately, with the aid of π–π stacking interaction, PAHs can be selectively detected by some special SERS substrates, such as single-walled carbon nanotubes [246], humic acids-based Ag NPs [247], calixarene-functionalized Ag NPs [248], 4-aminothiophenol (4-ATP) functionalized ZnO–Ag hybrid nanoflowers [249] and poly (sodium 4-styrenesulfonate) (PSSS)-decorated Ag NPs [250]. More recently, our group designed a novel SERS sensing platform named PSSS-decorated Ag NPs in one step under room temperature [250]. The as-prepared SERS substrate has no SERS background interference compared to humic acids-based Ag NPs with strong background noise. More importantly, it can sensitively detect the PAHs by the proposed π–π stacking interaction mechanism, which provides high SERS intensity and very low detection limits (FAD, 10 aM; fluorescein, 10 pM).

5.5. Immunoassays

It is well-known that cancer is the leading fatal cause human life, due to its widespread incidence and high mortality rate. Thus, early detection of cancer symptom screening is crucial to improve chances of survival. The levels of protein biomarkers in living cells or organisms are considered as the readouts of physiological and pathophysiological environments, because these protein biomarkers are typically released from cells or organs. For instances, α-Fetoprotein (AFP) is a well-established biomarker for early diagnosis of liver cancer [251], while carcino-embryonic antigen (CEA)

and neuron-specific enolase (NSE) are well-known biomarkers for lung cancer [121,252]. Notably, the cancer biomarkers usually exist in very low concentrations during the early stage of cancer, and are quite difficult to detect. To improve diagnostic accuracy and treatment response, development of an ultrasensitive assay for specific detection of biomarker proteins is preferred.

Among the specific antigen–antibody interactions, immunoassays are the most commonly used approaches for biological protein detection. Antibody is used as molecular recognition site because of its high affinity and specificity to a specific antigen. Moreover, each antibody has a unique affinity for a specific antigen. Thus, the antibody–antigen interaction is very strong. Recently, the integrated platform based on immunoassays and SERS has received great attention, because it can perfectly combine the advantages of both immunoassays and SERS, resulting in high detection sensitivity. SERS-based immunoassay sensing platforms are widely exploited in cancer screening [252,253] biomedical diagnostics [168,254], food safety [255,256] and environmental monitoring [257,258].

In many SERS-based immunoassay studies, indirect detection of proteins or biological molecules by labeling with an active Raman reporter molecule is a commonly used approach. An ultrasensitive SERS biosensor for detecting folic acid was reported by employing Au NP–Ag NP heterodimers, which were formed via antigen–antibody interaction [258]. Under slight stirring, the as-prepared Au NPs and Ag NPs were modified by antibody and antigen, respectively. Then the Raman reporter molecule 4-aminothiophenol (4-ATP) further was labeled on the surface of conjugated antibody-Au NPs and antigen-Ag NPs, respectively. In the absence of folic acid, the antibody-Au NPs and antigen-Ag NPs forms a dimer, which yield very strong SERS signals of 4-ATP. However, in the presence of folic acid, the antibody-Au NPs gets released from the dimer. As the SERS intensity of 4-ATP is inversely proportional to the folic acid content, the detection levels of folic acid can be quantified by measuring SERS intensity of 4-ATP. With the help of the dimer hotspots and antigen–antibody immunoassay mechanism, the SERS-based immunoassay sensor has achieved an ultrasensitive detection ranging from 0.005 ng mL^{-1} to 1 ng mL^{-1} and a detection limit of 0.86 pg mL^{-1}.

In addition, a sandwich assay is a commonly used approach for achieving ultrasensitive SERS detection of analytes, because it can create more enhancement hotspots. There are three main components in a sandwich model including a supporting substrate labeled with analyte-specific antibodies, analytes, and analyte-specific SERS tags. Here, the SERS tag is usually a noble metal substrate labeled with the specific antibodies and Raman reporter molecules. Once the sandwich structure is formed, the concentrations of analytes can be qualitatively or quantitatively detected by measuring SERS signals of the labeled Raman reporter.

Song et al. [252] reported a highly sensitive, specific and simultaneous SERS-based sandwich immunoassay for two protein markers carcinoembryonic antigen (CEA) and neuron-specific enolase (NSE), which are strongly related with lung cancer screening. In the typical sandwich immunoassay, there are two analyte-specific SERS tags (CEA SERS tags, NSE SERS tags), two analytes (CEA, NSE) and a supporting substrate, namely gold coated magnetic NPs (GMNPs) modified with two targeted analyte specific antibodies, as depicted in Fig. 16. The CEA SERS tags are prepared by consecutive surface modifications of flower-like Au NPs with Raman reporter molecule 4-mercaptobenzoic acid, 1-ethyl-3-(3-dimethylaminopropyl) carbodiimide (EDC), N-hydroxysuccinimide (NHS) and antibody-CEA. The fabrication of NSE SERS tags is similar to the process of CEA SERS tags with a slight difference in the Raman reporter molecule and antibody for NSE SERS tags being 5,5-dithiobis-(2-nitrobenzoic acid) (DTNB) and antibody-NSE, respectively. On the other hand, the immune supporting substrate is synthesized by labeling both anti-CEA and anti-NSE on surface of GMNPs. The detection principle is simple; two types of SERS tags will bind together with the immune supporting substrate via their corresponding specific antigens and form sandwich-like composite, providing excellent SERS enhancement hotspots. The SERS-based immunoassay results show excellent specificity and ultrahigh sensitivity. The detection limit of CEA and NSE in human serum specimens is 1.48 pg mL^{-1} and 2.04 pg mL^{-1}, respectively. Thus, the proposed SERS-based immunoassays are expected to provide another reliable approach for early cancer screening in clinical diagnostics.

6. Multifunctional SERS sensing platform

In order to address the issue of fluctuation of SERS signals and poor reproducibility of SERS events at ultralow detection levels, multifunctional integrated SERS sensing platform is a new emerging detection system, which not only integrates the advantages of analytical approaches such as microfluidics [259,260], optofluidics [261,262], dielectrophoretics [263,264] and capillary electrophoresis [265,266] but also allows one to quantitatively detect analytes in highly diluted solutions. In addition, the introduction of paper-based plasmonic platforms into SERS-based ultrasensitive sensing study [267,268] has received considerable attention in recent years, because of their low cost, light weight, easy to control, wide accessibility, and low-carbon footprint making paper a perfect alternative to traditional substrate materials such as glass, semiconductors, and plastics.

Yang and coworkers [269] proposed a new ultrasensitive detection strategy named dynamic surface enhanced Raman spectroscopy (DSERS), which is based on measuring the Raman signals of the mixture solution containing nanoparticles and target analytes from wet state to dry state during the state translation process of SERS substrate. This detection technique demonstrated good capability of achieving ultrahigh detection sensitivity. Herein, the three types of functionalized SERS sensing platform and their practical applications will be outlined briefly.

6.1. Microfluidics-assisted SERS sensing platform

The isolation of useful SERS signals from SERS signals fluctuations and blinking originating from diffusion motions of both target analytes and noble metal NPs, inhomogeneous distributions of adsorbed analytes on metal surface, and possible laser forces exerted on either metal NPs or analytes are the major challenges to achieve quantitative analysis of target analytes in highly diluted concentrations [49,270]. Fortunately, the implementation of microfluidic techniques into SERS-based detection can address and suppress the unwanted signals, because microfluidics can confine and manipulate a solution, liquid, and colloids-type suspension in micro-scaled channels. In contrast to the commonly used macroscopic devices such as sample cell and capillary, microfluidic chips integrated with SERS detection offer many advantages, such as extremely small sample consumption, short response time, high portability, and high detection sensitivity [271,272]. To date, there are two main types of microfluidics-assisted SERS sensing platforms such as metal colloids-based microfluidics SERS systems capable of manipulating a mixture composed of metallic NPs and analytes within a liquid, and second, highly ordered metal nanostructure-embedded microfluidic systems that possess plasmonic nanostructure coated on channel interface with fixed gaps for tailored plasmonic enhancement [273]. For metal colloids-based microfluidics platform, the obtained SERS signals highly depend on the electromagnetic hotspots induced by plasmonic nanoparticles aggregation. However, uniform nanostructure-

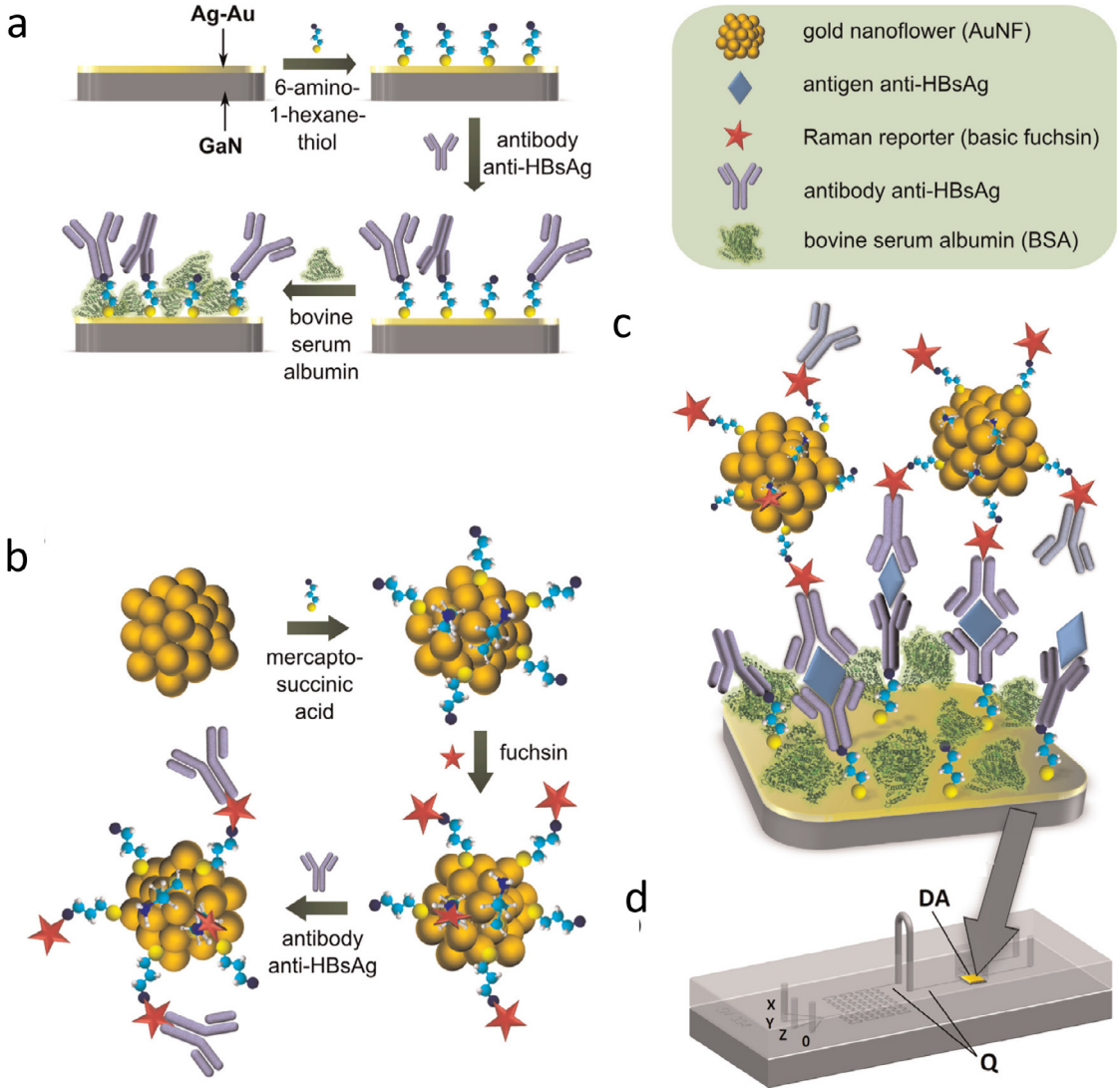

Fig. 17. Microfluidic system for the quantitative detection of HBsAg antigen by a SERS immunoassay. (a) Preparation of the capturing substrate, (b) Synthesis of the Raman reporter-labeled immuno-Au nanoflowers, (c) SERS detection of the sandwich interactions, (d) integration of a microfluidic device with the SERS-active substrate (Reproduced from Ref. [288] with permission of Elsevier B. V.)

embedded microfluidics platform can afford identical SERS enhancement sites for analytes due to their ordered distribution of hotspots.

6.1.1. Metal colloids-based microfluidics-SERS platform

Injecting small amount of mixture solutions (metal colloids and diluted target analytes solutions) into microfluidic channels not only serves as an efficient platform for monitoring mixture solutions, but also significantly improves SERS sensing sensitivity. Under high power laser irradiation, continuous flow in channels can effectively dissipate heat energy and protect analyte molecules from being damaged by laser [274]. More importantly, the SERS signals can be repeatedly detected by processing the Raman signals in a continuous detection volume replacing previous static conditions. Thus, the combination of microfluidics with SERS redefines multifunctional SERS-based sensing platforms, which are superior to common SERS detection study. In recent years, microfluidics-assisted SERS sensing platforms have been applied in various bio-analytical studies such as protein detection [275,276], immune-sensors [277,278], DNA/RNA assay [279–281], cells sorting/identification [282,283] and environment monitoring [284].

Recently, Zhou et al. [285] presented a rapid and sensitive detection method for determining bovine serum albumin (BSA) on a microfluidic chip incorporated with SERS spectroscopy. The microfluidic chip contains a T-shaped channel and two modified pneumatic valves. Interestingly, at the bottom of the channel, there is a modified poly (dimethylsiloxane) (PDMS) pneumatic valve and nanopost arrays, which are used to trap gold nanoparticles and form gold aggregates, producing efficient hotspots for SERS detection. When there is a pressure on the nanopost arrays, the channel becomes narrow in front of the valve, resulting in trapped Au NPs. Quantitative detection analysis of BSA is performed in the region forming Au aggregates by measuring the peak intensity at 1615 cm^{-1} ascribed to BSA fingerprint vibration. With the help of the proposed microfluidic chip, the detection limit of BSA can reach as low as picomolar level. Lately, a quite simple and rapid silica gel-based microfluidic platform for glycoprotein and streptavidin sensing was demonstrated with a femtomolar level detection sensitivity [286]. The microfluidic system was prepared by combining silica gel-based thin layer chromatography (TLC) plate and multifunctionalized silver coated gold NP (Ag@Au nanoparticle) enabling plasmonic enhancement. In silica gel, micrometer-

scaled pores and channels act similar to microchannels in a microfluidic device. For SERS substrate, multifunctional Ag@Au NPs are modified with 4-mercaptopyridine and glucose, respectively. The 4-mercaptopyridine acts as Raman reporter, while glucose interacts with proteins. After injecting protein solutions and Ag@Au NPs colloids into two individual channels, the aggregation of Ag@Au NPs induced by protein in channel interface can provide significant EM enhancement effects. The resulting SERS signal of 4-mercaptopyridine molecule is used for labeling concentration, with a reproducible detection limit of 1 fM and 10 fM for glycoprotein and streptavidin, respectively.

Immunoassay sensor is the most popular approach to detect disease-related biomarkers. Recently, a novel SERS-based immunoassay sensor for quantitative and sensitive detection of anthrax biomarker poly-γ-d-glutamic acid (PGA) was developed in a microfluidic device [287]. PGA can compete with PGA-conjugated gold nanoparticles to adsorb anti-PGA-immobilized magnetic beads in the microfluidic channel. Subsequently, magnetic immune-complexes are trapped by solenoids embedded within the microfluidic device, and their SERS signals can be directly measured. With the help of SERS-based microfluidic sensor, the detection limit of PGA in human serum can be determined as low as 100 pg mL^{-1}.

In addition, another efficient SERS immunoassay for quantitative detection of HBsAg antigen with a level of 0.01 IU mL^{-1} was presented in a microfluidic system [288]. In the study, the SERS immunoassays were performed on a sandwich structure with three layers (Fig. 17a–c), such as Hepatitis B virus antibodies (anti-HBsAg) anchored on GaN/Au–Ag surface through a 6-amino-1-hexanethiol (AHT) layer, Hepatitis B virus surface (HBsAg) antigen captured by anti-HBsAg, and Raman reporter basic fuchsin-labeled Au nanoflowers (antibody–FC–AuNFs). More importantly, the microfluidic chip allows us to perform and manipulate each step of the whole immunoassay process (Fig. 17d). There are four inlets (X, Y, Z, and O) used for injecting the following reagents: Bovine serum albumin (BSA) in PBS buffer solution, Hepatitis B virus surface (HBsAg) antigen in human blood plasma, Raman reporter-labeled Au-nanoflowers, PBS buffer solution, respectively. The labeled detection area (DA) is the place where sandwich structures are formed and detected by SERS. Hepatitis B virus surface (HBsAg) antigen can is quantified in this channel by measuring SERS signal of basic fuchsin (FC). It can be envisioned that the proposed SERS immunoassay could provide useful reference for other important biomarkers and point-of-care analysis in the disease diagnosis field.

Living cell is a class of complex organism composed of many biological components such as proteins, DNA, lipids, and carbohydrates, *etc*. SERS spectroscopy is well-suited to specifically detect target analytes having multiplexed components, while microfluidic chips are excellent systems employed to trap and capture cells in liquid solutions. Recently, a synergistic and portable system for specific identification, rapid detection and monitoring bacteria was demonstrated by combination of nanostructured dielectrophoresis (DEP) with SERS [289]. In the study, a nanoelectrode array made of vertically aligned carbon nanofibers was embedded in a microfluidic chip for capturing and concentration bacteria into a 200 μm × 200 μm region. In addition, a SERS substrate composed of iron oxide–gold (IO–Au) core–shell nanoovals (50 nm) labeled with a Raman reporter QSY21 was employed to attach and label bacteria via specific immunochemistry technique. The concentration of *E. coli* can be determined by measuring the SERS signal of Raman reporter QSY21. For pathogen *E. coli* cells, the integration of SERS and effective microfluidic DEP nanotechnology can significantly shorten detection time and improve detection sensitivity with a detection limit s of *E. coli* as low as 210 cfu ml^{-1}.

6.1.2. Uniform nanostructure-embedded microfluidics-SERS platform

Interestingly, metal colloids-based SERS microfluidic chips can essentially support the ultrasensitive detection of targeted analytes in a controllable flow, however the implementation of metal colloids in microfluidic channel may introduce new problems, such as a longer mixing reaction time between analyte molecules and metal NPs, cross-contamination and channel clogging due to large scaled aggregation of metal NPs. Nevertheless, these problems can be overcome by employing highly ordered metal nanostructure-embedded microfluidics device [273,290]. In these systems, the ordered nanostructure arrays do not flow with target analytes. More importantly, the regular nanostructure arrays can generate a uniform distribution of hotspots, which guarantee a huge EM enhancement gain and high reproducibility. In recent years, an increasing trend in SERS-based sensitive detection study resorts to the introduction of uniform nanostructure arrays embedded into solid-state microfluidics chip [291,292].

The following two steps are required to fabricate ordered nanostructure arrays embedded into microfluidics system- first, *in-situ* preparation of uniform SERS nanostructures inside microfluidic channel, and second, construction of microfluidic channels on top of uniform SERS nanostructures. Parisi et al. [293] demonstrated a microfluidic system with integrated novel Ag NPs decorated nanowall structures for ultrasensitive detection of crystal violet. At room temperature, Ag NP decorated nanowall structure was prepared in a microfluidic channel through *in situ* electrodeposition of Cu-core/C-sheath nanowall structure and subsequent galvanic replacement reaction. In the microfluidic channel, Ag NP decorated nanowalls produce highly quality hotspots for SERS detection. When crystal violet was used as the target analyte, the microfluidic system integrated-SERS substrate provided a detection limit as low as 50 pM. In addition, a SERS-based microfluidic device embedded with highly uniformed Ag nanodot arrays was demonstrated for performing multiplexed detection of low-concentration target analytes [294]. The highly ordered Ag nanodot array was prepared by depositing Ag on an ultrathin anodic aluminium oxide (AAO) film. Because of huge gain in EM field arising from Ag nanodot array, the multiplexed SERS signals of adenine and thiram can be realized in an ultralow detection concentration. More recently, a novel device for specific detection of polychlorinated biphenyls (PCB77) using aptamer-based SERS-microfluidic sensor was proposed [295]. To construct the microfluidic chip, the ordered Ag nanocrown arrays used for producing hotspots were embedded in a microfluidic channel at the bottom of ordered structure polydimethylsiloxane (PDMS) film. Another similar PDMS sheet was integrated with the ordered PDMS sheet forming a microfluidic chip. Moreover, with the assistance of a thiolated aptamer by forming Ag-S bonds, the target analyte molecules (PCB77) can be immobilized on SERS detection area, further developing SERS detection sensitivity of PCB77. This SERS-based microfluidic chip can obtain a lowest detectable concentration of 1.0×10^{-8} M, indicating its application for trace detection of organic pollutants.

6.1.3. Optofluidics-based SERS platform

Optofluidics is an emerging platform, which can synergistically integrate the optical systems and microfluidics [296,297] to develop the performance of analytical measurements at the microscale, such as refractive index sensing [298], fluorescence [299], optical trapping and manipulation [300,301] and SERS [302,303]. Optofluidics-based SERS platform is perfectly suited for sensitive detection of chemicals and biological analytes in extremely diluted concentrations because it can provide more reproducible and reliable SERS detection sensitivity compared with common SERS or microfluidics system. To date, many optofluidics-based SERS plat-

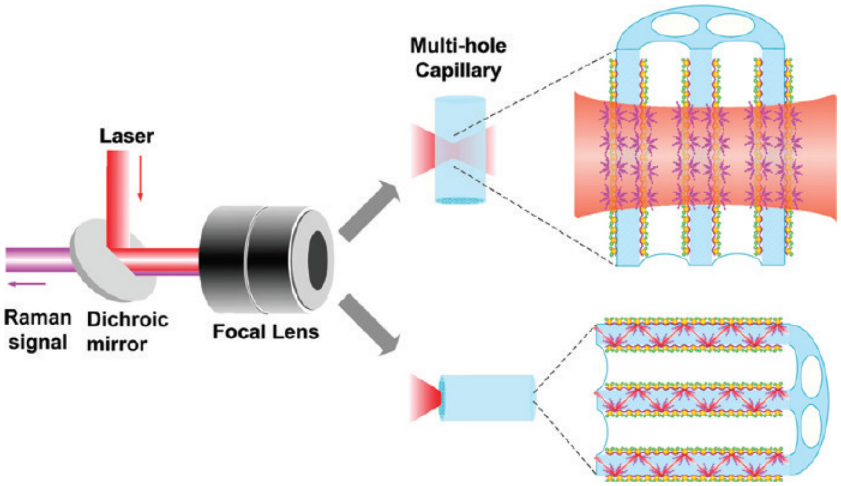

Fig. 18. Schematic of a flow-through optofluidic Raman system based on a multihole capillary. The SERS excitation and detection are arranged transversely (top) or longitudinally (bottom) with respect to the capillary. (Reproduced from Ref. [310] with permission of American chemical society.)

forms for chemicals and biological sensing have been reported [304–306]. Previously, an optofluidic ring resonator was designed to work as SERS-based sensing platform, which acted both as microfluidic sample delivery function and as a ring resonator, resulting in a detectable concentration of R6G as low as 400 pM [307]. Later, White et al. [308] reported a 3D optofluidic network system composed of packed nanoporous silica microspheres, which can be employed to trap and capture Ag NPs and adsorbed analytes, resulting in significantly improved SERS detection performance. A detectable limit of R6G is as low as 400 aM can be reached in 2 minutes after loading of R6G solutions into microfluidic channels. Thereafter, the research group developed an optofluidic SERS system based on the porous microfluidic matrix by integrating an automated micromixer and optical fibers into the device, affording an estimated detection limit of 63 ppb, 50 ppt for food contaminant melamine and fungicide thiram, respectively [309].

Guo et al. [310] developed a novel optofluidics-based SERS platform using a flow-through multihole capillary, which can provide a rapid, reliable, and 3D ultrasensitive detection for target molecule R6G, because of its large contact area for sample adsorption, inherent fluidic channels for sample delivery, and ordered structure for waveguide. Prior to injecting R6G solution into the channel, Au NPs were deposited on the inner surface of channel. Interestingly, the detection manner can be performed in two models including transverse and longitudinal method (Fig. 18). In the transverse method, the excitation laser is perpendicular to the capillary, and detectable SERS signals are determined by detection volume. However, due to the SERS excitation direction parallel to the capillary in the longitudinal method, the excitation light can be guided within the wall by total internal reflection, and quasi-guided by the hole via multi-reflection. Finally, the collected SERS signal is coupled back and guided into detectors by the wall and hole. The proposed optofluidics-based SERS system can provide a detection limit better than 100 fM for R6G. In addition, Deng et al. [309] developed an optofluidic-based SERS platform by integrating quasi-3D gold plasmonic nanostructure arrays in a poly-(dimethylsiloxane) (PDMS) chip. The excellent performance of the optofluidic SERS platform was tested by measuring the signals of pesticide malathion. Highly reproducible SERS signals of malathion can be obtained in low concentrations ranging from 0.01 to 10 ppm. Moreover, when the flow rate was increased to 0.3 mL min^{-1}, the obtained detection sensitivity was as low as 0.001 ppm. More recently, a novel optoelectrofluidic platform for SERS detection of 4, 4-bipyridine *in situ* was developed via Au decorated polystyrene microparticles, which showed highly active hotspots [311]. Owing to dielectrophoretic force mechanism, the Au/polystyrene microparticles can be concentrated at the middle of gold electrodes. Under optimal experimental conditions, the dielectrophoretic-assisted optofluidic platform can detect 4, 4-bipyridine in 100 pM levels. All in all, the combination of optofluidic and SERS can provide an automated sensing platform for on-site, highly sensitive detection of food and water contaminants.

6.2. Paper-based SERS sensing platform

As a class of both cheap and versatile materials, paper has been widely used for traditional writing, printing, packaging, and wiping for a long time in our daily life. However, with the development of modern technology, the innovative applications of paper have been developed into many scientific and technological fields far beyond its conventional functions, such as point-of-care clinical diagnosis [312–314], food safety [315], forensics [316], and environmental monitoring [317–319]. Moreover, there is an increasing demand for paper-based sensors for our daily-life applications, e.g. pH testing paper, pregnancy testing strips, blood glucose dipsticks, and urinalysis dipsticks, *etc.* Multifunctional paper-based plasmonic sensing platforms [220,320–322] integrated with plasmonic nanostructures and SERS have received tremendous attention, due to its light weight, flexibility, low cost, high accessibility, and good biodegradability. In addition, the 3D, porous, and heterogeneous interface of paper is well-suited to fabricate multifunctional SERS substrates not only possessing a number of hotspots, but also offer other important functions such as high specificity, multiplexed detection, sample separation and concentration. These excellent advantages of paper make it a promising alternative for ultrasensitive detection of analytes in practical applications. Extensive studies in recent years have attempted to integrate plasmonic nanostructures onto various papers, such as filter paper [323,324], printing paper [325] and cellulose paper [326]. The paper-based SERS substrates are usually prepared by depositing concentrated metal nanoparticles on paper surface using various approaches such as inkjet printing [326,327], screen printing [324,328], dip coating [147,329,330], *in situ* growth [331,332], vacuum deposition [333] and laser irradiation [334,335].

Recently, a paper-based SERS platform was demonstrated for non-invasive and highly sensitive cancer screening [336]. In the study, the SERS substrate was prepared by using dip coating

approach. A piece of common laboratory used filter paper was immersed into plasmonic gold nanorods solution for 24 hours to form a three-dimensional heterogeneous SERS substrate. Owing to the specific molecular changes between cancer and normal cells, the cancer screening can be performed by characterizing the two peak intensity ratios ($I_{1600/1440}$ and $I_{1440/1340}$). The diagnostic results show that the paper-based SERS platform can effectively distinguish cancer cells from normal cells in 20 patients, affording a sensitivity of 100% and specificity of 100%, respectively. Bardhan et al. [337] designed novel paper-based SERS dipsticks and swabs for sensitive detection of chemicals, proteins, and pesticide residues on a real fruit apple by incorporating multi-branched plasmonic gold nanoantennas on a filter paper. Typically, the as-prepared gold nanoantennas consisted of a spherical core with some protrusions, the tip of which could produce huge EM field gain. Thus, the paper-based SERS substrate was obtained by soaking cellulose filter paper in concentrated gold nano-antennas solution. Using 1,4-benzenedithiol and human serum albumin as target analytes, paper-based SERS dipsticks can give a detectable limit of 100 pM and 100 fM, respectively. More importantly, the paper-based SERS swabs can detect 4-aminothiophenol (62.5 pg) in solid state form, and methyl parathion (26.3 mg) on a real-life apple.

Additionally, a multifunctional paper-based SERS sensing system was prepared by dipping self-assembled Au NPs arrays onto the sharp tip (30°) of an arrow-shaped chromatographic paper strip [338]. As a plasmonic SERS substrate, the self-assembled Au NPs monolayer on the paper surface was employed to generate numerous SERS hotspots. In addition, the paper-based SERS platform also integrates two important functions such as separation and pre-concentration because of capillary force and polarity difference. Owing to tip enhanced capillary-driven force, the small tip area of the paper strip can produce much faster drying of solvent than other regions. Using R6G as analytes, the multifunctional paper-based SERS sensing system can provide a sub-attomolar detection limit of 50×10^{-18} M. More recently, an eco-friendly and ultrasensitive paper-based SERS substrate was designed by deep-ultraviolet laser irradiation method [335]. Prior to laser illumination, discontinuous metal films were prepared by depositing metal film on a hydrophobic treated filter paper. Owing to the photothermal effect induced by laser and low thermal conductivity of paper, highly density quasi-3D NP arrays were formed on the paper surface, which can provide a great number of highly effective hot spots for SERS detection. Moreover, the paper-based SERS substrate can provide stable and reproducible SERS signals within the efficient detection area. Using R6G as target analyte, the paper platform can achieve a detection limit of attomolar (10^{-18} M), which almost approaches single molecule detection performance.

Through successive ionic layer absorption and reaction (SILAR) method, Kim et al. [339] introduced an innovative fabrication approach to directly synthesize Ag NPs onto the paper surface employed for real biosensing. Interestingly, the surface of paper consists of two parts such as a hydrophilic area and a hydrophobic area. The former is employed to synthesize Ag NPs and measure SERS signals of sample, while the latter is used to prevent Ag NPs from depositing onto the paper surface. One SILAR fabrication cycle consists of treating the as-prepared paper substrate in silver nitrate solutions followed by rinsing with distilled water. Next, the paper substrate is transferred into sodium borohydride solutions for 30 s and rinsed with distilled water again. The plasmonic enhancement capacity of Ag NPs grown on paper surface can be monitored by tuning concentration of reactive solutions and treated cycle times. Owing to capillary effects, rough and porous properties of paper, the Ag NPs stacked 3D nanostructure can produce strong plasmonic coupling effect between inter-particles as well as inter-layers. The applicability of the proposed paper-based SERS platform was tested by using two real samples such as HPV-infected human cervical fluid and carcinogenesis-associated MG solution. The multifunctional paper-based SERS platform can not only specially distinguish three types of HPV (HPV-16, HPV-52, and HPV-58) in low detection concentration, but also obtain a MG detection as low as 10 pM (<0.004 ppb), which is much less than the standard limit of 2 ppb in experimental testing.

6.3. Dynamic SERS-based sensing platform

Since initial discovery of SERS in 1974, highly sensitive detection approaches based on SERS have been developed by many famous research groups, such as Van Duyne's group, Kneipp's group, Etchegoin and Le Ru's group, Nie shuming's group, Tian zhongqun's group, Halas and Moskovits's group, et al. In general, the widely used and accepted method for SERS detection is either plasmonic nanostructure-enhanced readout in wet state (*eg.*, metal colloids) or in dry state (*eg.*, films, self-assembled arrays, islands, *etc.*). Recently, Liu et al. [269,340] have proposed another new strategy to achieve ultrahigh sensitive detection of target analytes. The new approach called dynamic surface enhanced Raman spectroscopy (DSERS) can perfectly bridge wet state and dry state of metal nanostructures by measuring time-dependent SERS signals from the wet state to the dry state.

Unlike wet state-based and dry state-based detection methods, the performance of DSERS approach is highly related with the state translation of metal nanostructures from wet state to dry state. During the solvent evaporation process, SERS signals of target analytes are repeatedly collected in a fixed integration time. In addition, with the aid of capillary force, the Raman signal amplification of analytes is switched by the hotspots through forming self-closed metal nanostructure, which works in agreement with the previously reported Au nanofingers for analyte trapping and SERS sensing [341]. Thus, the basic detection strategy is that, in wet state, the metal nanostructures show a self-approach performance through the solvent capillary forces, resulting in the spontaneous formation of hotspots in a 3D place, which are beneficial for ultrasensitive SERS detection and molecule trapping [342]. However, when the metal nanostructures are completely transformed into a dry state, the solvent capillary forces disappear immediately, and the metal nanostructures recover their original positions, indicating the evanescence of Raman hotspots.

In contrast to wet state or dry state detection for SERS, DSERS possesses obvious advantages. First, DSERS is a very simple and recyclable process and does not involve any complicated nanostructure fabrication [343]. Second, it can guarantee a high detection sensitivity and good reproducibility of SERS events. Third, the used solvent acts as a switch for signal measurement, and some negative effects generated by laser illumination, such as photobleaching, photo-degradation, and photo-heating, can be significantly weakened. Due to these outstanding advantages, D-SERS has become a practical sensing platform in many scientific fields, *e.g.*, cellular secretion assays [344], pesticide residue monitoring [345,346], drugs tracing [347] and illegal additives identification [348].

Qian et al. [340] presented an extremely simple and sensitive DSERS approach for R6G detection. Prior to DSERS detection, the plasmonic substrate was simply prepared by dropping 5 μL mixture composed of Ag-shell/sphere colloids with R6G ethanol solution. With the help of D-SERS strategy, the fingerprint Raman signal ascribed to R6G can be achieved with a concentration at 10^{-16} M, which significantly superior to traditional SERS method using Ag nanospheres substrate without any signal of R6G when the concentration is at 10^{-8} M. Later, a visual online detection and rapid accurate identification of drugs in body fluid has been proposed using DSERS [347]. Due to its huge enhancement effects and good reproducibility, the Au nanorods were used as D-SERS

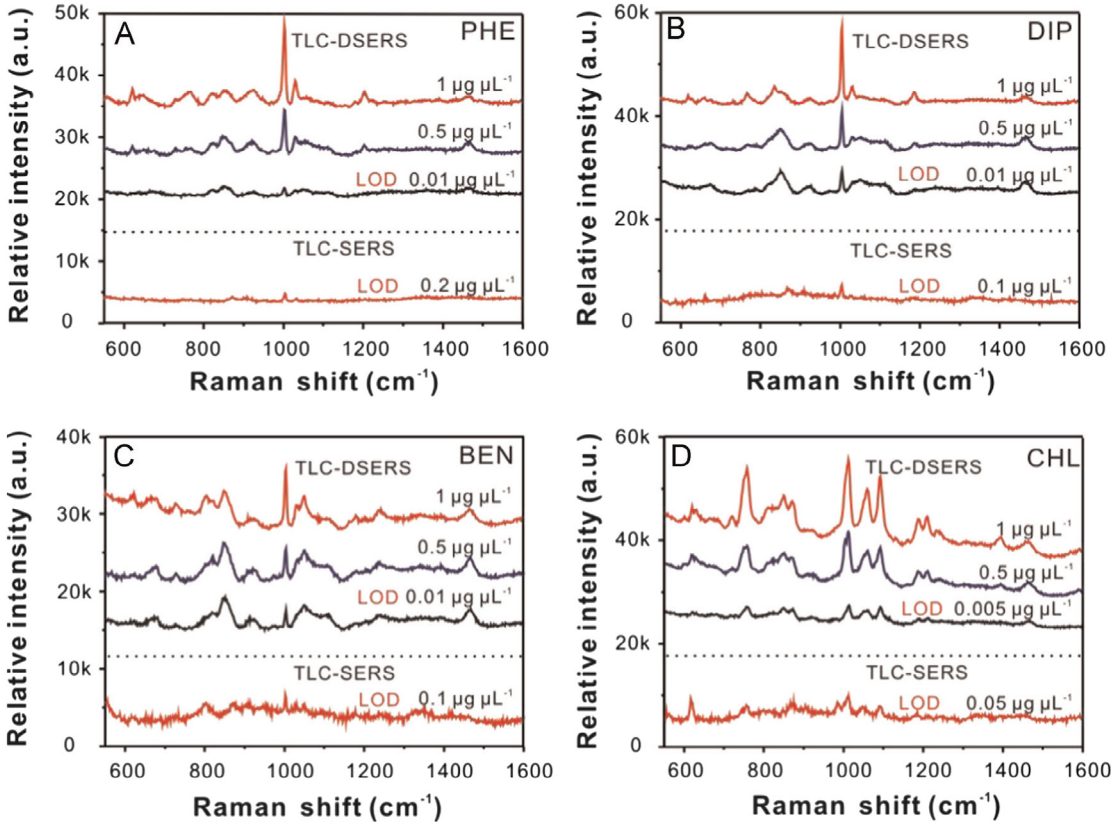

Fig. 19. SERS spectra of different drugs (A – PHE, B – DIP, C – BEN, and D – CHL) with different concentrations adulterated in BDS using 'TLC–DSERS' method versus 'TLC–SERS' method. (Reproduced from Ref. [348] with permission of Elsevier B. V.)

substrates. Without any sample pretreatment, the SERS spectra of urine and methamphetamine (MAMP) in urine were recorded by a portable Raman spectrometer. With the assistant of DSERS and support vector machine (SVM) model, a screening readout was performed to determine the presence of drugs in urine. The multifunctional sensing platform requires only 2 μL of human urine and takes no more than 2 min to complete the testing process. More importantly, when the concentration of drug MAMP is down to 0.1 ppm, it still affords an identification accuracy of better than 90%.

Very recently, a novel method DSERS combined with thin layer chromatography (TLC) was proposed and used for sensitive, online detection of illegally adulterants in botanical dietary supplements. [348]Under UV illumination, four commonly used reference adulterants (PHE, DIP, BEN and CHL) in BDS were separated on a TLC plate, respectively. Using 50% glycerol silver colloids as plasmonic substrate, the DSERS detection was continuously performed in 120 seconds, and integration time for every spectrum was 10 seconds. The strongest SERS spectra of four chemicals in various detection concentrations are shown in Fig. 19. In contrast to the obtained detection limit of TLC-SERS by used of silver colloids, the detection limits of TLC–DSERS for chemicals (PHE, DIP, BEN and CHL) was increased by 1–2 orders of magnitude, yielding 0.01 μg μL^{-1} for PHE, 0.01 μg μL^{-1} for DIP, 0.01 μg μL^{-1} for BEN, and 0.005 μg μL^{-1} for CHL, respectively. Moreover, the novel TLC–DSERS method can successfully indentify one sample containing BEN in ten real-life BDA samples.

7. Summary and future outlook

In summary, SERS-based ultrasensitive sensing platforms are the most promising approach to monitor and identify targeted analytes including molecules and inorganic ions in ultralow concentrations, and they have been successfully employed in various interdisciplinary applications related with chemistry, biology, medical, nanoscience and biophotonics. In the article, we systematically reviewed and discussed the ultrasensitive sensing strategies based on the latest practical applications by introducing resonance enhancement techniques, high quality nanostructures, highly efficient adsorption mechanisms, and multifunctional integrated SERS-based sensing platforms.

Various studies have confirmed that the SERS platforms incorporated with resonance enhancement techniques and devices including resonant adsorption, optical coherence, and optical waveguide, can essentially develop a higher ultrasensitive detection capability compared to common SERS. However, some major challenges restrict their use for real-life applications. For example, due to limited output wavelength, and matching the plasmonic resonance frequency efficiently with frequency of electronic transition of analytes in SERRS study are still a reason of concern. A possible solution to address this issue is to design the SERS substrates with a wide SPA band region or multiple resonance band, which can efficiently match the plasmonic coupling between incident light and SERS substrates, and absorption excitation between incident light and targeted analytes. Recently, the appearance of double resonance SERS substrates which can provide much higher enhancement gain than the single resonance model has been reported [349,350].

The SECARS technique involves the use of expensive femtosecond or picosecond lasers as light sources, which can lead to melting, change in shape and even fragmentation of nanoparticles. Prior to SECARS detection, the coating and decoration of nanoparticles needs to be performed to protect nanoparticles from damage. While low spectral resolution induced by ultrashort pulses and

strong non-resonant background interference also hinder the performance of SECARS, these drawbacks can be suppressed by optical approaches, such as laser pulse shaping and time-resolved detection [351]. Since CARS is a weak third-order nonlinear process, the main challenge for SECARS detection is tailoring the plasmonic substrates to achieve the strongest CARS enhancement effects such that the pump, Stokes and anti-Stokes photons are resonant with the SECARS substrates simultaneously in the same spatial position. The Fano resonance model are presently the ideal plasmonic metamaterials with strong plasmonic coupling to address this concern [352–355]. Thus, more novel, sensitive, stable, and specific plasmonic Fano resonance nanostructures need to be proposed for improved CARS detection sensitivity.

Optical waveguide-based sensing platforms have also demonstrated high performance for SERS detection. Among various waveguide devices, the famous Kretschmann configuration semicylindrical prism is the most widely used model for SERS sensing. The SERS-active sensing layers are usually noble metal NPs or films which provide plasmonic EM enhancement gain. Additionally, the coating of semiconducting and polymeric materials can further generate SERS effects due to the development of charge-transfer. Meanwhile, it should be noted that semicylindrical prism cannot be employed to detect analytes in liquid solutions. Fortunately, the development of optical fiber waveguide sensor addresses the dilemma. Due to its ultra-high detection sensitivity, the optical fiber waveguide sensors are considered as ideal candidates for the next generation SERS substrate. Typically, the optical fiber sensor integrated-microfluidic device is expected to dominate SERS detection as it improves the detection sensitivity considerably as well as performing quantitative measurement of target analytes.

Plasmonic nanostructures play the important role of mediators that couple incident light with targeted analytes. We have summarized various plasmonic nanostructures with ultrahigh SERS enhancement capability, such as nanoaggregates, nanoassemblies, ordered plasmonic nanostructures, alloys, carbon-based materials, Si-based nanomaterials, magnetic nanomaterials, MOFs, and 3D nanostructured arrays. A number of practical studies in biosensing, bioimaging, bioseparation, cancer screening/therapy, biomedical diagnostics, pollutant monitoring, and food safety, *etc.*, have confirmed the ultrahigh SERS detection capability of plasmonic nanosensors by optimizing of their SPR features such as morphology, size, composition, surface modification, and dimensionality. However, external force-driven nanoaggregates usually exhibit random morphology and unexpected enhancement hotspots. Therefore, good reproducibility of SERS events remains a major bottleneck which needs to be addressed. A possible solution at present, is to employ electron beam lithography and nanoimprinting methods, which can design software-aided random nanostructures. In summary, designing and creating novel plasmonic nanostructures with high sensitivity, high specificity, high reproducibility, high compatibility, and high stability needs major focus of the future research to bring SERS based ultrasensitive sensing at the forefront.

The roles of efficient adsorption mechanisms including covalent bonding, hydrophobic interaction, charge-selective mechanism, π-π stacking interaction, and immunoassays are elaborated in developing the adsorption efficiency of plasmonic nanostructures towards various target analytes, and further improve their SERS detection sensitivity. For SERS detection, covalent bonding is suitable for the analytes containing active heterocyclic atoms (*eg.*, S, N, O), while positive-type target analytes prefer to be adsorbed on the surface of oppositely charged plasmonic nanostructures via electrostatic interaction. Super hydrophobic nanostructure surface not only enables a liquid droplet containing target analytes to maintain its quasi-spherical shape for a long time, but also can efficiently regulate and concentrate water-insoluble target molecules onto plasmonic hotspots area, resulting in huge amplification of SERS signals originating from target analytes. More interestingly, π-π stacking interaction is a typical non-covalent method to immobilize and capture aromatic analytes close to the plasmonic nanostructure. Thus, it provides an effective guideline for monitoring the aromatic molecules that have low affinity to metal surfaces. An important factor to keep in mind is the creation of plasmonic SERS substrate possessing π-π stacking adsorption capacity. Polymer-decorated NPs may offer a possible solution to this, wherein the used polymer template consists of a number of aromatic moieties (π donators), which can be capped and wrapped on the metal NPs surface. Poly (styrenesulfonate) (PSS)-based polymer family can be used as potential templates as they provide excellent π donators. In addition, another possible approach is to fabricate carbon-based hybrid nanomaterials such as graphene-based, graphene oxide-based, carbon nanotubes-based nanocomposites, because of their abundant π electron systems in molecular structure. Furthermore, immunoassays offer high affinity and specificity between antibodies and antigens. The famous sandwich configuration of the SERS-based immunoassays platforms is widely employed in biophotonics and nanomedicine fields for disease biomarker monitoring, cancer screening and biomedical diagnostics. Thus, more novel SERS-based immunosensors capable of precisely *in vivo* bioimaging and cancer therapy would be preferred and valuable for future study.

In the past decades, various multifunctional integrated SERS sensing platforms have sprung up for addressing the quantitative analysis issue of SERS. The integration of SERS with microfluidic or optofluidic chips has helped to overcome the SERS signal variation issue in highly diluted solutions as well as to achieve the quantitative determination for analytes with ultralow detection sensitivity. However, one major challenge for developing multifunctional microfluidics-based and optofluidics-based systems is the high cost and sophisticated fabrication techniques involved (focused ion beam (FIB) and electron beam lithography (EBL)) in integrating the uniform solid plasmonic arrays into microchannels. For a larger practical outlook, the SERS substrates prepared by low cost and simple fabrication methods are more reasonable. For example, the introduction of inexpensive and versatile paper-based plasmonic substrates into microfluidics device has demonstrated its great potential in SERS detection [356,357]. In addition, the portable miniaturization of optofluidics-based SERS devices integrated with lasers and Raman spectrometers may possibly set the standard for designing next generation SERS-based detection platform for on-site measurement. Unlike the classical wet and dry state SERS detection strategies, D-SERS is the latest emerging sensing approach, which can bridge the wet state and dry state approaches. Recent research developments and applications of using DSERS as outlined in the review have confirmed that it indeed possesses ultrahigh detection capability by monitoring the state transformation of metal nanoparticles, providing a new methodology for future SERS detection study. Overall, with the rapid advancement of modern technology, we foresee that there will be more ultrasensitive detection strategies related with SERS to emerge within the next few years.

Acknowledgements

Parts of this work was supported by the National Natural Science Foundation of China (61605121/61620106016/61525503/61378091/61405123); the National Basic Research Program of China (2015CB352005); Guangdong Natural Science Foundation Innovation Team (2014A030312008); Hong Kong, Macao and Taiwan cooperation innovation platform & major projects of international cooperation in Colleges and Universities in Guangdong Province (2015KGJHZ002); and Shenzhen Basic Research

Project (JCYJ20150930104948169/JCYJ20160328144746940/GJHZ20160226202139185); the Training Plan of Guangdong Province Outstanding Young Teachers in Higher Education Institutions (Yq2013142). Authors also acknowledge Singapore Ministry of Education (Grants Tier 2 MOE2010-T2-2-010 (M4020020.040 ARC2/11) and Tier 1 M4010360.040 RG29/10), NTU-NHG Innovation Collaboration Grant (No. M4061202.040), NTU-A*STAR Silicon Technologies, Centre of Excellence under the program grant (No. 11235100003), NEWRI seed funding (No. NEWRI SF20140901) and School of Electrical and Electronic Engineering at NTU for funding and support.

References

[1] J. Homola, Chem. Rev. 108 (2008) 462–493.
[2] D.M. Rissin, C.W. Kan, T.G. Campbell, S.C. Howes, D.R. Fournier, L. Song, T. Piech, P.P. Patel, L. Chang, A.J. Rivnak, E.P. Ferrell, J.D. Randall, G.K. Provuncher, D.R. Walt, D.C. Duffy, Nat. Biotechnol. 28 (2010) 595–599.
[3] O.R. Miranda, H.T. Chen, C.C. You, D.E. Mortenson, X.C. Yang, U.H.F. Bunz, V.M. Rotello, J. Am. Chem. Soc. 132 (2010) 5285–5289.
[4] H.X. Jia, Z.P. Li, C.H. Liu, Y.Q. Cheng, Angew. Chem. Int. Ed. 49 (2010) 5498–5501.
[5] L. Guerrini, Z. Krpetic, D. van Lierop, R.A. Alvarez-Puebla, D. Graham, Angew. Chem. Int. Ed. 54 (2015) 1144–1148.
[6] C.Y. Zhang, H.C. Yeh, M.T. Kuroki, T.H. Wang, Nat. Mater. 4 (2005) 826–831.
[7] D.A. Giljohann, C.A. Mirkin, Nature 462 (2009) 461–464.
[8] J.E. Reiner, A. Balijepalli, J.W.F. Robertson, J. Campbell, J. Suehle, J.J. Kasianowicz, Chem. Rev. 112 (2012) 6431–6451.
[9] F. Patolsky, G.F. Zheng, C.M. Lieber, Nat. Protoc. 1 (2006) 1711–1724.
[10] F. Patolsky, G. Zheng, C.M. Lieber, Nanomedicine-Uk 1 (2006) 51–65.
[11] J.F. Li, Y.F. Huang, Y. Ding, Z.L. Yang, S.B. Li, X.S. Zhou, F.R. Fan, W. Zhang, Z.Y. Zhou, D.Y. Wu, B. Ren, Z.L. Wang, Z.Q. Tian, Nature 464 (2010) 392–395.
[12] N.F. Xu, L.G. Xu, W. Ma, L.Q. Liu, H. Kuang, C.L. Xu, Food Agric. Immunol. 26 (2015) 635–644.
[13] C. Muehlethaler, M. Leona, J.R. Lombardi, Anal. Chem. 88 (2016) 152–169.
[14] M.B. Pushkarsky, I.G. Dunayevskiy, M. Prasanna, A.G. Tsekoun, R. Go, C.K.N. Patel, Proc. Natl. Acad. Sci. U.S.A. 103 (2006) 19630–19634.
[15] J.S. Lee, M.S. Han, C.A. Mirkin, Angew. Chem. Int. Ed. 46 (2007) 4093–4096.
[16] R.A. Alvarez-Puebla, R. Contreras-Caceres, I. Pastoriza-Santos, J. Perez-Juste, L. M. Liz-Marzan, Angew. Chem. Int. Ed. 48 (2009) 138–143.
[17] S.R. Lipsky, M.M. Shahin, Nature 197 (1963), 625-&.
[18] M. Martelanc, L. Ziberna, S. Passamonti, M. Franko, Talanta 154 (2016) 92–98.
[19] A.C. Manetta, L. Di Giuseppe, M. Giammarco, I. Fusaro, A. Simonella, A. Gramenzi, A. Formigoni, J. Chromatogr. A 1083 (2005) 219–222.
[20] W.J. Xie, A.S. Xu, E.S. Yeung, Anal. Chem. 81 (2009) 1280–1284.
[21] J. Singer, W.C. Schnute, J.E. Shively, C.W. Todd, A.D. Riggs, Anal. Biochem. 94 (1979) 297–301.
[22] S. Kinani, S. Bouchonnet, N. Milan, I. Ricordel, J. Chromatogr. A 1141 (2007) 131–137.
[23] A.S. Reisch, O. Elpeleg, Method Cell Biol. 80 (2007) 199–222.
[24] J.N. Bixler, M.T. Cone, B.H. Hokr, J.D. Mason, E. Figueroa, E.S. Fry, V.V. Yakovlev, M.O. Scully, Proc. Natl. Acad. Sci. U.S.A. 111 (2014) 7208–7211.
[25] P. Zhang, H. Liu, S.Z. Ma, S. Men, Q.Z. Li, X. Yang, H.N. Wang, A.Y. Zhang, Biosens. Bioelectron. 80 (2016) 538–542.
[26] K. Kneipp, H. Kneipp, I. Itzkan, R.R. Dasari, M.S. Feld, Chem. Rev. 99 (1999) 2957.
[27] K. Kneipp, H. Kneipp, J. Kneipp, Accounts Chem. Res. 39 (2006) 443–450.
[28] P.L. Stiles, J.A. Dieringer, N.C. Shah, R.R. Van Duyne, Ann. Rev. Anal. Chem. 1 (2008) 601–626.
[29] E.C.L. Ru, P.G. Etchegoin, Principles of Surface-Enhanced Raman Spectroscopy, 2009.
[30] A. Campion, P. Kambhampati, Chem. Soc. Rev. 27 (1998) 241–250.
[31] L.A. Lane, X. Qian, S. Nie, Chem. Rev. 115 (2015) 10489–10529.
[32] S. Schlucker, Angew. Chem. 53 (2014) 4756–4795.
[33] M.E. Stewart, C.R. Anderton, L.B. Thompson, J. Maria, S.K. Gray, J.A. Rogers, R. G. Nuzzo, Chem. Rev. 108 (2008) 494–521.
[34] S. Zeng, D. Baillargeat, H.-P. Ho, K.-T. Yong, Chem. Soc. Rev. 43 (2014) 3426–3452.
[35] W.C. Law, K.T. Yong, A. Baev, P.N. Prasad, ACS Nano 5 (2011) 4858–4864.
[36] J.H. Xian, L.C. Chen, H.B. Niu, J.L. Qu, J. Song, Nanoscale 6 (2014) 13994–14001.
[37] Y.Q. Wang, B. Yan, L.X. Chen, Chem. Rev. 113 (2013) 1391–1428.
[38] D. Grasseschi, H.E. Toma, Coord. Chem. Rev. 333 (2017) 108–131.
[39] X. Tan, J. Melkersson, S. Wu, L. Wang, J. Zhang, Chemphyschem 17 (2016) 2630–2639.
[40] W.R. Browne, J.J. McGarvey, Coord. Chem. Rev. 251 (2007) 454–473.
[41] A. Krolikowska, Electrochim. Acta 111 (2013) 952–995.
[42] M.G. Sceats, J. Opt. Soc. Am. 70 (1980), 639-639.
[43] J.P. Bravo-Vasquez, H. Fenniri, J. Phys. Chem. C 113 (2009) 12897–12900.
[44] N.P.W. Pieczonka, G. Moula, R.F. Aroca, Langmuir 25 (2009) 11261–11264.
[45] D.V. Chulhai, Z.W. Hu, J.E. Moore, X. Chen, L. Jensen, Annu. Rev. Phys. Chem. 67 (2016) 541–564.
[46] J.N. He, C.Z. Fan, P. Ding, S.M. Zhu, E.J. Liang, Sci. Rep.-Uk 6 (2016).
[47] H. Hakkinen, Nat. Chem. 4 (2012) 443–455.
[48] S. Adams, J.Z. Zhang, Coord. Chem. Rev. 320 (2016) 18–37.
[49] S.M. Nie, S.R. Emery, Science 275 (1997) 1102–1106.
[50] H.X. Xu, E.J. Bjerneld, M. Kall, L. Borjesson, Phys. Rev. Lett. 83 (1999) 4357–4360.
[51] H.B. Zhou, S.Y. Lin, Y.C. Nie, D.T. Yang, Q.Q. Wang, W.J. Chen, N. Huang, Z.J. Jiang, S.Z. Chen, Analyst 140 (2015) 7518–7521.
[52] L. Li, S.F. Lim, A.A. Puretzky, R. Riehn, H.D. Hallen, Appl. Phys. Lett. 101 (2012).
[53] D.O. Sigle, E. Perkins, J.J. Baumberg, S. Mahajan, J. Phys. Chem. Lett. 4 (2013) 1449–1452.
[54] T. Ding, D.O. Sigle, L.O. Hermann, D. Wolverson, J.J. Baumberg, Acs Appl. Mater. Interface 6 (2014) 17358–17363.
[55] S.K. Jha, Z. Ahmed, M. Agio, Y. Ekinci, J.F. Loffler, J. Am. Chem. Soc. 134 (2012) 1966–1969.
[56] S.K. Jha, Y. Ekinci, M. Agio, J.F. Loffler, Analyst 140 (2015) 5671–5677.
[57] W.G. Qu, L.Q. Lu, L. Lin, A.W. Xu, Nanoscale 4 (2012) 7358–7361.
[58] J. Song, J. Qu, M.T. Swihart, P.N. Prasad, Nanomed. Nanotechnol. Biol. Med. 12 (2016) 771–788.
[59] X.M. Qian, X.H. Peng, D.O. Ansari, Q. Yin-Goen, G.Z. Chen, D.M. Shin, L. Yang, A. N. Young, M.D. Wang, S.M. Nie, Nat. Biotechnol. 26 (2008) 83–90.
[60] A. Samanta, K.K. Maiti, K.S. Soh, X.J. Liao, M. Vendrell, U.S. Dinish, S.W. Yun, R. Bhuvaneswari, H. Kim, S. Rautela, J.H. Chung, M. Olivo, Y.T. Chang, Angew. Chem. Int. Ed. 50 (2011) 6089–6092.
[61] G. von Maltzahn, A. Centrone, J.H. Park, R. Ramanathan, M.J. Sailor, T.A. Hatton, S.N. Bhatia, Adv. Mater. 21 (2009) 3175.
[62] S. Harmsen, M.A. Bedics, M.A. Wall, R.M. Huang, M.R. Detty, M.F. Kircher, Nat. Commun. 6 (2015).
[63] S. Harmsen, R.M. Huang, M.A. Wall, H. Karabeber, J.M. Samii, M. Spaliviero, J.R. White, S. Monette, R. O'Connor, K.L. Pitter, S.A. Sastra, M. Saborowski, E.C. Holland, S. Singer, K.P. Olive, S.W. Lowe, R.G. Blasberg, M.F. Kircher, Sci. Transl. Med. 7 (2015).
[64] R. Huang, S. Harmsen, J.M. Samii, H. Karabeber, K.L. Pitter, E.C. Holland, M.F. Kircher, Theranostics 6 (2016) 1075–1084.
[65] X. Hua, D.V. Voronine, C.W. Ballmann, A.M. Sinyukov, A.V. Sokolov, M.O. Scully, Phys. Rev. A 89 (2014).
[66] P.D. Maker, R.W. Terhune, Phys. Rev. 148 (1966), 990-990.
[67] C.L. Evans, X.S. Xie, Ann. Rev. Anal. Chem. 1 (2008) 883–909.
[68] H. Chew, D.S. Wang, M. Kerker, J. Opt. Soc. Am. B 1 (1984) 56–66.
[69] E.J. Liang, A. Weippert, J.M. Funk, A. Materny, W. Kiefer, Chem. Phys. Lett. 227 (1994) 115–120.
[70] T.W. Koo, S. Chan, A.A. Berlin, Opt. Lett. 30 (2005) 1024–1026.
[71] J.A. Fan, K. Bao, C.H. Wu, J.M. Bao, R. Bardhan, N.J. Halas, V.N. Manoharan, G. Shvets, P. Nordlander, F. Capasso, Nano Lett. 10 (2010) 4680–4685.
[72] Y. Zhang, Y.-R. Zhen, O. Neumann, J.K. Day, P. Nordlander, N.J. Halas, Nat. Commun. 5 (2014) 4424.
[73] C. Steuwe, C.F. Kaminski, J.J. Baumberg, S. Mahajan, Nano Lett. 11 (2011) 5339–5343.
[74] S. Yampolsky, D.A. Fishman, S. Dey, E. Hulkko, M. Banik, E.O. Potma, V.A. Apkarian, Nat. Photonics 8 (2014) 650–656.
[75] Y.F. Wang, W.D. Ruan, J.H. Zhang, B. Yang, W.Q. Xu, B. Zhao, J.R. Lombardi, J. Raman Spectrosc. 40 (2009) 1072–1077.
[76] S.J. Pearce, M.E. Pollard, S.Z. Oo, R. Chen, M.D.B. Charlton, Appl. Phys. Lett. 105 (2014).
[77] D.B. Hu, Z.M. Qi, J. Phys. Chem. C 117 (2013) 16175–16181.
[78] B. Dong, W. Zhang, Z.P. Li, M.T. Sun, Plasmonics 6 (2011) 189–193.
[79] S. Wang, Z.Y. Wu, L. Chen, Y.J. Gu, H.L. Wang, S.P. Xu, W.Q. Xu, J. Phys. Chem. C 119 (2015) 24942–24949.
[80] Y.J. Gu, S.P. Xu, H.B. Li, S.Y. Wang, M. Cong, J.R. Lombardi, W.Q. Xu, J. Phys. Chem. Lett. 4 (2013) 3153–3157.
[81] Y. Lee, J. Lee, T.K. Lee, J. Park, M. Ha, S.K. Kwak, H. Ko, ACS Appl. Mater. Interface 7 (2015) 26421–26429.
[82] C.C. Fu, Y.J. Gu, Z.Y. Wu, Y.Y. Wang, S.P. Xu, W.Q. Xu, Sensor Actuat. B-Chem. 201 (2014) 173–176.
[83] D.-B. Hu, Z.-M. Qi, J. Phys. Chem. C 117 (2013) 16175–16181.
[84] F. Peyskens, A. Dhakal, P. Van Dorpe, N. Le Thomas, R. Baets, ACS Photonics 3 (2016) 102–108.
[85] A. Amezcua-Correa, J. Yang, C.E. Finlayson, A.C. Peacock, J.R. Hayes, P.J.A. Sazio, J.J. Baumberg, S.M. Howdle, Adv. Funct. Mater. 17 (2007) 2024–2030.
[86] S.Y. Wang, C.Y. Liu, H.L. Wang, G. Chen, M. Cong, W. Song, Q. Jia, S.P. Xu, W.Q. Xu, ACS Appl. Mater. Interface 6 (2014) 11706–11713.
[87] T. Gong, Y. Cui, D. Goh, K.K. Voon, P.P. Shum, G. Humbert, J.-L. Auguste, X.-Q. Dinh, K.-T. Yong, M. Olivo, Biosens. Bioelectron. 64 (2015) 227–233.
[88] P.C. Lee, D. Meisel, J. Phys. Chem. 86 (1982) 3391–3395.
[89] K. Kneipp, Y. Wang, H. Kneipp, L.T. Perelman, I. Itzkan, R. Dasari, M.S. Feld, Phys. Rev. Lett. 78 (1997) 1667–1670.
[90] K. Kneipp, H. Kneipp, V.B. Kartha, R. Manoharan, G. Deinum, I. Itzkan, R.R. Dasari, M.S. Feld, Phys. Rev. E 57 (1998) R6281–R6284.
[91] X.H. Zhang, C.Y. Lin, Q.Y. Liu, A.H. Liang, RSC Adv. 4 (2014) 959–962.
[92] Y. Fang, Science 322 (2008), 1790-1790.
[93] Y. Fang, N.H. Seong, D.D. Dlott, Science 321 (2008) 388–392.
[94] N.A. Abu Hatab, J.M. Oran, M.J. Sepaniak, ACS Nano 2 (2008) 377–385.
[95] S.M. Wells, S.D. Retterer, J.M. Oran, M.J. Sepaniak, ACS Nano 3 (2009) 3845–3853.
[96] J.J. Liang, H.W. Liu, C.H. Huang, C.Z. Yao, Q.Q. Fu, X.Q. Li, D.L. Cao, Z. Luo, Y. Tang, Anal. Chem. 87 (2015) 5790–5796.

[97] B. Yang, X.C. Chen, R.Y. Liu, B.H. Liu, C.L. Jiang, RSC Adv. 5 (2015) 77755–77759.
[98] T. Yang, J. Ma, S.J. Zhen, C.Z. Huang, ACS Appl. Mater. Interface 8 (2016) 14802–14811.
[99] Y.H. Zheng, L. Rosa, T. Thai, S.H. Ng, D.E. Gomez, H. Ohshima, U. Bach, J. Mater. Chem. A 3 (2015) 240–249.
[100] J.B. Song, B. Duan, C.X. Wang, J.J. Zhou, L. Pu, Z. Fang, P. Wang, T.T. Lim, H.W. Duan, J. Am. Chem. Soc. 136 (2014) 6838–6841.
[101] Y.D. Sun, Z.Z. Han, H.L. Liu, S.N. He, L.B. Yang, J.H. Liu, Nanoscale 7 (2015) 6619–6626.
[102] L. Fabris, M. Dante, T.Q. Nguyen, J.B.H. Tok, G.C. Bazan, Adv. Funct. Mater. 18 (2008) 2518–2525.
[103] N. Guarrotxena, G.C. Bazan, Chem. Commun. 47 (2011) 8784–8786.
[104] H.L. Marks, M.V. Pishko, G.W. Jackson, G.L. Cote, Anal. Chem. 86 (2014) 11614–11619.
[105] Y.Y. Zhu, H. Kuang, L.G. Xu, W. Ma, C.F. Peng, Y.F. Hua, L.B. Wang, C.L. Xu, J. Mater. Chem. 22 (2012) 2387–2391.
[106] C.G. Wang, Y. Chen, T.T. Wang, Z.F. Ma, Z.M. Su, Adv. Funct. Mater. 18 (2008) 355–361.
[107] Y.X. Li, Z.F. Ma, Nanotechnology 24 (2013).
[108] L.B. Zhong, J. Yin, Y.M. Zheng, Q. Liu, X.X. Cheng, F.H. Luo, Anal. Chem. 86 (2014) 6262–6267.
[109] R.G. Freeman, K.C. Grabar, K.J. Allison, R.M. Bright, J.A. Davis, A.P. Guthrie, M. B. Hommer, M.A. Jackson, P.C. Smith, D.G. Walter, M.J. Natan, Science 267 (1995) 1629–1632.
[110] T. Dadosh, Y. Gordin, R. Krahne, I. Khivrich, D. Mahalu, V. Frydman, J. Sperling, A. Yacoby, I. Bar-Joseph, Nature 436 (2005) 677–680.
[111] A.S.D.S. Indrasekara, B.J. Paladini, D.J. Naczynski, V. Starovoytov, P.V. Moghe, L. Fabris, Adv. Healthcare Mater. 2 (2013) 1370–1376.
[112] X.L. Wu, P. Fu, W. Ma, L.G. Xu, H. Kuang, C.L. Xu, RSC Adv. 5 (2015) 73395–73398.
[113] L.G. Xu, H.H. Yin, W. Ma, H. Kuang, L.B. Wang, C.L. Xu, Biosens. Bioelectron. 67 (2015) 472–476.
[114] S. Li, L. Xu, W. Ma, H. Kuang, L. Wang, C. Xu, Small 11 (2015) 3435–3439.
[115] L.G. Xu, S. Zhao, W. Ma, X.L. Wu, S. Li, H. Kuang, L.B. Wang, C.L. Xu, Adv. Funct. Mater. 26 (2016) 1602–1608.
[116] M.L. Shi, J. Zheng, C.H. Liu, G.X. Tan, Z.H. Qing, S. Yang, J.F. Yang, Y.J. Tan, R.H. Yang, Biosens. Bioelectron. 77 (2016) 673–680.
[117] M.D. Sonntag, J.M. Klingsporn, A.B. Zrimsek, B. Sharma, L.K. Ruvuna, R.P. Van Duyne, Chem. Soc. Rev. 43 (2014) 1230–1247.
[118] J. Lee, B. Hua, S. Park, M. Ha, Y. Lee, Z. Fan, H. Ko, Nanoscale 6 (2014) 616–623.
[119] A. Li, L. Tang, D. Song, S. Song, W. Ma, L. Xu, H. Kuang, X. Wu, L. Liu, X. Chen, C. Xu, Nanoscale 8 (2016) 1873–1878.
[120] L. Cheng, C.S. Ma, G. Yang, H.J. You, J.X. Fang, J. Mater. Chem. A 2 (2014) 4534–4542.
[121] C.Y. Song, L.H. Min, N. Zhou, Y.J. Yang, B.Y. Yang, L. Zhang, S. Su, L.H. Wang, RSC Adv. 4 (2014) 41666–41669.
[122] J.P. Xie, Q.B. Zhang, J.Y. Lee, D.I.C. Wang, ACS Nano 2 (2008) 2473–2480.
[123] G.N. Zhang, J.R. Li, A.G. Shen, J.M. Hu, Phys. Chem. Chem. Phys. 17 (2015) 21261–21267.
[124] H.M. Song, L. Deng, N.M. Khashab, Nanoscale 5 (2013) 4321–4329.
[125] A. Dandapat, T.K. Lee, Y.M. Zhang, S.K. Kwak, E.C. Cho, D.H. Kim, ACS Appl. Mater. Interface 7 (2015) 14793–14800.
[126] S.Y. Chou, C.C. Yu, Y.T. Yen, K.T. Lin, H.L. Chen, W.F. Su, Anal. Chem. 87 (2015) 6017–6024.
[127] S. Botti, L. Cantarini, S. Almaviva, A. Puiu, A. Rufoloni, Chem. Phys. Lett. 592 (2014) 277–281.
[128] P. Wang, M. Xia, O. Liang, K. Sun, A.F. Cipriano, T. Schroeder, H.N. Liu, Y.H. Xie, Anal. Chem. 87 (2015) 10255–10261.
[129] S. Zhao, W. Ma, L.G. Xu, X.L. Wu, H. Kuang, L.B. Wang, C.L. Xu, Biosens. Bioelectron. 68 (2015) 593–597.
[130] L. Xu, W. Yan, W. Ma, H. Kuang, X. Wu, L. Liu, Y. Zhao, L. Wang, C. Xu, Adv. Mater. 27 (2015) 1706–1711.
[131] J.J. Feng, X.L. Wu, W. Ma, H. Kuang, L.G. Xu, C.L. Xu, Chem. Commun. 51 (2015) 14761–14763.
[132] M. Ma, H.H. Yin, L.G. Xu, X.L. Wu, H. Kuang, L.B. Wang, C.L. Xu, Chem. Commun. 50 (2014) 9737–9740.
[133] W. Fan, Y.H. Lee, S. Pedireddy, Q. Zhang, T.X. Liu, X.Y. Ling, Nanoscale 6 (2014) 4843–4851.
[134] D. Yim, H. Kang, S.J. Jeon, H.I. Kim, J.K. Yang, T.W. Kang, S. Lee, J. Choo, Y.S. Lee, J.W. Kim, J.H. Kim, Analyst 140 (2015) 3362–3367.
[135] L.L. Zhang, C.L. Jiang, Z.P. Zhang, Nanoscale 5 (2013) 3773–3779.
[136] Y. Zhao, W.C. Zeng, Z.C. Tao, P.H. Xiong, Y. Qu, Y.W. Zhu, Chem. Commun. 51 (2015) 866–869.
[137] M.M. Liu, W. Chen, Biosens. Bioelectron. 46 (2013) 68–73.
[138] Z. Fan, R. Kanchanapally, P.C. Ray, J. Phys. Chem. Lett. 4 (2013) 3813–3818.
[139] H.L. Chen, Z.M. Liu, S.Y. Li, C.K. Su, X.J. Qiu, H.Q. Zhong, Z.Y. Guo, Theranostics 6 (2016) 1096–1104.
[140] L.L. Wang, J. Zheng, Y.H. Li, S. Yang, C.H. Liu, Y. Xiao, J.S. Li, Z. Cao, R.H. Yang, Anal. Chem. 86 (2014) 12348–12354.
[141] J. Ge, Y. Li, J. Wang, Y. Pu, W.D. Xue, X.G. Liu, J. Alloy. Compd. 663 (2016) 166–171.
[142] F.M. Zou, H.J. Zhou, T.V. Tan, J. Kim, K. Koh, J. Lee, ACS Appl. Mater. Interface 7 (2015) 12168–12175.
[143] D.A. Heller, S. Baik, T.E. Eurell, M.S. Strano, Adv. Mater. 17 (2005) 2793.
[144] M.L. Schipper, N. Nakayama-Ratchford, C.R. Davis, N.W.S. Kam, P. Chu, Z. Liu, X.M. Sun, H.J. Dai, S.S. Gambhir, Nat. Nanotechnol. 3 (2008) 216–221.
[145] Z. Chen, S.M. Tabakman, A.P. Goodwin, M.G. Kattah, D. Daranciang, X.R. Wang, G.Y. Zhang, X.L. Li, Z. Liu, P.J. Utz, K.L. Jiang, S.S. Fan, H.J. Dai, Nat. Biotechnol. 26 (2008) 1285–1292.
[146] T.P. McNicholas, K. Zhao, C.H. Yang, S.C. Hernandez, A. Mulchandani, N.V. Myung, M.A. Deshusses, J. Phys. Chem. C 115 (2011) 13927–13931.
[147] K. Zhang, J. Ji, X.N. Fang, L. Yan, B.H. Liu, Analyst 140 (2015) 134–139.
[148] M. Shaban, A.R. Galaly, Sci Rep-Uk 6 (2016).
[149] Y. He, C.H. Fan, S.T. Lee, Nano Today 5 (2010) 282–295.
[150] F. Peng, Y.Y. Su, Y.L. Zhong, C.H. Fan, S.T. Lee, Y. He, Accounts Chem. Res. 47 (2014) 612–623.
[151] M.L. Zhang, X. Fan, H.W. Zhou, M.W. Shao, J.A. Zapien, N.B. Wong, S.T. Lee, J. Phys. Chem. C 114 (2010) 1969–1975.
[152] H.Y. Wang, X.X. Jiang, S.T. Lee, Y. He, Small 10 (2014) 4455–4468.
[153] P.P. Zhang, J. Gao, X.H. Sun, Appl. Phys. Lett. 106 (2015).
[154] H.S. Gill, S. Thota, L. Li, H.Z. Ren, R. Mosurkal, J. Kumar, Sensor Actuat. B-Chem. 220 (2015) 794–798.
[155] Y.X. Du, R.Y. Liu, B.H. Liu, S.H. Wang, M.Y. Han, Z.P. Zhang, Anal. Chem. 85 (2013) 3160–3165.
[156] E. Galopin, J. Barbillat, Y. Coffinier, S. Szunerits, G. Patriarche, R. Boukherroub, ACS Appl. Mater. Interface 1 (2009) 1396–1403.
[157] Y. He, S. Su, T.T. Xu, Y.L. Zhong, J.A. Zapien, J. Li, C.H. Fan, S.T. Lee, Nano Today 6 (2011) 122–130.
[158] C.X. Zhang, L. Su, Y.F. Chan, Z.L. Wu, Y.M. Zhao, H.J. Xu, X.M. Sun, Nanotechnology 24 (2013).
[159] M.F. Peng, H.Y. Xu, M.W. Shao, Appl. Phys. Lett. 104 (2014).
[160] B. Sun, X.X. Jiang, H.Y. Wang, B. Song, Y. Zhu, H. Wang, Y.Y. Su, Y. He, Anal. Chem. 87 (2015) 1250–1256.
[161] O. Olea-Mejia, M. Fernandez-Mondragon, G. Rodriguez-de la Concha, M. Camacho-Lopez, Appl. Surf. Sci. 348 (2015) 66–70.
[162] T. Fu, J. Fang, C.S. Wang, J.B. Zhao, J. Mater. Chem. A 4 (2016) 8803–8811.
[163] Y. Zhao, Y. Yang, Y. Luo, X. Yang, M. Li, Q. Song, ACS Appl. Mater. Interface 7 (2015) 21780–21786.
[164] E. Chung, J. Jeon, J. Yu, C. Lee, J. Choo, Biosens. Bioelectron. 64 (2015) 560–565.
[165] D. Depan, R.D.K. Misra, Nanoscale 4 (2012) 6325–6335.
[166] H.T. Ngo, N. Gandra, A.M. Fales, S.M. Taylor, T. Vo-Dinh, Biosens. Bioelectron. 81 (2016) 8–14.
[167] L. Zhang, J.J. Xu, L. Mi, H. Gong, S.Y. Jiang, Q.M. Yu, Biosens. Bioelectron. 31 (2012) 130–136.
[168] J. Yoon, N. Choi, J. Ko, K. Kim, S. Lee, J. Choo, Biosens. Bioelectron. 47 (2013) 62–67.
[169] H.B. Hu, Z.H. Wang, L. Pan, S.P. Zhao, S.Y. Zhu, J. Phys. Chem. C 114 (2010) 7738–7742.
[170] D. Song, R. Yang, C.W. Wang, R. Xiao, F. Long, Sci. Rep. 6 (2016).
[171] A. Zengin, U. Tamer, T. Caykara, Biomacromolecules 14 (2013) 3001–3009.
[172] Y.F. Pang, C.W. Wang, J. Wang, Z.W. Sun, R. Xiao, S.Q. Wang, Biosens. Bioelectron. 79 (2016) 574–580.
[173] Y. Qiu, D. Deng, Q. Deng, P. Wu, H. Zhang, C. Cai, J. Mater. Chem. B 3 (2015) 4487–4495.
[174] M.L. Foo, R. Matsuda, S. Kitagawa, Chem. Mater. 26 (2014) 310–322.
[175] R. Ricco, L. Malfatti, M. Takahashi, A.J. Hill, P. Falcaro, J. Mater. Chem. A 1 (2013) 13033–13045.
[176] S. Furukawa, J. Reboul, S. Diring, K. Sumida, S. Kitagawa, Chem. Soc. Rev. 43 (2014) 5700–5734.
[177] K. Sugikawa, Y. Furukawa, K. Sada, Chem. Mater. 23 (2011) 3132–3134.
[178] K. Sugikawa, S. Nagata, Y. Furukawa, K. Kokado, K. Sada, Chem. Mater. 25 (2013) 2565–2570.
[179] X. Kuang, S.J. Ye, X.Y. Li, Y. Ma, C.Y. Zhang, B. Tang, Chem. Commun. 52 (2016) 5432–5435.
[180] L.E. Kreno, N.G. Greeneltch, O.K. Farha, J.T. Hupp, R.P. Van Duyne, Analyst 139 (2014) 4073–4080.
[181] Y.L. Hu, J. Liao, D.M. Wang, G.K. Li, Anal. Chem. 86 (2014) 3955–3963.
[182] Z.W. Jiang, P.F. Gao, L. Yang, C.Z. Huang, Y.F. Li, Anal. Chem. 87 (2015) 12177–12182.
[183] Y. He, Y. Wang, X. Yang, S. Xie, R. Yuan, Y. Chai, ACS Appl. Mater. Interface 8 (2016) 7683–7690.
[184] D. Prezgot, A. Ianoul, J. Phys. Chem. C 119 (2015) 3293–3301.
[185] S. Saverot, X. Geng, W. Leng, P.J. Vikesland, T.Z. Grove, L.R. Bickford, RSC Adv. 6 (2016) 29669–29673.
[186] R.A. Alvarez-Puebla, E.R. Zubarev, N.A. Kotov, L.M. Liz-Marzan, Nano Today 7 (2012) 6–9.
[187] V. Lopez-Puente, P.C. Angelome, G.J.A.A. Soler-Illia, L.M. Liz-Marzan, ACS Appl. Mater. Interface 7 (2015) 25633–25640.
[188] H.L. Liu, Z.L. Yang, L.Y. Meng, Y.D. Sun, J. Wang, L.B. Yang, J.H. Liu, Z.Q. Tian, J. Am. Chem. Soc. 136 (2014) 5332–5341.
[189] H.Y. Wang, J.M. Fang, J.F. Xu, F. Wang, B. Sun, S.N. He, G.P. Sun, H.L. Liu, Analyst 140 (2015) 2973–2978.
[190] S. Yang, X. Dai, B.B. Stogin, T.S. Wong, Proc. Natl. Acad. Sci. U.S.A. 113 (2016) 268–273.
[191] Y. Liu, L. Zhao, J.Z. Su, M.T. Li, L.J. Guo, ACS Appl. Mater. Interface 7 (2015) 3532–3538.
[192] Y.W. Tan, J.J. Gu, W. Xu, Z.P. Chen, D.X. Liu, Q.L. Liu, D. Zhang, ACS Appl. Mater. Interface 5 (2013) 9878–9882.

[193] C.Y. Zhang, Y. Lu, B. Zhao, Y.W. Hao, Y.Q. Liu, Appl. Surf. Sci. 377 (2016) 167–173.
[194] S.Y. Lee, S.H. Kim, M.P. Kim, H.C. Jeon, H. Kang, H.J. Kim, B.J. Kim, S.M. Yang, Chem. Mater. 25 (2013) 2421–2426.
[195] C.C. Ho, K. Zhao, T.Y. Lee, Nanoscale 6 (2014) 8606–8611.
[196] G.C. Phan-Quang, H.K. Lee, I.Y. Phang, X.Y. Ling, Angew. Chem. Int. Ed. 54 (2015) 9691–9695.
[197] I. Izquierdo-Lorenzo, S. Jradi, P.M. Adam, RSC Adv. 4 (2014) 4128–4133.
[198] B. Chen, G.W. Meng, Q. Huang, Z.L. Huang, Q.L. Xu, C.H. Zhu, Y.W. Qian, Y. Ding, ACS Appl. Mater. Interface 6 (2014) 15667–15675.
[199] M. Li, S.K. Cushing, J.M. Zhang, S. Suri, R. Evans, W.P. Petros, L.F. Gibson, D.L. Ma, Y.X. Liu, N.Q. Wu, ACS Nano 7 (2013) 4967–4976.
[200] Z.B. Li, G.W. Meng, Q. Huang, X.Y. Hu, X. He, H.B. Tang, Z.W. Wang, F.D. Li, Small 11 (2015) 5452–5459.
[201] J. Huang, D.Y. Ma, F. Chen, M. Bai, K.W. Xu, Y.X. Zhao, Anal. Chem. 87 (2015) 10527–10534.
[202] S. Picciolini, N. Castagnetti, R. Vanna, D. Mehn, M. Bedoni, F. Gramatica, M. Villani, D. Calestani, M. Pavesi, L. Lazzarini, A. Zappettini, C. Morasso, RSC Adv. 5 (2015) 93644–93651.
[203] E.Z. Tan, P.G. Yin, T.T. You, H. Wang, L. Guo, ACS Appl. Mater. Interface 4 (2012) 3432–3437.
[204] Z.G. Dai, G.M. Wang, X.H. Xiao, W. Wu, W.Q. Li, J.J. Ying, J.F. Zheng, F. Mei, L. Fu, J. Wang, C.Z. Jiang, J. Phys. Chem. C 118 (2014) 22711–22718.
[205] C. Zhang, S.Z. Jiang, C. Yang, C.H. Li, Y.Y. Huo, X.Y. Liu, A.H. Liu, Q. Wei, S.S. Gao, X.G. Gao, B.Y. Man, Sci. Rep.-Uk 6 (2016).
[206] A.M. Gabudean, D. Biro, S. Astilean, J. Mol. Struct. 993 (2011) 420–424.
[207] L. Zhang, R. Zhang, M.X. Gao, X.M. Zhang, Talanta 158 (2016) 315–321.
[208] D.S. Grubisha, R.J. Lipert, H.Y. Park, J. Driskell, M.D. Porter, Anal. Chem. 75 (2003) 5936–5943.
[209] K. Faulds, W.E. Smith, D. Graham, Analyst 130 (2005) 1125–1131.
[210] E. Papadopoulou, N. Gale, J.F. Thompson, T.A. Fleming, T. Brown, P.N. Bartlett, Chem. Sci. 7 (2016) 386–393.
[211] X.C. Sun, S. Stagon, H.C. Huang, J. Chen, Y. Lei, RSC Adv. 4 (2014) 23382–23388.
[212] F. Sun, T. Bai, L. Zhang, J.R. Ella-Menye, S.J. Liu, A.K. Nowinski, S.Y. Jiang, Q.M. Yu, Anal. Chem. 86 (2014) 2387–2394.
[213] Y. Chen, L.H. Wu, Y.H. Chen, N. Bi, X. Zheng, H.B. Qi, M.H. Qin, X. Liao, H.Q. Zhang, Y. Tian, Microchim. Acta 177 (2012) 341–348.
[214] A.R. Bizzarri, S. Cannistraro, Nanomed-Nanotechnol. 3 (2007) 306–310.
[215] A. Accardo, F. Gentile, F. Mecarini, F. De Angelis, M. Bughammer, E. Di Fabrizio, C. Riekel, Langmuir 26 (2010) 15057–15064.
[216] M. Reyssat, A. Pepin, F. Marty, Y. Chen, D. Quere, Europhys. Lett. 74 (2006) 306–312.
[217] M.J. Liu, Y.M. Zheng, J. Zhai, L. Jiang, Acc. Chem. Res. 43 (2010) 368–377.
[218] Y.W. Su, B.H. Ji, Y. Huang, K.C. Hwang, Langmuir 26 (2010) 18926–18937.
[219] H.Y. Zhao, J. Jin, W.J. Tian, R. Li, Z. Yu, W. Song, Q. Cong, B. Zhao, Y. Ozaki, J. Mater. Chem. A 3 (2015) 4330–4337.
[220] J.D. Shao, L.P. Tong, S.Y. Tang, Z.N. Guo, H. Zhang, P.H. Li, H.Y. Wang, C. Du, X.F. Yu, ACS Appl. Mater. Interface 7 (2015) 5391–5399.
[221] F. De Angelis, F. Gentile, F. Mecarini, G. Das, M. Moretti, P. Candeloro, M.L. Coluccio, G. Cojoc, A. Accardo, C. Liberale, R.P. Zaccaria, G. Perozziello, L. Tirinato, A. Toma, G. Cuda, R. Cingolani, E. Di Fabrizio, Nat. Photon 5 (2011) 682–687.
[222] P. Lovera, N. Creedon, H. Alatawi, M. Mitchell, M. Burke, A.J. Quinn, A. O'Riordan, Nanotechnology 25 (2014).
[223] N.D. Jayram, S. Sonia, S. Poongodi, P.S. Kumar, Y. Masuda, D. Mangalaraj, N. Ponpandian, C. Viswanathan, Appl. Surf. Sci. 355 (2015) 969–977.
[224] N.D. Jayrarn, D. Aishwarya, S. Sonia, D. Mangalaraj, P.S. Kumar, G.M. Rao, J. Colloid. Interface Sci. 477 (2016) 209–219.
[225] K. Bhatt, S.S. Tan, S. Karumuri, A.K. Kalkan, Nano Lett. 10 (2010) 3880–3887.
[226] A.Y. Panarin, S.N. Terekhov, K.I. Kholostov, V.P. Bondarenko, Appl. Surf. Sci. 256 (2010) 6969–6976.
[227] S.Y. Baik, Y.J. Cho, Y.R. Lim, H.S. Im, D.M. Jang, Y. Myung, J. Park, H.S. Kang, ACS Nano 6 (2012) 2459–2470.
[228] S.S.R. Dasary, A.K. Singh, D. Senapati, H.T. Yu, P.C. Ray, J. Am. Chem. Soc. 131 (2009) 13806–13812.
[229] W. Ren, Y.X. Fang, E.K. Wang, ACS Nano 5 (2011) 6425–6433.
[230] Y.H. Guo, X.T. Wang, B. Miao, Y. Li, W.R. Yao, Y.F. Xie, J.D. Li, D.M. Wu, R.J. Pei, RSC Adv. 5 (2015) 98724–98729.
[231] S. Hussain, A.H. Malik, M.A. Afroz, P.K. Iyer, Chem. Commun. 51 (2015) 7207–7210.
[232] Z. Guo, J. Hwang, B. Zhao, J.H. Chung, S.G. Cho, S.-J. Baek, J. Choo, Analyst 139 (2014) 807–812.
[233] G.H. Qi, C.C. Fu, G. Chen, S.P. Xu, W.Q. Xu, RSC Adv. 5 (2015) 49759–49764.
[234] Z.L. Sun, J.L. Du, L. Yan, S. Chen, Z.L. Yang, C.Y. Jing, ACS Appl. Mater. Interface 8 (2016) 3056–3062.
[235] Y.Q. Zhu, L. Zhang, L.B. Yang, Mater. Res. Bull. 63 (2015) 199–204.
[236] C.W. Wang, H.T. Chang, Anal. Chem. 86 (2014) 7606–7611.
[237] P. He, Y. Zhang, L.J. Liu, W.P. Qiao, S.S. Zhang, Chem-Eur. J. 19 (2013) 7452–7460.
[238] L.X. Chen, X.L. Fu, J.H. Li, Nanoscale 5 (2013) 5905–5911.
[239] P. Mignon, S. Loverix, J. Steyaert, P. Geerlings, Nucleic Acids Res. 33 (2005) 1779–1789.
[240] J.J. Schwinefus, J. McDevitt, Biophys. J. 98 (2010), 41a-41a.
[241] K.A. Wilson, J.L. Kellie, S.D. Wetmore, Nucleic Acids Res. 42 (2014) 6726–6741.
[242] Q. Wang, X.Q. Li, S. Ma, Chem. J. Chin. 35 (2014) 2674–2679.
[243] D. Sadhukhan, M. Maiti, G. Pilet, A. Bauza, A. Frontera, S. Mitra, Eur. J. Inorg. Chem. (2015) 1958–1972.
[244] A.S. Mahadevi, G.N. Sastry, Chem. Rev. 113 (2013) 2100–2138.
[245] E.A. Meyer, R.K. Castellano, F. Diederich, Angew. Chem. Int. Ed. 42 (2003) 1210–1250.
[246] P. Leyton, J.S. Gomez-Jeria, S. Sanchez-Cortes, C. Domingo, M. Campos-Vallette, J. Phys. Chem. B 110 (2006) 6470–6474.
[247] L.L. Qu, Y.T. Li, D.W. Li, J.Q. Xue, J.S. Fossey, Y.T. Long, Analyst 138 (2013) 1523–1528.
[248] P. Leyton, S. Sanchez-Cortes, J.V. Garcia-Ramos, C. Domingo, M. Campos-Vallette, C. Saitz, R.E. Clavijo, J. Phys. Chem. B 108 (2004) 17484–17490.
[249] X. He, H. Wang, Z.B. Li, D. Chen, Q. Zhang, Phys. Chem. Chem. Phys. 16 (2014) 14706–14712.
[250] Y.F. Yuan, X.T. Yu, Q. Zhang, M.F. Chang, L. Li, T.Q. Yang, Y.T. Chen, H.F. Pan, S.J. Zhang, L. Li, J.H. Xu, Anal. Chem. 88 (2016) 4328–4335.
[251] A. Arzumanyan, H.M.G.P.V. Reis, M.A. Feitelson, Nat. Rev. Cancer 13 (2013) 123–135.
[252] C. Song, Y. Yang, B. Yang, L. Min, L. Wang, J. Mater. Chem. B 4 (2016) 1811–1817.
[253] B.C. Tang, J.J. Wang, J.A. Hutchison, L. Ma, N. Zhang, H. Guo, Z.B. Hu, M. Li, Y.L. Zhao, ACS Nano 10 (2016) 871–879.
[254] S.J. Ye, X.M. Zhai, Y.Y. Wu, S.P. Kuang, Biosens. Bioelectron. 79 (2016) 130–135.
[255] M.X. Li, H. Yang, S.Q. Li, K. Zhao, J.G. Li, D.N. Jiang, L.L. Sun, A.P. Deng, J. Agric. Food Chem. 62 (2014) 10896–10902.
[256] C.W. Fang, C. Wei, M.M. Xu, Y.X. Yuan, R.A. Gu, J.L. Yao, RSC Adv. 6 (2016) 61325–61333.
[257] Y.Z. Wang, S. Chen, C. Wei, M.M. Xu, J.L. Yao, Y. Li, A.P. Deng, R.A. Gu, Chem. Commun. 50 (2014) 9112–9114.
[258] X.L. Wu, X. Chen, F.L. Gan, W. Ma, L.G. Xu, H. Kuang, A.K. Li, C.L. Xu, Biosens. Bioelectron. 75 (2016) 55–58.
[259] I.J. Hidi, M. Jahn, K. Weber, D. Cialla-May, J. Popp, Phys. Chem. Chem. Phys. 17 (2015) 21236–21242.
[260] J. Qi, J.B. Zeng, F.S. Zhao, S.H. Lin, B. Raja, U. Strych, R.C. Willson, W.C. Shih, Nanoscale 6 (2014) 8521–8526.
[261] D. Choi, T. Kang, H. Cho, Y. Choi, L.P. Lee, Lab Chip 9 (2009) 239–243.
[262] A. Lamberti, A. Virga, A. Chiado, A. Chiodoni, K. Bejtka, P. Rivolo, F. Giorgis, J. Mater. Chem. C 3 (2015) 6868–6875.
[263] S. Heeg, A. Oikonomou, R. Fernandez-Garcia, C. Lehmann, S.A. Maier, A. Vijayaraghavan, S. Reich, Nano Lett. 14 (2014) 1762–1768.
[264] L. Lesser-Rojas, P. Ebbinghaus, G. Vasan, M.L. Chu, A. Erbe, C.F. Chou, Nano Lett. 14 (2014) 2242–2250.
[265] P. Negri, R.J. Flaherty, O.O. Dada, Z.D. Schultz, Chem. Commun. 50 (2014) 2707–2710.
[266] P. Negri, S.A. Sarver, N.M. Schiavone, N.J. Dovichi, Z.D. Schultz, Analyst 140 (2015) 1516–1522.
[267] C.H. Lee, L.M. Tian, S. Singamaneni, ACS Appl. Mater. Interface 2 (2010) 3429–3435.
[268] J.E.L. Villa, R.J. Poppi, Analyst 141 (2016) 1966–1972.
[269] L.B. Yang, P. Li, H.L. Liu, X.H. Tang, J.H. Liu, Chem. Soc. Rev. 44 (2015) 2837–2848.
[270] P.G. Etchegoin, E.C. Le Ru, Phys. Chem. Chem. Phys. 10 (2008) 6079–6089.
[271] J.S. Sun, Y.L. Xianyu, X.Y. Jiang, Chem. Soc. Rev. 43 (2014) 6239–6253.
[272] C. Wang, C.X. Yu, Nanotechnology 26 (2015).
[273] J.A. Huang, Y.L. Zhang, H. Ding, H.B. Sun, Adv. Opt. Mater. 3 (2015) 618–633.
[274] A.F. Chrimes, K. Khoshmanesh, P.R. Stoddart, A. Mitchell, K. Kalantar-zadeh, Chem. Soc. Rev. 42 (2013) 5880–5906.
[275] Y.L. Xing, A. Wyss, N. Esser, P.S. Dittrich, Analyst 140 (2015) 7896–7901.
[276] A.H. Nguyen, J. Lee, H.I. Choi, H.S. Kwak, S.J. Sim, Biosens. Bioelectron. 70 (2015) 358–365.
[277] M. Lee, K. Lee, K.H. Kim, K.W. Oh, J. Choo, Lab Chip 12 (2012) 3720–3727.
[278] L. Wu, Z.Y. Wang, K.Q. Fan, S.F. Zong, Y.P. Cui, Small 11 (2015) 2798–2806.
[279] J. Morla-Folch, H.N. Xie, P. Gisbert-Quilis, S. Gomez-de Pedro, N. Pazos-Perez, R.A. Alvarez-Puebla, L. Guerrini, Angew. Chem. Int. Ed. 54 (2015) 13650–13654.
[280] K.K. Strelau, R. Kretschmer, R. Moller, W. Fritzsche, J. Popp, Anal. Bioanal. Chem. 396 (2010) 1381–1384.
[281] E. Prado, A. Colin, L. Servant, S. Lecomte, J. Phys. Chem. C 118 (2014) 13965–13971.
[282] P.R. Zhang, L.H. Ren, X. Zhang, Y.F. Shan, Y. Wang, Y.T. Ji, H.B. Yin, W.E. Huang, J. Xu, B. Ma, Anal. Chem. 87 (2015) 2282–2289.
[283] Q. Zhang, P.R. Zhang, H.L. Gou, C.B. Mou, W.E. Huang, M.L. Yang, J. Xu, B. Ma, Analyst 140 (2015) 6163–6174.
[284] R. Gao, N. Choi, S.I. Chang, E.K. Lee, J. Choo, Nanoscale 6 (2014) 8781–8786.
[285] J.H. Zhou, K.N. Ren, Y.H. Zhao, W. Dai, H.K. Wu, Anal. Bioanal. Chem. 402 (2012) 1601–1609.
[286] A. Saha, N.R. Jana, ACS Appl. Mater. Interface 7 (2015) 996–1003.
[287] R. Gao, J. Ko, K. Cha, J.H. Jeon, G.E. Rhie, J. Choi, A.J. deMello, J. Choo Biosens Bioelectron. 72 (2015) 230–236.
[288] A. Kamińska, E. Witkowska, K. Winkler, I. Dzięcielewski, J.L. Weyher, J. Waluk, Biosens. Bioelectron. 66 (2015) 461–467.
[289] F.R. Madiyar, S. Bhana, L.Z. Swisher, C.T. Culbertson, X.H. Huang, J. Li, Nanoscale 7 (2015) 3726–3736.
[290] H.Y. Mao, W.G. Wu, D.D. She, G.C. Sun, P.P. Lv, J. Xu, Small 10 (2014) 127–134.

[291] Y.Q. Zhao, Y.L. Zhang, J.A. Huang, Z.Y. Zhang, X.F. Chen, W.J. Zhang, J. Mater. Chem. A 3 (2015) 6408–6413.
[292] R. Wilson, S.A. Bowden, J. Parnell, J.M. Cooper, Anal. Chem. 82 (2010) 2119–2123.
[293] J. Parisi, L. Su, Y. Lei, Lab Chip 13 (2013) 1501–1508.
[294] G. Chen, Y.Y. Wang, H.L. Wang, M. Cong, L. Chen, Y.G. Yang, Y.J. Geng, H.B. Li, S.P. Xu, W.Q. Xu, RSC Adv. 4 (2014) 54434–54440.
[295] C.C. Fu, Y. Wang, G. Chen, L.Y. Yang, S.P. Xu, W. Xu, Anal. Chem. 87 (2015) 9555–9558.
[296] D. Psaltis, S.R. Quake, C.H. Yang, Nature 442 (2006) 381–386.
[297] C. Monat, P. Domachuk, B.J. Eggleton, Nat. Photonics 1 (2007) 106–114.
[298] J.C. Yang, J. Ji, J.M. Hogle, D.N. Larson, Nano Lett. 8 (2008) 2718–2724.
[299] N. Ganesh, W. Zhang, P.C. Mathias, E. Chow, J.A.N.T. Soares, V. Malyarchuk, A. D. Smith, B.T. Cunningham, Nat. Nanotechnol. 2 (2007) 515–520.
[300] T.H. Wang, Y.H. Peng, C.Y. Zhang, P.K. Wong, C.M. Ho, J. Am. Chem. Soc. 127 (2005) 5354–5359.
[301] K. Wang, E. Schonbrun, P. Steinvurzel, K.B. Crozier, Nano Lett. 10 (2010) 3506–3511.
[302] S.M. Park, Y.S. Huh, H.G. Craighead, D. Erickson, Proc. Natl. Acad. Sci. U.S.A. 106 (2009) 15549–15554.
[303] M.K.K. Oo, Y. Han, J. Kanka, S. Sukhishvili, H. Du, Opt. Lett. 35 (2010) 466–468.
[304] X.D. Fan, I.M. White, Nat. Photonics 5 (2011) 591–597.
[305] Y. Yin, T. Qiu, W.J. Zhang, P.K. Chu, J. Mater. Res. 26 (2011) 170–185.
[306] C. Lim, J. Hong, B.G. Chung, A.J. deMello, J. Choo Analyst 135 (2010) 837–844.
[307] I.M. White, J. Gohring, X.D. Fan, Opt. Express 15 (2007) 17433–17442.
[308] S.H. Yazdi, I.M. White, Biomicrofluidics 6 (2012).
[309] Y. Deng, M.N. Idso, D.D. Galvan, Q.M. Yu, Anal. Chim. Acta 863 (2015) 41–48.
[310] Y. Guo, M.K. Khaing, K. Reddy, X. Fan, ACS Nano 6 (2012) 381–388.
[311] A. Yamaguchi, T. Fukuoka, R. Takahashi, R. Hara, Y. Utsumi, Sensor Actuat. B-Chem. 230 (2016) 94–100.
[312] A.W. Martinez, S.T. Phillips, M.J. Butte, G.M. Whitesides, Angew. Chem. Int. Ed. 46 (2007) 1318–1320.
[313] L.Y. Guan, J.F. Tian, R. Cao, M.S. Li, Z.X. Cai, W. Shen, Anal. Chem. 86 (2014) 11362–11367.
[314] S. Ahmed, M.P.N. Bui, A. Abbas, Biosens. Bioelectron. 77 (2016) 249–263.
[315] S.M.Z. Hossain, R.E. Luckham, M.J. McFadden, J.D. Brennan, Anal. Chem. 81 (2009) 9055–9064.
[316] Y.X. Ma, H. Li, S. Peng, L.Y. Wang, Anal. Chem. 84 (2012) 8415–8421.
[317] L.B. Wang, W. Chen, D.H. Xu, B.S. Shim, Y.Y. Zhu, F.X. Sun, L.Q. Liu, C.F. Peng, Z. Y. Jin, C.L. Xu, N.A. Kotov, Nano Lett. 9 (2009) 4147–4152.
[318] S. Chaiyo, W. Siangproh, A. Apilux, O. Chailapakul, Anal. Chim. Acta 866 (2015) 75–83.
[319] J.C. Cunningham, P.R. DeGregory, R.M. Crooks, Ann. Rev. Anal. Chem. 9 (2016) 183–202.
[320] L. Polavarapu, A. La Porta, S.M. Novikov, M. Coronado-Puchau, L.M. Liz-Marzan, Small 10 (2014) 3065–3071.
[321] Y.H. Ngo, D. Li, G.P. Simon, G. Garnier, Langmuir 28 (2012) 8782–8790.
[322] C.H. Lee, M.E. Hankus, L. Tian, P.M. Pellegrino, S. Singamaneni, Anal. Chem. 83 (2011) 8953–8958.
[323] A. Abbas, A. Brimer, J.M. Slocik, L.M. Tian, R.R. Naik, S. Singamaneni, Anal. Chem. 85 (2013) 3977–3983.
[324] L.L. Qu, D.W. Li, J.Q. Xue, W.L. Zhai, J.S. Fossey, Y.T. Long, Lab Chip 12 (2012) 876–881.
[325] W.W. Yu, I.M. White, Analyst 138 (2013) 3679–3686.
[326] W.W. Yu, I.M. White, Anal. Chem. 82 (2010) 9626–9630.
[327] E.P. Hoppmann, W.W. Yu, I.M. White, Methods 63 (2013) 219–224.
[328] W. Dungchai, O. Chailapakul, C.S. Henry, Analyst 136 (2011) 77–82.
[329] R. Gottesman, S. Shukla, N. Perkas, L.A. Solovyov, Y. Nitzan, A. Gedanken, Langmuir 27 (2011) 720–726.
[330] W.W. Yu, I.M. White, Analyst 137 (2012) 1168–1173.
[331] M.L. Cheng, B.C. Tsai, J. Yang, Anal. Chim. Acta 708 (2011) 89–96.
[332] Y.J. Meng, Y.C. Lai, X.H. Jiang, Q.Q. Zhao, J.H. Zhan, Analyst 138 (2013) 2090–2095.
[333] R. Zhang, B.B. Xu, X.Q. Liu, Y.L. Zhang, Y. Xu, Q.D. Chen, H.B. Sun, Chem. Commun. 48 (2012) 5913–5915.
[334] Y.K. Han, Z. Liang, H.L. Sun, H. Xiao, H.L. Tsai, Appl. Phys. A-Mater. 102 (2011) 415–419.
[335] C.C. Yu, S.Y. Chou, Y.C. Tseng, S.C. Tseng, Y.T. Yen, H.L. Chen, Nanoscale 7 (2015) 1667–1677.
[336] Q. Liu, J.H. Wang, B.K. Wang, Z. Li, H. Huang, C.Z. Li, X.F. Yu, P.K. Chu, Biosens. Bioelectron. 54 (2014) 128–134.
[337] J.A. Webb, J. Aufrecht, C. Hungerford, R. Bardhan, J. Mater. Chem. C 2 (2014) 10446–10454.
[338] K. Zhang, J.J. Zhao, H.Y. Xu, Y.X. Li, J. Ji, B.H. Liu, ACS Appl. Mater. Interface 7 (2015) 16767–16774.
[339] W. Kim, Y.H. Kim, H.K. Park, S. Choi, ACS Appl. Mater. Interface 7 (2015) 27910–27917.
[340] K. Qian, L.B. Yang, Z.Y. Li, J.H. Liu, J. Raman Spectrosc. 44 (2013) 21–28.
[341] M. Hu, F.S. Ou, W. Wu, I. Naumov, X.M. Li, A.M. Bratkovsky, R.S. Williams, Z.Y. Li, J. Am. Chem. Soc. 132 (2010) 12820–12822.
[342] H.L. Liu, Y.D. Sun, Z. Jin, L.B. Yang, J.H. Liu, Chem. Sci. 4 (2013) 3490–3496.
[343] L.B. Yang, H.L. Liu, J. Wang, F. Zhou, Z.Q. Tian, J.H. Liu, Chem. Commun. 47 (2011) 3583–3585.
[344] F. Lussier, T. Brule, M. Vishwakarma, T. Das, J.P. Spatz, J.F. Masson, Nano Lett. 16 (2016) 3866–3871.
[345] P. Li, H.L. Liu, L.B. Yang, J.H. Liu, Talanta 117 (2013) 39–44.
[346] P. Li, R.L. Dong, Y.P. Wu, H.L. Liu, L.T. Kong, L.B. Yang, Talanta 127 (2014) 269–275.
[347] R.L. Dong, S.Z. Weng, L.B. Yang, J.H. Liu, Anal. Chem. 87 (2015) 2937–2944.
[348] F. Fang, Y. Qi, F. Lu, L. Yang, Talanta 146 (2016) 351–357.
[349] M.G. Banaee, K.B. Crozier, ACS Nano 5 (2011) 307–314.
[350] N.A. Cinel, S. Butun, G. Ertas, E. Ozbay, Small 9 (2013) 531–537.
[351] D.V. Voronine, A.M. Sinyukov, X. Hua, K. Wang, P.K. Jha, E. Munusamy, S.E. Wheeler, G. Welch, A.V. Sokolov, M.O. Scully, Sci. Rep.-Uk 2 (2012).
[352] A.A. Yanik, A.E. Cetin, M. Huang, A. Artar, S.H. Mousavi, A. Khanikaev, J.H. Connor, G. Shvets, H. Altug, Proc. Natl. Acad. Sci. U.S.A. 108 (2011) 11784–11789.
[353] R.B. Jiang, F. Qin, Q.F. Ruan, J.F. Wang, C.J. Jin, Adv. Funct. Mater. 24 (2014) 7328–7337.
[354] S.L. Dodson, C. Cao, H. Zaribafzadeh, S.Z. Li, Q.H. Xiong, Biosens. Bioelectron. 63 (2015) 472–477.
[355] F. Cheng, X.D. Yang, J. Gao, Sci. Rep.-Uk 5 (2015).
[356] H. Torul, H. Ciftci, D. Cetin, Z. Suludere, I.H. Boyaci, U. Tamer, Anal. Bioanal. Chem. 407 (2015) 8243–8251.
[357] Y.S. Huh, A.J. Chung, B. Cordovez, D. Erickson, Lab Chip 9 (2009) 433–439.